

Structural Design and Fabrication of Multifunctional Nanocarbon Materials for Extreme Environmental Applications

Sijia Wu, Huajian Li, Don N. Futaba, Guohai Chen, Chen Chen, Kechen Zhou, Qifan Zhang, Miao Li, Zonglin Ye, and Ming Xu*

Extreme environments represent numerous harsh environmental conditions, such as temperature, pressure, corrosion, and radiation. The tolerance of applications in extreme environments exemplifies significant challenges to both materials and their structures. Given the superior mechanical strength, electrical conductivity, thermal stability, and chemical stability of nanocarbon materials, such as carbon nanotubes (CNTs) and graphene, they are widely investigated as base materials for extreme environmental applications and have shown numerous breakthroughs in the fields of wide-temperature structural-material construction, low-temperature energy storage, underwater sensing, and electronics operated at high temperatures. Here, the critical aspects of structural design and fabrication of nanocarbon materials for extreme environments are reviewed, including a description of the underlying mechanism supporting the performance of nanocarbon materials against extreme environments, the principles of structural design of nanocarbon materials for the optimization of extreme environmental performances, and the fabrication processes developed for the realization of specific extreme environmental applications. Finally, perspectives on how CNTs and graphene can further contribute to the development of extreme environmental applications are presented.

1. Introduction

Extreme environments refer to numerous varieties of harsh conditions under which materials and devices fail to operate. This concept includes not only regions of extreme temperatures extending from below 256 or higher than 313 K (e.g., the south pole regions with an annual average temperature of 243–248 K and the lowest temperature of 183 K, deserts with

peak temperatures of ≈353 K), but also acid–alkaline environments with the pH values lower than 5 or higher than 9 (e.g., Tamagawa Onsen with the pH value of 1 and Soda lake with the pH around 10), high salinity environments with salinity equal to or greater than 3.5% (e.g., oceans or Dead Sea), high-pressure environments with the pressure larger than 20 MPa (e.g., deep sea or ultradeep Earth with the pressure as high as 100 MPa), and outer space which contains various forms of radiation with energies ranging from 1 keV to hundreds of megaelectronvolts (Figure 1).^[1] The operation of devices and instruments in such extreme environments faces tremendous challenges because temperature, pressure, pH, salinity, and radiation degrade the structural properties of materials and thus deteriorate their performances.

There are many examples throughout industry and research showing the detrimental effects of extreme environments. For example, the long-term operation of

automatic observation systems used for the scientific exploration of Antarctic relies on the proper function of small-scale energy-storage devices. However, significant decays in capacitances are common occurrence to the observation system due to the reduced transport of ions and electrons in electrodes.^[2] This reduces the running time of such systems and degrades data transmission. In addition, electronic devices used in high temperature environments (>473 K), such as aerospace or underground mining and drilling, regularly suffer instability due to temperature effects on the resistors.^[3] Even the ocean represents a type of extreme environment as the ships, underwater robots, and pipelines all use metal (e.g., stainless steel) in their design as shells or architectural support. In this case, the corrosion of metals causes degradation of their mechanical strength and greatly shortens their service life.^[4] Detectors used for deep-sea exploration are required to withstand the high-pressure environment, where the materials are prone to deformation and damage compared to their counterparts operating under ambient conditions. Even in outer space, weakness to various types of radiation leads to the loss in communication data due to the sensitivity of both insulating and semiconducting components.^[5] Therefore, the use of devices in extreme environments represents a significant challenge due to environmental effects on the desired and

S. Wu, H. Li, C. Chen, K. Zhou, Q. Zhang, M. Li, Z. Ye, M. Xu

School of Materials Science and Engineering
State Key Laboratory of Material Processing and Die and Mould Technology

Huazhong University of Science and Technology
Wuhan 430074, China

E-mail: ming.xu@hust.edu.cn

D. N. Futaba, G. Chen
Nano Carbon Device Research Center
National Institute of Advanced Industrial Science and Technology (AIST)
Tsukuba 305-8565, Japan

 The ORCID identification number(s) for the author(s) of this article can be found under <https://doi.org/10.1002/adma.202201046>.

DOI: 10.1002/adma.202201046

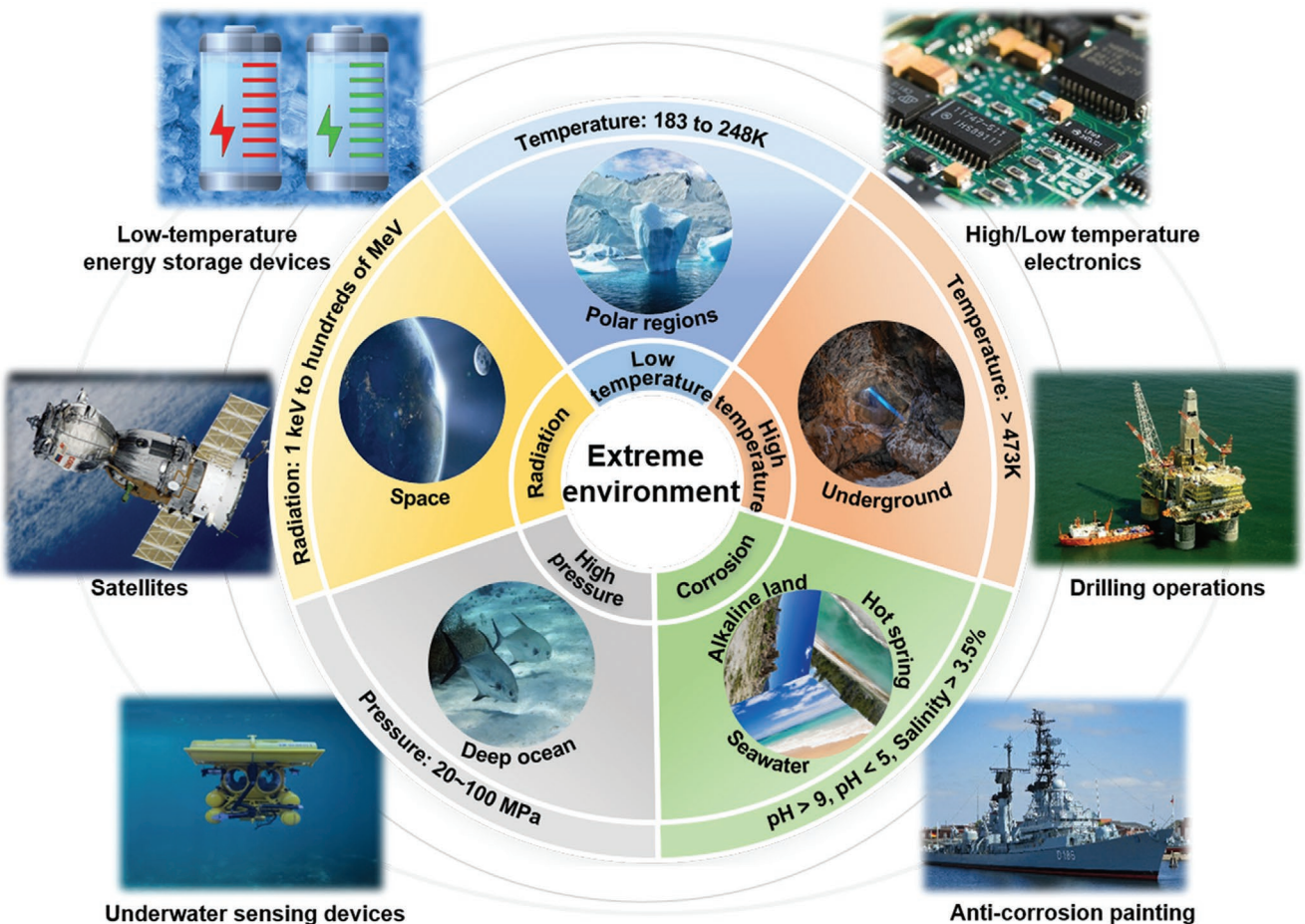


Figure 1. Extreme environments and the corresponding applications. All images are from Pixabay.

needed material properties. There is a need to develop new materials that can demonstrate superior environmental tolerances and thus overcome bottlenecks in the development of the applications in extreme environments.

Nanocarbon materials, exemplified by 1D carbon nanotubes (CNTs) and 2D graphene, possess excellent properties, such as low mass density, high electrical conductivity, high strength, chemical inertness, and thermal stability.^[6] In recent years, the applications of nanocarbon materials for extreme uses have greatly advanced in both academic and industry fields. For example, nanocarbon materials have been reported for stable mechanical and adhesive properties across wide temperature ranges from 4 to 1273 K^[7] and played important roles in high- and low-temperature energy-storage devices working commonly across 203–323 K.^[8] In addition, nanocarbon materials can act as nanofillers for composite materials used as textiles, coatings, adhesives, and electromagnetic interference (EMI) shields in extreme environments, which have attracted the attention across wide industrial areas.^[9] Furthermore, the radiation-resistant properties of nanocarbon materials also make them promising in the applications of the next-generation space electronic devices and nuclear industries. At present, CNTs and graphene have already been used in the applications of helicopter rotor blades in the AH-64 Apache, gas detectors/chemical sensors, anticorrosion coatings, and heating films.^[10]

This review covers the advantages of nanocarbon materials under extreme conditions, the principles of structural design and fabrication technologies developed for nanocarbon materials intended to operate in extreme environments, and the examples of realized devices in extreme environments including wide operating temperatures and underwater conditions. Reliability issues and failure mechanisms are provided from a fundamental standpoint to illustrate the significant challenges of operations in extreme environments. The future application prospects of nanocarbon materials in extreme environments are also discussed.

2. Advantages of Nanocarbon Materials for Extreme Environments

2.1. Factors Governing the Performances of Materials against Extreme Environments

2.1.1. The Effect of Extreme Environments on the Performances of Materials

Extreme environments, including high and low temperatures, high pressures, corrosion, and radiation, can affect the microstructures of materials, resulting in the degradation in their intrinsic mechanical, electrical, and thermal performances.

Fundamentally, variations in temperature affect the thermal vibrations of atoms and molecules of materials. High temperatures stimulate atomic and molecular vibrations, causing the weakening of bonds. The degradation of stiffness always occurs in materials at increased temperatures and decomposition and melting can occur at sufficiently high temperatures. By contrast, at low temperatures, these thermal atomic and molecular vibrations are suppressed, triggering the embrittlement and fracture of materials.^[11]

On the aspect of material functions, the activation of atomic thermal vibration (i.e., phonon modes) of metals increases the difficulty of electron transport due to phonon-electron scattering. As a result, with increased temperature, their electrical and thermal conductivities decrease. By contrast, for amorphous or noncrystalline ceramics and polymeric materials where the thermal conductivity stems from the phonon transfer atomically or via molecular chains, thermal conductivities increase with temperature increasing, causing the degradation of their insulating properties.^[12]

In addition, several other environments can act to degrade material properties. High pressure environments can cause pressure-induced deformation or fracture. In acidic, alkaline, and corrosive environments with high salinity, a variety of chemical reactions can readily occur to materials, especially to metals possessing dangling bonds. This leads to the decrease in stiffness and electrical conductivity of materials.^[13] In radiation environments, high-energy particles, such as gamma rays, electrons, and neutrons impact the surface of materials, which leads to electron ionization, atomic dislocations, and atomic nuclei decay, ultimately induces swelling and embrittlement of the exposed materials.^[14]

2.1.2. Strategies of Performance Improvement against Extreme Environments

To withstand the influence of extreme environments, consideration of both interatomic bonding (e.g., covalent, ionic, metallic, van der Waals (vdW), and hydrogen bonds) and the microstructures (e.g., crystal structure, grain size, molecular chain configuration) of materials is necessary. For example, to withstand the influence of high temperatures on the thermal insulation of materials, porous structures with tortuous thermal pathway are often adopted to reduce the heat conduction throughout the materials.^[15] He et al. reported a highly porous composite material by using mullite fibers as matrix and ZrO₂-SiO₂ aerogel as fillers.^[15a] Combining the thermal stability of ceramics and the high porosity of material structure, high insulation performance with a thermal conductivity of only 0.083–0.18 W m⁻¹ K⁻¹ was achieved across 773–1473 K. To resist embrittlement of polymeric materials at low temperatures, the application of flexible molecular chains is one efficient route. For example, an elastomer was reported to possess excellent elasticity and ductility down to 163 K through the construction of ultraflexible perfluoropolyether chains cross-linked by dynamic urethane chemistry.^[16]

To counter the influence of high pressure on the structural stability of materials, interatomic bonding has been utilized to improve both material stiffness and toughness. The typical

cases are specially designed alloys.^[17] Another way is to design composite structures, aiming to resist microcracks caused by high pressures. For example, Yang et al. used highly ductile silk and strong carbon fibers as the fillers to double the impact resistance of epoxy resin matrix.^[18] To counter the influence of corrosion of metals, reducing the chemical reactivity of the surfaces is necessary, which can be realized by passivating metal surfaces directly or applying polymeric coatings. For example, Peng et al. achieved a 20-fold improvement in the corrosion resistance of copper with an ultrathin surface passivation layer of 200 nm by crystallographic reconstructing copper atoms of outermost surface from copper (Cu) (111) to Cu (110).^[19]

The ways to overcome the influence of radiation exposure of metals include the enhancement of interatomic bonding and tailoring of microstructures to eliminate the interstitial atoms and vacancies generated by radiation, while preventing the migration and aggregation of interstitial atoms.^[20] For example, Lu et al. prepared a series of nickel alloys to minimize atomic mobility by tuning elemental composition of the alloys, including NiFe, NiCoFe, NiCoFeCr, and NiCoFeCrMn.^[21] In doing so, the radiation resistance of nickel was improved evidenced by the reduction of swelling degree from 9.4% to 0.1% after an exposure to 3 MeV ion irradiation at 773 K.

As described, the mechanical properties of materials depend greatly on the interatomic bonding and the microstructure. Similarly, the functions of materials (e.g., electrical and thermal properties) depend on the electronic structure of atoms and the electron movement (rotation, scattering, excitation, transition, etc.) throughout the materials. To counter the influence of extreme environments, bond strengthening and structural optimization represent two aspects which require attention.

2.2. Features of Nanocarbon Materials for Extreme Environments

2.2.1. Feature Properties of Individual Nanocarbon Components against Extreme Environments

To understand the underlying mechanism of the behaviors of nanocarbon materials in extreme environments, we begin with the introduction of structural properties of individual nanocarbon components (i.e., individual CNTs and graphene).

From the structural aspect, graphene possesses 2D honeycomb-like planar structure which is formed by a hexagonal array of sp² hybridized carbon atoms. The thickness of single layer graphene (SLG) is only a single atomic layer, representing the thinnest possible flat layer.^[22] Graphene represents one of the strongest materials with a Young's modulus reaching 1 TPa based on its unique structure.^[23] CNTs can be considered as the seamlessly rolled sheets of graphene. Although the strain energy is increased in the curved structure, the total energy of the tubular structure is reduced due to the decrease in the number of dangling bonds, promoting the structural stability of CNTs. Therefore, in theory, CNTs are capable of withstanding the pressure of 5.5 GPa at 300 K and temperature of 3070 K in vacuum.^[24]

From a functional aspect, compared with 3D structural materials, 2D planar structure of graphene significantly decreases phonon-boundary scattering. Thus, the thermal conductivity of

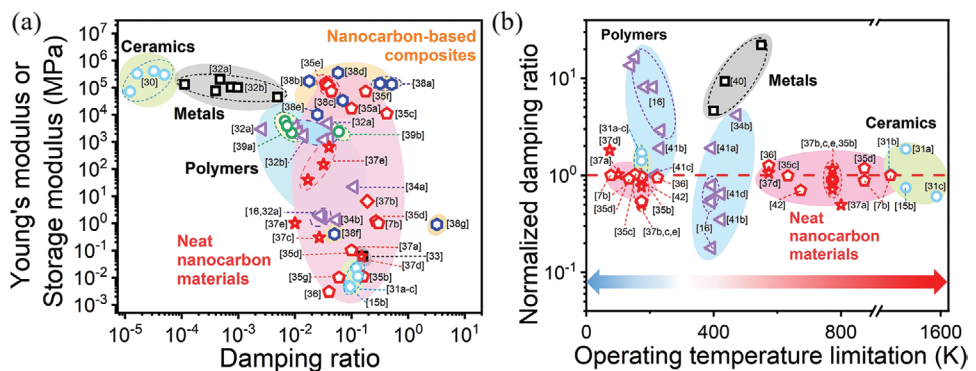


Figure 2. Mechanical properties of ceramics, metals, polymer materials, and nanocarbon materials. a) Ashby map of damping ratio versus storage modulus of ceramics^[30] and aerogel,^[15b,31] metals^[32] and nickel microlattice,^[33] polymer materials (e.g., plastic,^[32] rubber^[16,34]), nanocarbon materials (CNT,^[7b,35] graphene,^[36] hybrid^[37]) and their composites,^[38] and carbon/carbon composites.^[39] b) Ashby map of operating temperature limitation versus normalized damping ratio of ceramics aerogel,^[15b,31] plastic metals,^[40] polymers,^[16,34b,41] and nanocarbon materials.^[7b,35b-d,36,37,42]

SLG is theoretically predicted to be $10\,000\text{ W m}^{-1}\text{ K}^{-1}$, while experimentally it has been measured as high as $5300\text{ W m}^{-1}\text{ K}^{-1}$, 10 times higher than that of copper ($400\text{ W m}^{-1}\text{ K}^{-1}$).^[25] In addition, graphene is a zero-bandgap material with ultrahigh carrier mobility ($2 \times 10^5\text{ cm}^2\text{ V}^{-1}\text{ s}^{-1}$), which is 100 times higher than that of monocrystalline silicon.^[26] By contrast, the electronic characteristics (semiconducting/metallic) of CNTs vary based on its diameter and helicity. The bandgap of a single-walled CNT (SWCNT) varies from 0 to $\approx 1\text{ eV}$. In addition, CNTs present quantum confinement effects by showing ballistic transport of electrons in the axial direction with the electrical conductivity experimentally reaching 10^8 S m^{-1} .^[27] The thermal conductivity of CNTs is also governed by their diameter, chirality, and length, which can be conducted through electron transport and wave transmission through the lattice.^[28] The thermal conductivity of CNTs also shows anisotropy with the axial thermal conductivity up to $7000\text{ W m}^{-1}\text{ K}^{-1}$.^[28c] Commonly quoted values for individual CNTs are $3000\text{ W m}^{-1}\text{ K}^{-1}$ for multiwall CNTs (MWCNTs) and $3500\text{ W m}^{-1}\text{ K}^{-1}$ for SWCNTs at room temperature.^[28b,29] In addition, due to the strong C=C covalent bonds, nanocarbon materials are among the most chemically stable materials, which can withstand the corrosion of strong acid and alkali.

Compared with conventional materials, individual nanocarbon components possess excellent chemical stability, highest thermal conductivity and electrical conductivity based on the nature of C=C covalent bond and their low-dimensional feature, which can be very useful building blocks for the architecture of materials for the use in extreme environments.

2.2.2. Feature Properties of Nanocarbon Materials in Extreme Environments

While acting as the building blocks for the architecture of materials for the use in extreme environments, the distinctive properties of individual nanocarbon components bring out numerous macroscopic properties distinguishing them from conventional materials when exposed to extreme environments.

Since temperature is the most general and significant environmental factor, we compare the temperature dependence of

mechanical, electrical, and thermal properties between nanocarbon materials and conventional materials using examples to highlight the differing properties of macroscopic-scale nanocarbon materials in extreme environments.

Temperature Dependence of Mechanical Properties of Nanocarbon Materials: For the mechanical behavior of materials, the stiffness (represented by storage modulus) and energy dissipation ability (represented by damping ratio) are mutually exclusive in conventional materials. This mutual exclusivity stems from the origins of these two properties. Storage modulus arises from the bonding strength in materials, while the damping ratio relies on the mobility of the microstructures of materials (e.g., internal friction of molecular chains of polymers).

As seen in Figure 2a, the storage modulus of ceramics, metals, polymers, and carbon–carbon (C/C) composites spans the range from 7×10^4 to $5 \times 10^5\text{ MPa}$ (green area),^[32b] 1.3×10^4 to $2 \times 10^5\text{ MPa}$ (gray area),^[32] 2.15×10^3 to $5.92 \times 10^3\text{ MPa}$ (yellow area),^[39] and 0.3×10^3 to $5 \times 10^3\text{ MPa}$ (blue area),^[16,32,34a] respectively. The decrease in the storage modulus is attributed to the decrease of their bonding strength, giving rise to the increasing trend of the damping ratio from $\approx 1 \times 10^{-5}$ to $\approx 5 \times 10^{-5}$ for ceramics, $\approx 1 \times 10^{-4}$ to 4×10^{-3} for metals, $\approx 6.7 \times 10^{-3}$ to 6×10^{-2} for C/C composites, and 8×10^{-4} to 0.11 for polymers. For conventional materials, this is a necessary trade-off.

In contrast to such materials, nanocarbon materials exhibit distinct trends of mechanical behaviors (red area in Figure 2a) that their storage moduli range from 3×10^{-3} to $1.51 \times 10^5\text{ MPa}$, spanning eight orders of magnitude without a trade-off in the damping ratio (2.7×10^{-2} to 0.42).^[7b,35a,c-f,36,37,42] This is because the stiffness and energy dissipation ability of nanocarbon materials originate from the same mechanism; that is, the amount of vdW interactions between individual nanocarbon components, which not only provides structural strength, but also the mobility of individual nanocarbon components.^[35d] In addition, nanocarbon materials can also be combined in a composite with other materials to effectively increase the stiffness and energy dissipation. An ultrahigh value of storage modulus of $3.5 \times 10^5\text{ MPa}$ has been reported for CNT/polymer (bis-maleimide) composites^[38d] and a high damping ratio of 0.54 for CNT-reinforced natural rubber.^[38g]

The origin of mechanical strength and energy dissipation ability has afforded nanocarbon materials the unique mechanical stability across wide temperature ranges. We plotted the normalized damping ratio (i.e., the ratio of the damping ratio at extreme temperatures to the corresponding value at 293 K) versus operating temperature limitation of nanocarbon materials comparing with polymers, plastic alloys, and porous ceramic structures (Figure 2b). The operating temperature window for nanocarbon materials was found to be exceptionally wide, extending as low as 77 K^[37d] and as high as 1273 K^[7b,35d] with the normalized damping ratio close to 1. This indicates that the nanocarbon materials exhibit temperature invariant energy dissipation ability at least across 77–1273 K.^[7b,35b-d,36,37,42] In addition to energy dissipation, other representative performances can be referred with temperature-invariant viscoelasticity across 77–1273 K,^[7b] temperature-invariant compressive across 4–1273 K,^[7a] temperature-invariant superelasticity across 173–773 K,^[37c,e] etc. For comparison, the operating temperature limitations of polymers, plastic alloys, and porous ceramics are 139–473 K with the normalized damping ratio of 0.35–4.2,^[16,34b,41,43] 298–550 K with the normalized damping ratio of 4.63–22,^[40] 173–1573 K with the normalized damping ratio of 0.6–1.86,^[15b,31] respectively, which are much sensitive to the temperature variation.

Temperature Dependence of Electrical Properties of Nanocarbon Materials: The important indices to characterize electrical performances of materials are electrical conductivity and ampacity. The realization of high electrical conductivity requires a large number of free electrons in materials, while ampacity represents the current-carrying capacity of materials which relies on strong bonds to resist the current-induced atomic displacement (i.e., electromigration).^[46a,b] As seen in Figure 3a, the electrical conductivity of metals (i.e., Fe, Pt, Al, Cu, etc.) spans the region of $\approx 8.64 \times 10^6$ to $\approx 6.2 \times 10^7$ S m⁻¹ due to their large number of free electrons. However, due to the limitation of strong bonds, the ampacities of metals are limited within only $\approx 5.59 \times 10^4$ to $\approx 2.16 \times 10^6$ A cm⁻² (gray area).^[44]

Individual nanocarbon components possess reasonably high electrical conductivity as exemplified by SWCNTs and graphene nanoribbons with electrical conductivities of 10^8 and 10^6 S m⁻¹, respectively (purple dots).^[27,45c] However, the electrical

conductivities of double-walled CNT (DWCNT) fibers, CNT buckypapers, and CNT films have only been reported to be 10^4 – 10^6 S m⁻¹ because of imperfections in packing and high contact resistance between individual nanocarbon components.^[45a,b,48d,50] The electrical conductivities of neat nanocarbon materials have been shown to be improved to above 10^6 S m⁻¹ through doping or annealing, which increases the number of carriers and reduces defects in materials.^[45f,g,48c] Combined with the lightweight characteristics, the specific electrical conductivities of neat nanocarbon materials range from 0.5 to 19.6 kS m² kg⁻¹, which are comparable to that of metals.^[45g,48c,51] Different from the close linkage between ampacity and bonding strength of metals, the ampacity of neat nanocarbon materials benefits from both their heat dissipation ability and C=C bonds. The ampacity is 10^5 A cm⁻² for DWCNT fibers and 2.3×10^6 A cm⁻² for graphene fibers, which shows similar range as metals.^[45b,d]

Nanocarbon-based composites have been reported to take advantage of the properties of both the matrix material and nanocarbon materials. Subramaniam et al. prepared composites of Cu and aligned CNTs, demonstrating simultaneous improvement of electrical conductivity (4.7×10^7 S m⁻¹) and ampacity (6×10^8 A cm⁻²).^[46a] Furthermore, a number of nanocarbon-based metal composites including CNT–Ni–Cu and graphene–Cu have been shown to improve the electrical conductivity and ampacity to the range of 1.2×10^7 to 5.1×10^7 S m⁻¹ and 1.5×10^5 to 6×10^8 A cm⁻², respectively.^[46b-f]

Figure 3b plots the operating temperature limitation versus normalized electrical conductivity (i.e., the ratio of the electrical conductivity at highest/lowest operating temperature to that at 293 K). The operating limitation temperature of metals, represented by tungsten, reaches 2500 K; however, the normalized electrical conductivity is only 0.07, indicating that significant degradation of electrical conductivities of metals occurs at high temperatures.^[47e] By contrast, neat nanocarbon materials, including MWCNT bulk materials,^[48a] MWCNT sheets and MWCNT yarns,^[48b] have showed normalized electrical conductivities ranging from 3.1 to 4.4 across 973–1800 K. This illustrates the relatively weak temperature dependence. The lowest operating temperature has been demonstrated as low as 4–77 K.^[48c,d] MWCNT buckypapers,^[48d] annealed CNT fibers, and iodine-doped CNT fibers^[48c] have shown normalized electrical

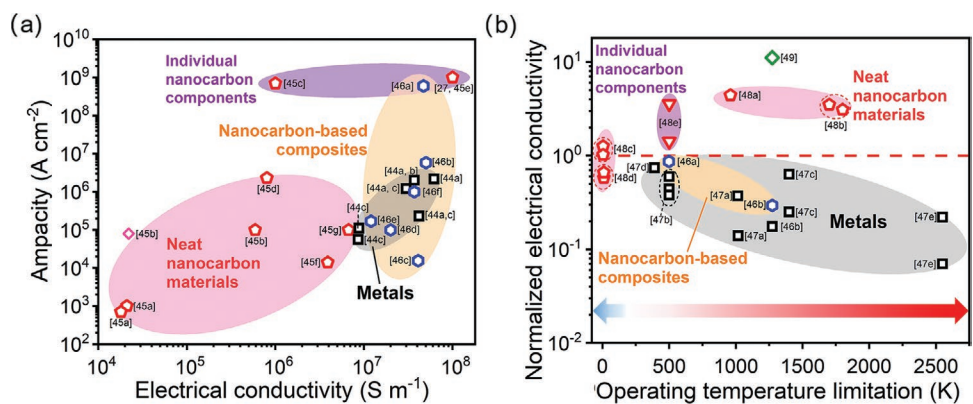


Figure 3. Electrical properties of ceramics, metals, polymer materials, and nanocarbon materials. a) Ashby map of electrical conductivity versus ampacity of metals,^[44] nanocarbon materials,^[27,45] and their composites.^[46] b) Ashby map of operating temperature limitation versus normalized electrical conductivity of metals,^[46a,b,47] nanocarbon materials,^[48] and their composites.^[46a,b,49]

conductivities of 0.4–1.26. Indeed, there is no unified and clear rule explaining the electrical performance of nanocarbon materials at low temperatures. As been reported in the literature, the electrical conductivities of CNTs were found to increase first and then decrease across 4–300 K due to the quasi-1D characteristic with the uncertain turning points appearing between 35 and 250 K, which was affected by CNT orientation, chirality, etc.^[52]

Furthermore, the addition of nanocarbon materials into metals can mitigate the decrease of electrical conductivity of metals at high temperatures. The normalized electrical conductivity of CNT/Cu and graphene/Cu composites is 0.86 and 0.29 at 500 and 1273 K, respectively, while that of pure Cu is 0.5 at 500 K and 0.175 at 1273 K, which is ascribed to the reduction in the electromigration of metal atoms through the addition of nanocarbon components.^[46a,b] A special case is the CNT adhesive–Cu foil reported by Xu et al., which showed the normalized electrical conductivity of 11.1 at 1300 K. The significantly increased electrical conductivity was attributed to the adhesion enhancement between CNTs and Cu foils.^[49]

In summary, the electrical conductivities of nanocarbon-based materials are shown to be affected by many structural factors including purity, porosity (packing), concentration, and alignment of nanocarbon components. Compared to metals, neat nanocarbon materials possess relatively stable electrical conductivity at extreme temperatures, while increased electrical conductivity at high temperatures can be attained based on the structural considerations.

Temperature Dependence of Thermal Properties of Nanocarbon Materials: Thermal properties, here, are mainly represented by thermal conductivity and thermal distortion parameter (TDP). Thermal conductivity is defined by the amount of heat per unit time per unit area that can be transferred through a plate of unit thickness of a given material (*x*-axis in Figure 4a). TDP is a mechanical characteristic representing the level of distortion of a material while being subjected to a certain amount of heat (*y*-axis in Figure 4a). The closer the absolute value of TDP to 0, the higher the ability of the material to resist thermal distortion. Since stiffer bonds tend to lead to a higher thermal conductivity, there is an increasing trend of thermal conductivity found with material species that polymers, metals, ceramics cover the

region of 0.08–0.44 W m⁻¹ K⁻¹ (blue area),^[32b] 10–429 W m⁻¹ K⁻¹ (gray area),^[25c,53] 4–223 W m⁻¹ K⁻¹ (green area),^[25c,32b] respectively. In addition, the stiffer bonds give rise to the enhanced resistance to thermal distortion so that the absolute values of TDP of metals (0.03–1.33 ppm m W⁻¹) and ceramics (\approx 0.01–4 ppm m W⁻¹) are much lower than that of polymers (300–3214 ppm m W⁻¹).

Due to the shortening of the bond length of in-plane sp² hybridized carbon atoms and stiff C=C bonds, the majority of carbon allotropes including CNTs possesses low or negative thermal expansion.^[61] Benefiting from this feature, neat nanocarbon materials have showed relatively small TDP values of -7.1×10^{-4} to -6.3×10^{-3} ppm m W⁻¹ (red area in Figure 4a).^[54a-d] This means that the thermal expansion/contraction occurred to neat nanocarbon materials upon the exposure to heat is \approx 1/2000 to \approx 1/10 of that of metals and ceramics. This highlights the excellent resistance of nanocarbon materials to thermal distortion. Although not being plotted in Figure 4a due to the lack of TDP data, there has been a significant amount of research reporting the superior thermal conductivities of neat nanocarbon materials as exemplified by nonaligned SWCNT film (30 W m⁻¹ K⁻¹), aligned SWCNT film (215 W m⁻¹ K⁻¹),^[59a] highly orientated graphene fibers (1290 W m⁻¹ K⁻¹),^[62] graphene papers (1434 W m⁻¹ K⁻¹),^[63] and graphene film (1870 W m⁻¹ K⁻¹).^[59b] It is worth noting that the orientation of nanocarbon components can significantly enhance thermal conductivity of neat nanocarbon materials by suppressing the phonon-boundary scattering.

In addition, nanocarbon materials can also be mixed with polymers to improve thermal conductivity and with metals to reduce their thermal distortion. Subramaniam et al. fabricated CNT/Cu composites using aligned CNT sheets to acquire continuous interfaces to promote heat conductivity and reported a combination of high thermal conductivity of 395 W m⁻¹ K⁻¹, which was close to Cu (400 W m⁻¹ K⁻¹) and low TDP of 1.26×10^{-3} ppm m W⁻¹.^[25c] Chen et al. further fabricated through-silicon-via interposers based on CNT–Cu composites and demonstrated Cu-level electrical conductivity (2.5×10^7 S m⁻¹) and Si-level coefficient of thermal expansion (7 ppm K⁻¹).^[64] Tseng et al. mixed polyimide (PI) with randomly dispersed graphene oxide (GO) nanosheets (20 wt%) and reported a TDP of

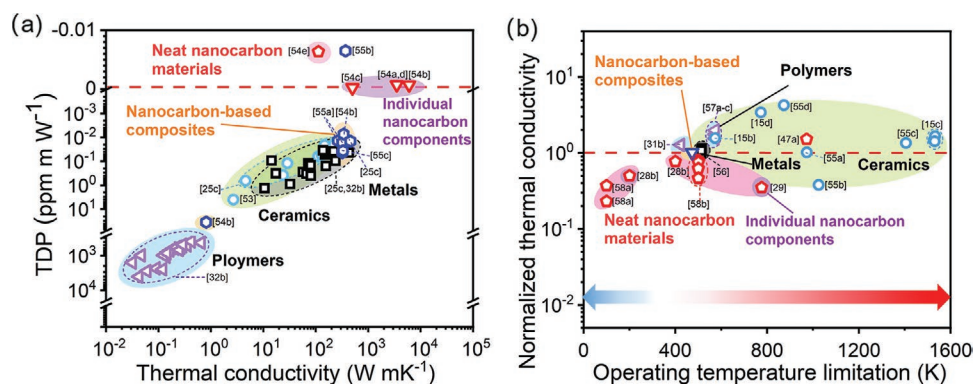


Figure 4. Thermal properties of ceramics, metals, polymer materials, and nanocarbon materials. a) Ashby map of thermal conductivity versus TDP of ceramics,^[25c,53] metals,^[25c,32b] polymer materials,^[32b] nanocarbon materials,^[54] and their composites.^[25c,54b,55] b) Ashby map of operating temperature limitation versus normalized thermal conductivity of ceramics,^[15b-d,31b,56] metals,^[25c,57] polymer materials,^[38b,58] nanocarbon materials,^[28b,29,48a,59] and their composites.^[60]

35 ppm m W⁻¹, only 1/10 of raw polymers, with a thermal conductivity of 0.81 W m⁻¹ K⁻¹.^[55b] It was interpreted that the low-dimensional and rigid GO nanosheets were able to enhance chain orientation of PI, thereby suppressing the thermal expansion of the PI matrix.

While porous polymers and ceramics are developed to serve as thermal insulators at the temperature ranges of 373–573^[38f,58] and 573–1780 K,^[15b-d,31b,56] respectively, nanocarbon materials have been mainly studied for heat dissipation with the highest operating temperature up to 958 K by utilizing their superior thermal conductivity (Figure 4b).^[48a] The normalized thermal conductivity (i.e., the ratio of thermal conductivity at extreme temperatures to the corresponding value at 293 K) of nanocarbon materials is 0.23–0.5 across 100–200 K^[28b,59a] and 0.35–1.51 across 400–958 K,^[28b,29,48a,59b] showing the different temperature dependence of nanocarbon materials as exemplified by SWCNT film,^[59a] individual SWCNT,^[29] individual MWCNT,^[28b] graphene film,^[59b] and MWCNT bulk.^[48a] The different trend can be interpreted by the increase of phonon-scattering across 100–958 K.^[28b,29,48a,59]

Similar with electrical conductivity, the thermal conductivity of nanocarbon materials is also a synergetic performance of structural factors, including chirality, defects, and orientation of nanocarbon components.^[28b,29,48a,59] Notably, with the combination of thermal conductivity at high temperatures and ultra-strong thermal distortion resistance (i.e., low TDP), nanocarbon materials have particular advantage as thermal management components in electronic devices, providing efficient cooling with minimal thermal expansion.^[63,65]

Feature Properties of Nanocarbon Materials against High Pressure, Corrosion, and Radiation: In addition to excellent performances at extreme temperatures, the unique atomic structure and low-dimensional characteristics have offered nanocarbon materials series of feature properties against high pressure, corrosion, and radiation, where nanocarbon materials commonly require to be combined with metals, ceramics, or polymer materials to make nanocarbon-based composites.

Benefiting from the high specific surface areas of nanocarbon components, nanocarbon-based composites possess abundant of nanoscale interfaces compared to the composites using Nanofiller,^[66] Kevlar,^[67] carbon fiber,^[68] carbon, and graphite^[69] as fillers.^[70] When subjected to high pressures, the interfacial sliding can provide efficient energy absorption and load transfer to release stress concentration. Many studies used nanocarbon materials as the dispersion or preform to develop the nanocarbon-based composites, such as MWCNT/epoxy,^[70a,b] GO/CNT/water polyurethane,^[70c,e] MWCNT/carbon-fiber-reinforced thermoplastic (CFRTP),^[68d,e] CNT/Kevlar,^[70f] etc., to optimize the impact resistance of composites. For example, a composite of MWCNTs and CFRTP can lead to a 24% increase in impact resistance from 191 to 231 kJ m⁻², as determined by a pendulum energy of 15 J.^[68d]

The feature of nanoscale interfaces can be also used to minimize the influence of radiation by trapping the defects generated by radiation. When nanocarbon materials combine with metals, such as graphene/tungsten film,^[71] CNT/Al,^[72] CNT/iron nanocrystals (Fe NCs),^[73] CNT/MgO,^[74] etc., the defects generated by radiation can be rehealed at interfaces to avoid the embrittlement of grain boundaries of the metal compo-

nents.^[20,71–75] A representative work is the incorporation of CNTs with Fe NCs.^[73] Randomly oriented CNTs were uniformly distributed along the abundant grain boundaries of iron matrix and formed a 3D CNT network to collect the radiation atoms and defects. Meanwhile, the CNTs provided rapid transport highways for the electrons and phonons to carry heat. This Fe–CNT composite could tolerate the irradiation from 150 keV He⁺ ions with a fluence of 5×10^{17} ions cm⁻² at 673 K and maintain the hardness, while the control sample exhibited cracking under the same radiation condition.

With the combination of chemical inertness and nanoscale feature, nanocarbon materials can play two roles in the composites, including “barrier” and “shielding.” The barrier effect is mainly due to the dense lattice structure and chemical inertness of graphene. As for shielding effects, nanocarbon components can fill the nanosized pores formed during the curing of the polymer coating for corrosion resistance, enhancing the inhibition of the diffusion of corrosive medium.^[76] For example, N-doped carbon quantum dot@graphene (N-CQD@Gr) was added to water-based epoxy (WEP) and coated on the metal surface.^[76f] The barrier of graphene layer, the extension of the diffusion path of corrosion medium, and the formation of passivation layer worked together to improve the corrosion resistance of metal materials. The impedance modulus of N-CQD@Gr/WEP coating was $10^9 \Omega \text{ cm}^2$, which was about 200 times higher than that of the epoxy coating after 90 days of immersion in 3.5 wt% NaCl solution. Another representative strategy was the direct deposition of a continuous graphene film on metal surfaces to completely isolate the corrosive medium for protection, which also effectively block corrosive substances such as oxygen, water, and salt ions.^[77]

2.3. Principle of Structural Design of Nanocarbon Materials for Extreme Environments

As described in Section 2.2.2, nanocarbon materials and their composites have varieties of properties, such as temperature-invariant damping properties across a wide temperature range, superior specific conductivity, and relative thermal stability, which can be expected to utilize in various extreme environments. To meet the specific requirements based on the extreme environmental applications, structural design is vital for the nanocarbon materials, which can be mainly divided into two categories: neat nanocarbon materials (Figure 5) and nanocarbon-based composite materials (Figure 6).

2.3.1. Neat Nanocarbon Materials for Operation across Wide Temperature Ranges

Xu et al. fabricated a class of CNT networked materials composed of traversing long CNTs with a very high density of intermittent physical interactions, analogous to entangled polymer chains but with much better thermal stability.^[7b] These CNT networked materials demonstrated temperature-invariant viscoelasticity across 77–1273 K, which was hundreds of degrees wider than conventional polymer materials (Figure 5a). Meanwhile, these CNT “rubbers” exhibited the fatigue

Neat nanocarbon materials

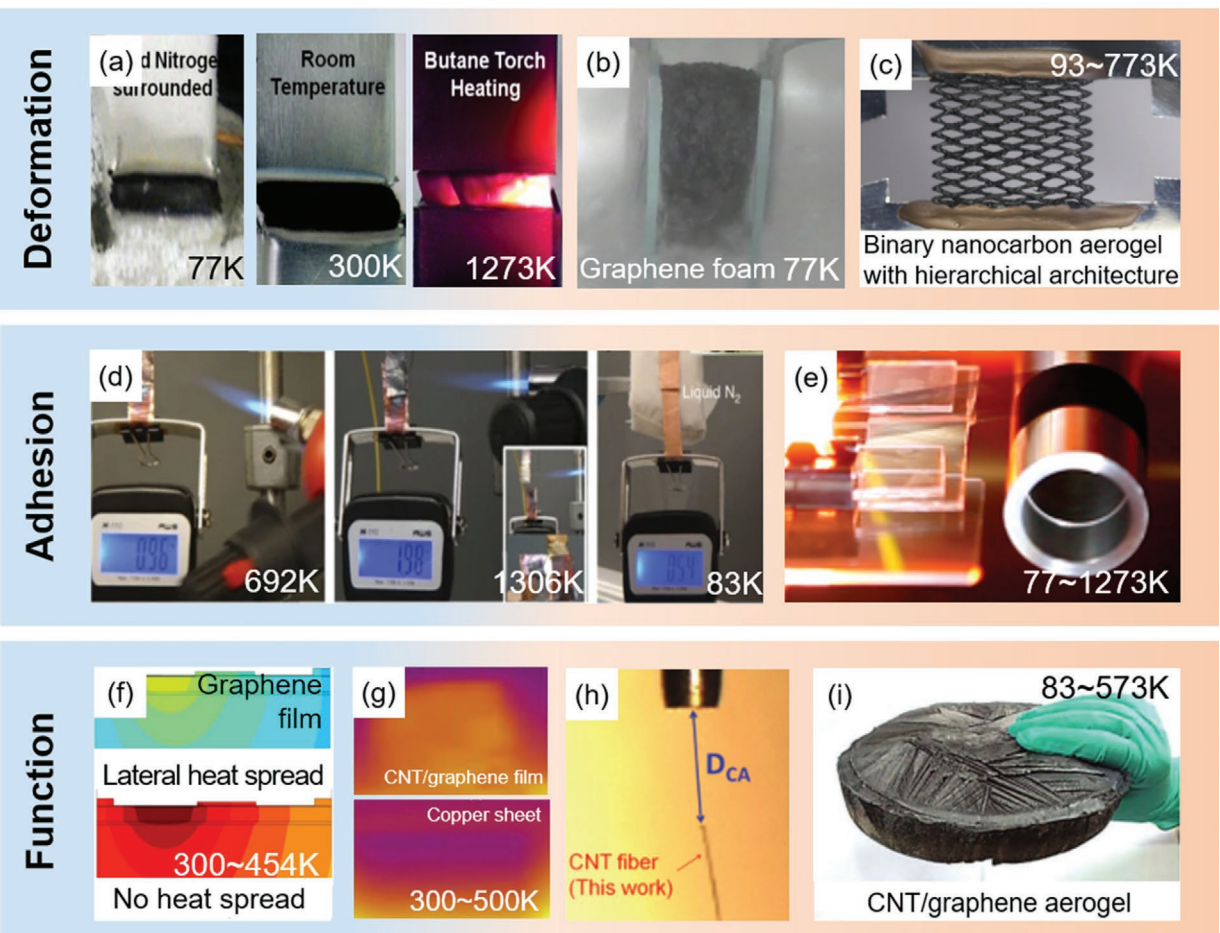


Figure 5. Structural design of neat nanocarbon materials for extreme environments. a) CNT rubbers with temperature-invariant viscoelasticity across 77–1273 K. Adapted with permission.^[7b] Copyright 2010, American Association for the Advancement of Science. b) Hyperelastic graphene foam with ≈90% reversible compressive deformation across 4–1273 K. Adapted with permission.^[36] Copyright 2015, Springer Nature. c) Binary nanocarbon aerogel with ultrahigh stretching ratio ($\approx 200\%$) across 93–773 K. Adapted under the terms of the CC-BY Creative Commons Attribution 4.0 International license (<https://creativecommons.org/licenses/by/4.0/>).^[37a] Copyright 2018, The Authors, published by Springer Nature. d) CNT array for adhesion across 83–1306 K. Adapted under the terms of the CC-BY Creative Commons Attribution 4.0 International license (<https://creativecommons.org/licenses/by/4.0/>).^[49] Copyright 2016, The Authors, published by Springer Nature. e) CNT tape with stable specific adhesion strength across 77–1273 K. Adapted with permission.^[78] Copyright 2019, American Chemical Society. f) Graphene film used as alternative heat-escaping channels across 300–454 K. Adapted with permission.^[65a] Copyright 2012, Springer Nature. g) CNT/graphene TIM with high thermal conductivity across 300–500 K. Adapted with permission.^[79] Copyright 2017, Elsevier. h) CNT fiber with high specific conductivity across 4–300 K. Adapted with permission.^[48c] Copyright 2013, American Association for the Advancement of Science. i) CNT/graphene aerogel with high structural stability across 83–573 K. Adapted with permission.^[37d] Copyright 2013, Wiley-VCH.

resistance by showing 10^6 cycles of torsional deformation across 133–873 K. In fact, it is expected that the temperature range is wider as the test temperatures were limited by the equipment. Chen and co-workers designed a hyperelastic graphene foam composed of cross-linked graphene sheets connected by covalent bonds.^[7a,36] These graphene foams exhibited ≈90% reversible compressive deformation with near-zero Poisson's ratio across 4–1273 K due to the synergistic combination of the intrinsic elastic/flexible properties of individual graphene sheets and the covalent junctions between the sheets (Figure 5b). Guo et al. fabricated a binary nanocarbon aerogel with a hierarchical architecture encompassing macroscopic trusses (the first order), Voronoi polygon cells enclosed by MWCNT-interconnected graphene laminates (the second order), folded cell walls that allowed reversible stretching (the third order), and syner-

gistic binary molecular building blocks (the fourth order).^[37a] It exhibited an ultrahigh stretching ratio ($\approx 200\%$) across 93–773 K due to the layered buckling structure and synergistic effects between CNTs and graphene (Figure 5c).

In addition to the deformable properties, neat nanocarbon materials have also demonstrated various exceptional and unique functions across wide temperature ranges. Xu et al. fabricated a unique CNT array with node top which could function as double-sided tape across a wide temperature range of 83–1306 K.^[49] Interestingly, the adhesive strength of this CNT tape increased monotonically with temperature and reached 143 N cm^{-2} at 1306 K, which was 6 times higher than that at room temperature (Figure 5d). In addition, Jin et al. prepared a CNT adhesive tape by drawing a CNT sheet from an as-grown CNT array and demonstrated a stable specific

Nanocarbon-based composite materials

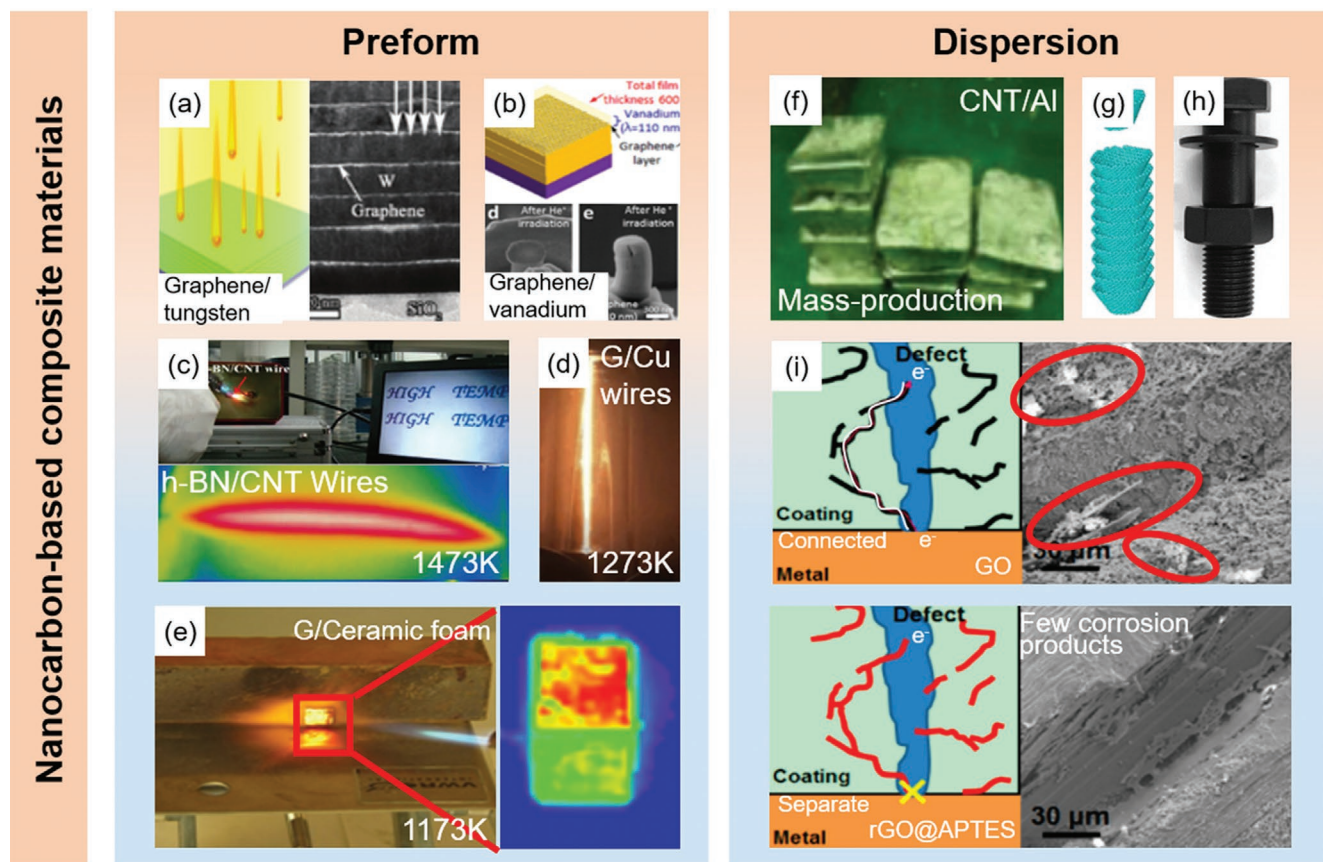


Figure 6. Structural design of nanocarbon-based composite materials for extreme environments. a) Graphene/tungsten (G/W) with high radiation resistance. Adapted with permission.^[71] Copyright 2017, Wiley-VCH. b) Graphene/vanadium (G/V) with high radiation resistance. Adapted under the terms of the CC-BY Creative Commons Attribution 4.0 International license (<https://creativecommons.org/licenses/by/4.0/>).^[75] Copyright 2016, The Authors, published by Springer Nature. c) h-BN/CNT wires with stable electrical resistance at 1473 K. Adapted with permission.^[82] Copyright 2019, Tsinghua University Press and Springer-Verlag GmbH Germany, part of Springer Nature. d) Graphene/Cu wires with high electrical conductivity at 1273 K. Adapted with permission.^[46b] Copyright 2019, Elsevier. e) Graphene/polymer-derived ceramic composite with high heat resistance up to 1173 K. Adapted with permission.^[83] Copyright 2018, Elsevier. f) CNT/Al composite with high radiation resistance. Adapted with permission.^[72] Copyright 2016, Elsevier. g) Structure of CSCNT. Adapted with permission.^[84] Copyright 2005, Elsevier. h) CSCNT/epoxy composite with high corrosion resistance used as coating of bolt. Adapted with permission.^[85] Copyright 2007, Wiley-VCH. i) rGO@APTES/PVB coatings with high corrosion resistance. Adapted with permission.^[76c] Copyright 2015, American Chemical Society.

adhesion strength of $1.1 \text{ N } \mu\text{g}^{-1}$ in the temperature range of 77–1273 K (Figure 5e).^[78] These works have showed the possibilities of CNT dry adhesives as thermal interfacial materials (TIMs) for the electronic devices required to work at high and low temperatures.

Nanocarbon materials have also been widely studied in the field of thermal management of electronic devices working in the environments up to 400 K. For example, Yan et al. and Zhang et al. used layer-structured graphene films as the heat dissipation components in transistors and chips to improve their temperature uniformity and reduce hotspots by 10–20 K, thus prolonging the service life of electronic devices (Figure 5f).^[65] Other research efforts have been devoted to developing nanocarbon-based TIMs. Not only the thermal conductivity being accounted, multifunctional TIMs have been reported. Lv et al. fabricated a superelastic TIM by using entangled CNT/graphene structured aerogel, which displayed a thermal conductivity up to $88.5 \text{ W m}^{-1} \text{ K}^{-1}$ and a thermal interface resistance as low as $13.6 \text{ mm}^2 \text{ K W}^{-1}$ at a high compres-

sion of 153 kPa.^[80] Hu et al. reported a robust TIM by using alternately stacked CNT/graphene sheets. An important process was the high-temperature annealing to remove the defects of this hybrid film and form covalent bonding between CNTs and graphene sheets, which improved the thermal conductivity to $800\text{--}1000 \text{ W m}^{-1} \text{ K}^{-1}$ across 300–500 K (Figure 5g).^[79]

Nanocarbon materials have also demonstrated stable electrical performance across a wide temperature range. For example, Behabtu et al. fabricated an iodine-doped CNT fiber with high degree of CNT alignment.^[48c] It showed the potential as a high-voltage wire by displaying a specific conductivity ($4.18 \text{ kS m}^2 \text{ kg}^{-1}$) across 4–300 K, which was higher than that of gold (Au) and close to that of Cu (Figure 5h). Xu et al. prepared a graphene aerogel fiber with interconnected pores, which could withstand a voltage of 3 V with the electrical conductivity above 2500 S m^{-1} across 50–300 K.^[81] Finally, the porous nature of neat nanocarbon materials can be considered for environmental protection. Sun et al. reported a CNT/graphene aerogel with a porosity of ≈99.9%, showing the oil absorption capacity

215–913 times of its own weight and the structural stability across 83–573 K (Figure 5i).^[37d]

2.3.2. Nanocarbon-Based Composite Materials for Extreme Environmental Applications

The nanocarbon-based composite materials can be divided into two basic types based on the fabrication method: composite fabricated from nanocarbon preforms (e.g., prepreg) and composite fabricated through solution-based processing (e.g., dispersion).

The properties of the composites fabricated based on using nanocarbon preforms rely on the custom designed and fabricated preform structures. For example, by tuning the alignment/orientation of nanocarbon materials in preforms, the anisotropy of composites can be independently controlled. Si et al. and Kim et al. designed a high-strength, radiation-resistant composite by intercalating the sheet-stacked graphene into metals.^[71,75] Benefiting from the high orientation of graphene, the composite showed excellent radiation tolerance of He ions with dosage of 13.5 displacements per atom (DPA) and 6.4 DPA, respectively (Figure 6a,b). Yang et al. prepared high-temperature wires by using CNT yarns as the preforms and epitaxially growing h-boron nitride (h-BN) as an insulating protective layer.^[82] The electrical resistance of the composite wire was maintained at 75–80 Ω when heated to 1473 K for 1200 s (Figure 6c). In addition, Zhao et al. designed an axially conductive wire composing the massive, strongly bonded, and super-helically arranged fine Cu fibers and interfacial graphene layers, showing electrical conductivity higher than pure Cu wire across 273–1273 K (Figure 6d).^[46b] Román-Manso et al. prepared a graphene/polymer-derived ceramic composite.^[83] The 3D-network-structured graphene preform was used to improve the heat resistance of the composite up to 1173 K by promoting the uniformity of temperature distribution in all directions (Figure 6e).

In contrast to preform-based composites, the properties of the composites fabricated from nanocarbon dispersion greatly rely on the content of nanocarbon fillers and the uniformity of dispersion, which are commonly used for applications requiring isotropic enhancement. So et al. mass-produced MWCNT/Al composites at 100 kg scale and verified that the uniformity of CNT dispersion contributed to the optimization of interfacial surface areas with the metal matrix, which inhibited the generation of pores in the matrix.^[72] There were no pores generated at 3.6 DPA by 100 keV He-ion irradiation with only a 1% volume content of MWCNTs (Figure 6f). Walker et al. fabricated graphene/Si₃N₄ composite, which could operate at temperature as high as 1923 K in air.^[86] The results also showed that the fracture toughness of the composite improved proportionately with the content of graphene and finally increased by 235% with 1.5 vol% graphene compared to raw materials (Si₃N₄) due to the expansion of the internal crack in multiple directions along graphene and the reduction of the stress concentration in the ceramic matrix. Taken together, although the content of nanocarbon materials is typically small, the presence of the nanocarbon plays a vital role in the functional characteristics of composites, especially in the improvement of the toughness of ceramics at high temperatures and the radiation resistance of metals.

Another form of nanocarbon composites is nanocarbon-based polymeric pastes for corrosion resistance which has also attracted huge attention. Hayashi et al. effectively improved the corrosion resistance of the epoxy matrix by 15 times through the addition of cup-stacked carbon nanotubes (CSCNTs), which not only inhibited the migration of ions in the corrosion solution to the matrix, but also reduced the internal defects of polymer coatings (Figure 6g,h).^[84,85] However, the addition of nanocarbon materials may also promote corrosion due to the formation of conductive network. Therefore, the content of the nanocarbon fillers needs to be precisely controlled. To inhibit the corrosion-promotion activity of nanocarbon materials, Sun et al. demonstrated a facile graphene encapsulation strategy by wrapping reduced graphene oxide (rGO) with (3-aminopropyl)-triethoxysilane (APTES) and then embedding rGO/APTES in polyvinyl butyral (PVB) coatings, which effectively enhanced the barrier properties by decreasing the corrosion rate from 0.392 to 0.006 μm year⁻¹ (Figure 6i).^[76c]

In summary, neat nanocarbon materials enable enhanced mechanical, electrical, and thermal stability across a wide temperature range. These stable properties provide interesting application prospects in extreme environments, such as aerospace, subterranean exploration, polar exploration, etc., which require high stability of structural properties. On the other hand, for applications in ocean, space, nuclear power plants, and other more complex extreme environments, such as anti-corrosion coating, antiradiation shell, high temperature cables, nanocarbon materials commonly require the combination with metals, ceramics, or polymer materials to improve density, air impermeability, and mechanical toughness at high temperatures with oxidation resistance.

3. Synthesis and Preparation of Nanocarbon-Based Materials for Extreme Environment Applications

It can be seen from Section 2 that the realization of functional characteristics of nanocarbon materials used in extreme environments depends greatly on its structure and assembly, while the realization of its structure and assembly depends on its synthesis and preparation.

3.1. Chemical Vapor Deposition (CVD) Growth Technologies

Currently, various neat nanocarbon materials such as CNT films,^[91] graphene films,^[92] CNT arrays,^[93] CNT forests,^[7b,35d,94] 3D CNT, and graphene structures^[95] for the extreme environments are synthetically prepared by CVD. The CVD process includes the main steps as followings. First, the carbon feedstock (e.g., methane (CH₄),^[91,95a] ethylene,^[7b,35d] acetylene,^[92a,93b,c] and alcohols^[95a,96]) decomposes to form carbon atoms due to the presence of heat or plasma, and dissolves into the catalyst nanoparticles. Then, these carbon atoms form nanocarbon materials depending on the shape and size of catalysts.

Catalysts play a critical role in affecting the morphology and quality of CNTs and graphene prepared via CVD. For the growth of CNTs, carbon feedstock is decomposed upon the

catalyst to release carbon and hydrogen. Carbon then precipitates from the catalyst nanoparticles as reaching the saturation state, forming tubular carbon.^[97] Fe, Ni, and Co are often popular choices as the catalysts for CNTs, since carbon atoms have high solubility and high diffusion rate in these metals.^[98] For the growth of graphene, the quality of the growth is dependent on the ability of the transition metal to improve dehydrogenation of hydrocarbon and carbon isolation. Cu and Ni are the popular choices as catalysts for graphene, yet they have fundamentally different mechanisms for growing graphenes. The low solubility of carbon (<0.001 at%) in Cu leads to a direct deposition and growth process of graphene, that is, the graphene is formed outward from the surface of Cu. Nickel has high carbon solubility (>0.1 at%), and the growth of graphene includes the processes of dissolution and pre-

cipitation, that is, indirect growth mode.^[99] Depending on the catalytic activity of metals, the growth temperatures are varied from 1073 to 1473 K for graphenes and from 873 to 1073 K for CNTs.^[100]

Through controlling the density and type of the catalysts with synthetic parameters, such as gas flow, carbon feedstock, temperature, etc., during the growth process, the structures of the individual nanocarbon components, including the wall number of CNTs (single-wall, double-wall, and multiwall), chirality (metallic and semiconducting), the layer number of graphene (single-layer, double-layer, and multilayer), layer size (nanometer–centimeter level), etc., and the structural properties of macroscopic aggregates, including density, height, and alignment, etc., can be precisely controlled (Figure 7a,b).

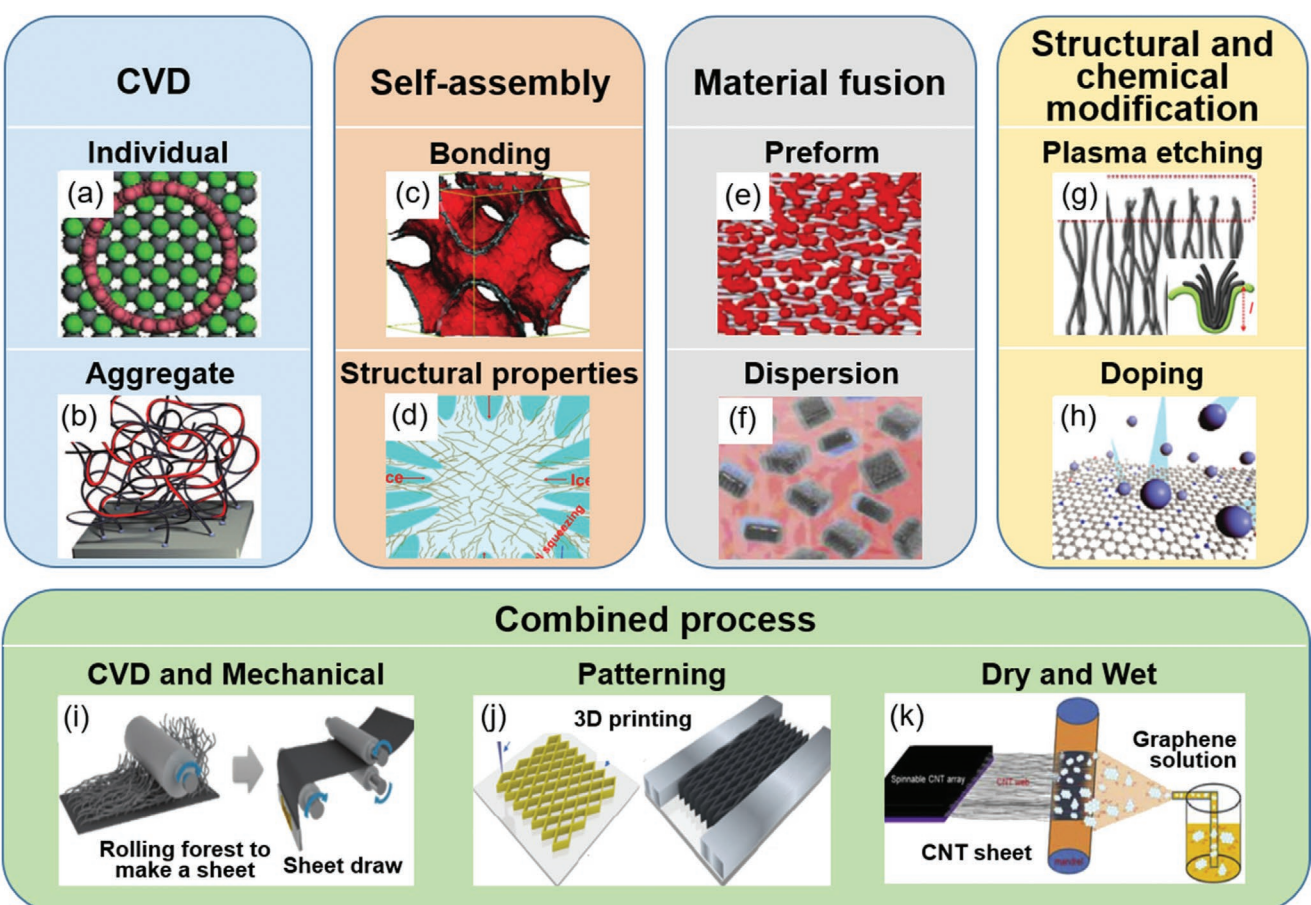


Figure 7. Five general preparation methods of nanocarbon-based materials. a,b) CVD can be used to control the structures of individual components and macroscopic aggregates. a) Individual material components; b) macroscopic aggregates. a) Adapted with permission.^[87] Copyright 2017, Springer Nature. b) Adapted with permission.^[7b] Copyright 2010, American Association for the Advancement of Science. c,d) Self-assembly can be used to control the interaction between the individual components and the structural properties of macroscopic aggregates. c) Bonding; d) structural properties of macroscopic aggregates. c) Adapted with permission.^[36] Copyright 2015, Springer Nature. d) Adapted with permission.^[42] Copyright 2016, Wiley-VCH. e,f) Material fusion: nanocarbon materials can be used as preform with orientation or dispersion. e) Preform; f) dispersion. e) Adapted with permission.^[46a] Copyright 2013, The Authors, published by Springer Nature. f) Adapted with permission.^[88] Copyright 2020, Elsevier. g,h) Structural and chemical modification of nanocarbon materials can be achieved by plasma etching or doping. g) Plasma etching; h) doping. g) Adapted under the terms of the CC-BY Creative Commons Attribution 4.0 International license (<https://creativecommons.org/licenses/by/4.0/>).^[49] Copyright 2016, The Authors, published by Springer Nature. h) Adapted with permission.^[89] Copyright 2011, American Chemical Society. i–k) Combined process can be used to realize the functional diversification of nanocarbon materials. i) CVD and mechanical; j) patterning; k) dry and wet. i) Adapted with permission.^[90] Copyright 2020, Wiley-VCH. j) Adapted under the terms of the CC-BY Creative Commons Attribution 4.0 International license (<https://creativecommons.org/licenses/by/4.0/>).^[37a] Copyright 2018, The Authors, published by Springer Nature. k) Adapted with permission.^[79] Copyright 2017, Elsevier.

3.1.1. Control of Individual Nanocarbon Components

The controllable preparation of the density,^[101] chirality,^[87] and wall number^[91b] of individual nanocarbon components are mainly achieved through the design of catalysts. For example, the chirality control of SWCNTs is usually achieved through the design of solid catalysts, which can maintain their crystalline structure at high temperatures. Zhang et al. used the uniform Mo₂C (001) plane with near sixfold symmetry as the catalyst, which matched the sixfold symmetry of (12, 6) SWCNTs, to synthesize SWCNTs with the abundance of (12, 6) nanotubes estimated to be greater than 90%.^[87]

Furthermore, to fabricate electronic devices that can be used at extreme temperatures, the length scales and wall/layer number of the prepared individual nanocarbon components need to be precisely controlled. Pei et al. prepared a horizontal SWCNT film by using a Cu catalyst with a lower catalytic activity and a relatively high total flow of CH₄/H₂ mixture gas (800/700 sccm) to achieve the precise control of wall number in a horizontal growth direction, which can be a candidate for the channel material of conventional Si-based transistors used at extreme temperatures (4.3–573 K).^[91b] Taking advantage of the low solubility of carbon in Cu, Li et al. synthesized centimeter-scale, large-area, single-layer graphene using a Cu substrate by CVD.^[92d] Its tolerance to 1800 K in vacuum made it a candidate to replace conventional thermionic cathodes and the channel material of conventional Si-based transistors.^[92a,b]

3.1.2. Control of Aggregates

CVD can also be used to precisely prepare the structural properties of macroscopic aggregates, such as mass density, height, porosity, tortuosity, etc., to conform to different extreme environmental applications. For example, to prepare materials that can maintain stable viscoelasticity over a wide temperature range, Xu et al. controlled the wall number (double-wall), tube diameter (3–5.5 nm), and density (3.3–44 mg cm⁻³) of CNTs by regulating the catalyst areal density (10¹⁰ to 5 × 10¹¹ catalyst cm⁻²) based on the CVD growth parameters (ethylene concentration of 7.5%, ethylene:water = 1000:1) used for aligned CNT forests.^[7b,35d,94] These flexible double-wall CNTs can act as polymer chains to create a 3D, randomly oriented CNT network, which tolerate a wide temperature range (77–1273 K).

To prepare 3D foam structures for use in extreme environments, Zhao et al. used polydimethylsiloxane as a template, 1,2-dichlorobenzene as carbon feedstock, and ferrocene as catalyst to prepare a 3D CNT sponge by CVD.^[95b] The structure was randomly interwoven with MWCNTs (diameter ≈ 70 nm) providing high porosity, compressibility, and mechanical recoverability, which could be used as a sensor in seawater (see details in Section 4.3). Based on a SiO₂ nanowire foam template, Song et al. prepared a hybrid foam for EMI shielding through a two-step CVD method without the use of metal catalysts.^[95a] A macroscopic CNT foam was first prepared using a template-directed CVD, and then multilayered graphene edge planes were in situ grown on the CNT foam with seamless junctions by plasma-enhanced CVD.

3.2. Selective Self-Assembly

Selective self-assembly is a technique in which individual components spontaneously form specific structures under the action of internal driving forces. This process can be used to prepare a variety of neat nanocarbon materials for extreme environment applications, such as fibers,^[48c] films,^[102] foams,^[7a,36] aerogels,^[37c–e,80,103] sponges,^[104] and other pseudo-1D, -2D, and -3D structural materials.^[81,105]

There are two critical factors for preparing these structures through self-assembly: 1) level of exfoliation of the nanocarbon dispersion and 2) strong interactions between the nanocarbon components, which leads to the assembly into the overlapped framework and retain the formed structure during and after removal of the liquid phase.^[6c] Through the controlling of the types, sizes, concentrations of individual nanocarbon components and internal drives, bonding of individual components (e.g., vdW interaction and covalent bonds) and structural properties of macroscopic aggregates (including density, porosity, Poisson's ratio, orientation, etc.) can be controlled (Figure 7c,d).

3.2.1. Bonding

To obtain superelasticity over a wide temperature range, the bondings including vdW interaction and covalent bonds of 3D nanocarbon aggregates are tailored through tuning the method of linkage.^[7a,36,37c–e,80,103] For example, Zhao et al. used GO sheets as the individual components and ethanol as the dispersant to achieve a superelastic GO foam with covalent connections (C—O, C=O, and C(=O)O) between sheets through hydrothermal self-assembly.^[7a] After annealing, the GO foam could maintain high mechanical resilience across 4–1273 K.

In addition to the introduction of covalent bonds, the foams with the enhanced vdW interaction by coating graphene on CNT contacts have also been reported for superelasticity across 83–773 K.^[37c–e,80,103] The representative results were reported by Lv et al. who prepared a class of entangled graphene/CNT aerogels (23–85 mg cm⁻³) by using a mixed dispersion of GO sheets and CNTs (diameter of 30–50 nm, length of 50–100 μm) with the concentration of 2–5 mg mL⁻¹,^[80] and Gao and co-workers who prepared a highly porous graphene/CNT aerogel (porosity of ≈99.9%) by using a mixed dispersion of giant GO sheets (average lateral size of 18.5 μm, thickness of GO of ≈0.8 nm^[106]) and CNTs with the concentration of 1.0 mg mL⁻¹.^[37d]

3.2.2. Structural Properties of Macroscopic Aggregates

While the size of individual components and the concentration of dispersion are tuned, structural properties of macroscopic aggregates (e.g., orientation,^[42,81,105] porosity,^[37d,42] and density^[36,80]) can be precisely controlled, generating series of unique properties for extreme environments.

For example, by controlling the concentration of the GO dispersion (0.20–5.00 mg mL⁻¹) and individual size of the GO flakes (≈20–50 μm in lateral dimension), zero-Poisson's ratio structures with different densities (0.3–14 mg cm⁻³) in a wide temperature range (223–573 K) were obtained.^[36] By using liquid

nitrogen as the coagulation bath followed by freeze-drying, a graphene aerogel fiber composing lamellar, concentrated GO liquid crystalline (LC) gels was constructed, exhibiting electrical conductivity of 2.6×10^3 to 4.9×10^3 S m $^{-1}$ across 50–300 K.^[81] Using the orientated growth through freeze-casting, graphene elastomers with anisotropic microstructures in two directions (i.e., hyperbolic patterns in the longitudinal and spoke-like network in the transverse) were formed, which displayed viscoelasticity across 173–673 K.^[42] The structural optimization of individual components including monolayer (1.2 nm) and GO size (area greater than 2000 μm^2) and the structural tuning of aggregates including porosity (59.65–99.65%) and macroscopic aspect ratio (L/D of 0.5–1.5) were all essential for the extreme-temperature viscoelastic performance.

3.3. Material Fusion

As addressed in Section 2.3, integration of CNTs or graphene into various matrices, such as metals, ceramics, and polymers, to form advanced composites used in extreme environment is one of the most promising and scalable routes for taking full advantage of their unique structures and properties.^[107] Incorporation of nanocarbon components with matrix materials mainly includes two types: fusion with nanocarbon preforms which can be a variety of structures such as fibers,^[46d,82] films,^[71,75] arrays,^[25c,46a,108] and fusion with nanocarbon dispersion^[72,76a–c,109] with the volume fraction of nanocarbon components being precisely tuned (Figure 7e,f).

3.3.1. Fusion with Nanocarbon Preforms

To construct composites with exceptional electrical and thermal transport for extreme environments, aligned arrays and fibers are preferred to be used as the preforms,^[25c,46a,d,82,108] while metal or ceramic materials are chosen to be the matrix materials being achieved by electrodeposition or CVD.

For example, Zou et al. reported a CNT/Ni/Cu composite fiber based on the continuous electrodeposition of a several-micrometer-thick Cu layer around a CNT fiber with a Ni nanobuffer layer of 0.5 wt% in between, which had a relatively stable electrical performance across 573–873 K by showing a lower temperature coefficient of resistivity of 1.14×10^{-3} K $^{-1}$ compared to 4.12×10^{-3} K $^{-1}$ of Cu.^[46d] Subramaniam et al. used vertically aligned CNT arrays (VACNTs) as preforms and adopted a two-stage electrodeposition approach to fabricate a homogeneous CNT/Cu composite film (45 vol% of CNTs). This composite exhibited a high thermal conductivity of 800 W m $^{-1}$ K $^{-1}$ and a 100 times higher ampacity (6×10^8 A cm $^{-2}$) accompanied by exceptional TDP (of 1.26×10^{-3} ppm m W $^{-1}$).^[25c,46a]

The operating temperature range can be further broadened by combining nanocarbon materials with ceramics. Zou et al. developed a CVD method to infiltrate Si into CNT arrays for this purpose.^[108] The CVD method allowed the simultaneous growth of ceramics throughout the surface of VACNTs, resulting in the improvement in the density and uniform distribution of VACNT/ceramic composites. The as-fabricated composite exhibited thermal stability up to 1673 K and high elec-

trical conductivity of 8.95 S m $^{-1}$ at 823 K. Yang et al. prepared a high-temperature coaxial h-BN/CNT wires by CVD epitaxial growth of h-BN on CNT yarn spun from a superaligned CNT array in a dry state, which could tolerate 1473 K in air.^[82]

3.3.2. Fusion with Nanocarbon Dispersion

To realize corrosion resistance, radiation resistance, and embrittlement resistance at low temperatures, composites with uniformly dispersed nanocarbon components have shown advanced properties compared to conventional materials. Fusion with nanocarbon dispersion follows the process of mixing a dispesion of nanocarbon components into the matrix of the desired composite compound (in solution or powder form) and then formed into the needed shape through blending (powder blending, melt blending, solution blending) or spark plasma sintering (SPS) to, respectively, prepare polymer, ceramic, and metal composites.^[72,76a–c,109]

For example, Sun et al. reported a rGO/PVB solution for an anticorrosion coating on Cu substrates.^[76a–c] The key step was the use of strong oxidants to graft functional groups (numerous hydroxyl, carboxyl, and epoxy) on GO sheets for the reaction with APTES, while APTES was used as passivation layer on GO and to promote uniform dispersion.^[76c] In addition, Wu et al. prepared graphene nanoplatelets (GNPs)/Al₂O₃ composites by colloidal process and SPS.^[109a] With the addition of only 1.0 vol% GNPs, the fracture toughness of GNPs/Al₂O₃ was increased by 20.04% at 77 K. Furthermore, So et al. reported a MWCNT (0.5 wt%)-reinforced Al composite for radiation resistance. The uniform dispersion was realized through a planetary ball-milling process, while SPS was used for the encapsulation of the dispersed CNTs and the further consolidation with Al particles to form Al–C covalent bonds.^[72,109b]

3.4. Structural and Chemical Modification

Currently, special structural design and chemical modification of nanocarbon materials for extreme environments can be achieved by techniques, such as plasma etching^[49,110] and doping^[48c,111] (Figure 7g,h).

3.4.1. Plasma Etching

Plasma etching has been commonly employed to create patterned^[110] or specifically structured^[49] nanocarbon materials for extreme environments. Driven by a strong electric field, bombardment by the plasma (e.g., a neutral collection of ions, electrons, and neutral particles) results in the destruction of low-energy chemical bonds, removal of surface impurities, and the reaction with the surface to induce etching.

For example, to obtain the bioinspired dry adhesive usable across a wide temperature range (77–1306 K), Xu et al. used well-controlled oxygen plasma etching (30 W, 1.5 min) to remove the nonaligned top of VACNTs, leading to the formation of a node structured top to realize “nano-interlock” adhesion mechanism.^[49] To obtain patterned desalination membranes that can

be used in high-pressure environments, Yang et al. used silicon dioxide as a mask to introduce nanopore structures (pore size of 0.3–1.2 nm) on the surface of graphene–CNT composite films by oxygen plasma etching. By the introduction of functional groups (e.g., hydroxyl groups) at the edges of the nanopores, the passage of ions could be prevented even at 57 MPa.^[110b] To obtain electronic devices with unique circuit patterns for the application at extreme temperatures (>423 K), Wang et al. prepared patterned superaligned carbon nanotube (SACNT) films using reactive ion etching for fabricating the thermionic electron microemitter arrays, which reached the temperatures as high as ≈2400 K.^[110d]

3.4.2. Doping

To improve the electrical performance at low temperatures, doping is adopted through CVD technology and solution process. These processes introduce active sites and defects on the surface of the materials, which further react with other radicals or ionized atoms/molecules to form new and relatively stable chemical bonds.

Lin et al. successfully synthesized in-plane graphitic nitrogen-cluster-doped graphene (Nc-G) with millimeter-sized single-crystalline domains, relying on an oxygen-assisted CVD growth strategy (oxygen flow rate of 0.2 sccm at 0.5 Pa) to eliminate the pyridinic N and to suppress the nucleation density and using acetonitrile as both nitrogen and carbon feedstock.^[111a] The as-prepared Nc-G exhibited high carrier mobility of 13 000 cm² V⁻¹ s⁻¹ at low temperature (1.9 K).

In addition to the CVD process, doping can be conducted during solution processing.^[48c,111b] Alvarenga et al. used KAuBr₄ as a dispersant in the wet spinning process of CNT wire for doping. This process resulted in a fivefold increase in electrical conductivity compared to that of the untreated fibers at the temperatures of 100–400 K.^[111b] Behabtu et al. used high-quality CNTs with a length of 5 μm as the individual material components and chlorosulfonic acid as the dispersant to prepare a LC solution with CNT concentration of 2–6 wt% to spin an iodine-doped CNT fiber, displaying a specific conductivity of 4.18 kS m² kg⁻¹ across 4–300 K.^[48c]

3.5. Combined Processes

In addition to the above individual preparation technologies, it is also necessary to combine multiple processes to realize the functional diversification of nanocarbon materials in extreme environments (Figure 7i–k).

3.5.1. CVD and Mechanical Means

The unique structures of neat nanocarbon materials, such as CNT yarns,^[112] CNT films with high alignment,^[78,90,113] CNT arrays with high density^[7b,35d] for the extreme environments are usually prepared by combining CVD with various mechanical means, such as dry-drawing,^[78,113] twist-spinning,^[112] rolling drawing,^[90] compression,^[7b,35d] etc. For example, Jin et al. pre-

pared SACNT films by combining CVD with dry-drawing, which can be used as dry adhesives across 77–1273 K.^[78] Lima et al. further prepared CNT yarns by twisting method based on CNT film obtained by dry-drawing.^[112] After infiltration with paraffin, the yarns demonstrated up to 7.3% hysteresis-free contraction when lifting heavy loads, as heated from ambient to incandescent temperature (2833 K). Furthermore, Zhang et al. performed both mechanical rolling and drawing on the CVD-grown CNTs to obtain dense CNT films filled with uniformly oriented nanogaps.^[90] This structure was essential for a highly sensitive electrochemical sensor in seawater. In addition, Xu et al. utilized reactive ion etching to the catalyst surface to grow randomly oriented CNT arrays using CVD and combined post-synthetic compression to prepare a class of CNT rubbers with the densities from 20 to 54 mg cm⁻³ for viscoelasticity across 77–1273 K.^[7b]

3.5.2. Patterning

Patterned structures could be prepared in combination with lithography technology. For example, Luo et al. combined CVD and electron beam lithography to fabricate graphene thermal emitters with bow-tie patterns, which was able to operate stably at 1600 K.^[114] Liu et al. obtained a CNT film array based on dry-drawn film, combined with screen printing and laser cutting, to achieve the luminescence function at temperatures up to 2070 K.^[113]

In addition, when it is necessary to design nanocarbon materials with a specialized structure to use in an extreme environment, 3D printing technology is often considered. Several multidimensional printing techniques have been developed to fabricate nanocarbon material architectures and their composites with designed properties and versatility (e.g., electrical conductivity, mechanical strength), such as inkjet printing^[37a] and direct ink writing (DIW).^[115] To obtain materials that are highly scalable at extreme temperatures, Guo et al. prepared a binary carbon aerogel composed of graphene and MWCNTs by 3D ink printing technology combined with self-assembly technology.^[37a] This method imparts macroscopic structural control, while microscale pore structures remain random. The structure demonstrated high stretchability with elongation of 200% across 93–773 K. Furthermore, DIW offers numerous benefits, including printing at room temperature, scalability, and versatility. To obtain probes operable at extremely high temperatures, Liang et al. used the extrusion-based DIW method to fabricate high-precision structural rGO probes with the size and shape of the probes being controlled by adjusting the printing parameters.^[115] Ultimately, the probe could remain thermally stable up to 3000 K.

3.5.3. Dry and Wet

By combining the aforementioned various techniques, neat nanocarbon materials and their composite materials for extreme temperatures can be obtained through the combination of dry and wet processing techniques.^[37b,79,116] For example, Hu et al. obtained CNT sheets from CVD-grown CNT arrays

by dry-drawing, further sprayed GO solution on the CNT sheets, and then annealed at 1600 K to prepare a CNT/graphene hybrid film.^[79] The CNT/graphene hybrid film was stably connected through covalent bonds and showed a high-temperature thermal conductivity of $\approx 870 \text{ W m}^{-1} \text{ K}^{-1}$ at 500 K. Furthermore, conductive CNT/graphene hybrid yarns with high electrical conductivity ($27.6 \times 10^3 \text{ S cm}^{-1}$) at low temperature (<80 K) were prepared by the electrospinning deposition of graphene flakes onto MWCNT sheets.^[116] In addition, Zhang et al. first prepared thin CNT aerogel hollow tubes by floating catalyst chemical vapor deposition, then densified a fiber formed from the aerogel using liquid as it was drawn from the reactor.^[117] The raw fiber was then twisted using a motor. As a result of the combined dry and wet processing, CNT fibers with strong tube-to-tube bonding were fabricated, which showed a Young's modulus of 3.1 GPa at 2673 K.

In conclusion, as stated previously, to realize the properties needed for use in extreme environments, the structure of the individual material component and the assembly into a particular structure are of upmost importance. In this section, we have outlined five general methods (CVD, self-assembly, material fusion, structural and chemical modification, and

combined processes) to realize the nanocarbon-based material structures unique for diverse extreme environment applications.

4. Examples of Applications of Nanocarbon-Based Devices in Extreme Environments

4.1. Structural Materials Serving for Wide Temperature Range

As described in Section 2.3, individual nanocarbon components, such as CNTs and graphene, possess extraordinary mechanical strength and thermal stability. Through various fabrication methods introduced in Section 3, the nanocarbon materials can be constructed into numerous forms of neat nanocarbon materials with stable mechanical performance across wide temperature ranges, which distinguishes them from other structural materials that possess strong temperature-dependent mechanical properties. These nanocarbon macroassemblies include yarns,^[124] fibers,^[35f,45d,81,118,123d,125] sheets,^[121] films,^[78,126] networks,^[35c] forests,^[7b,35d] solids,^[35a,105,123a] arrays,^[37b] foams,^[7a,36,123b,c] and aerogels^[35b,g,37a,c-e,123e] (Figure 8a–i), which can have tunable

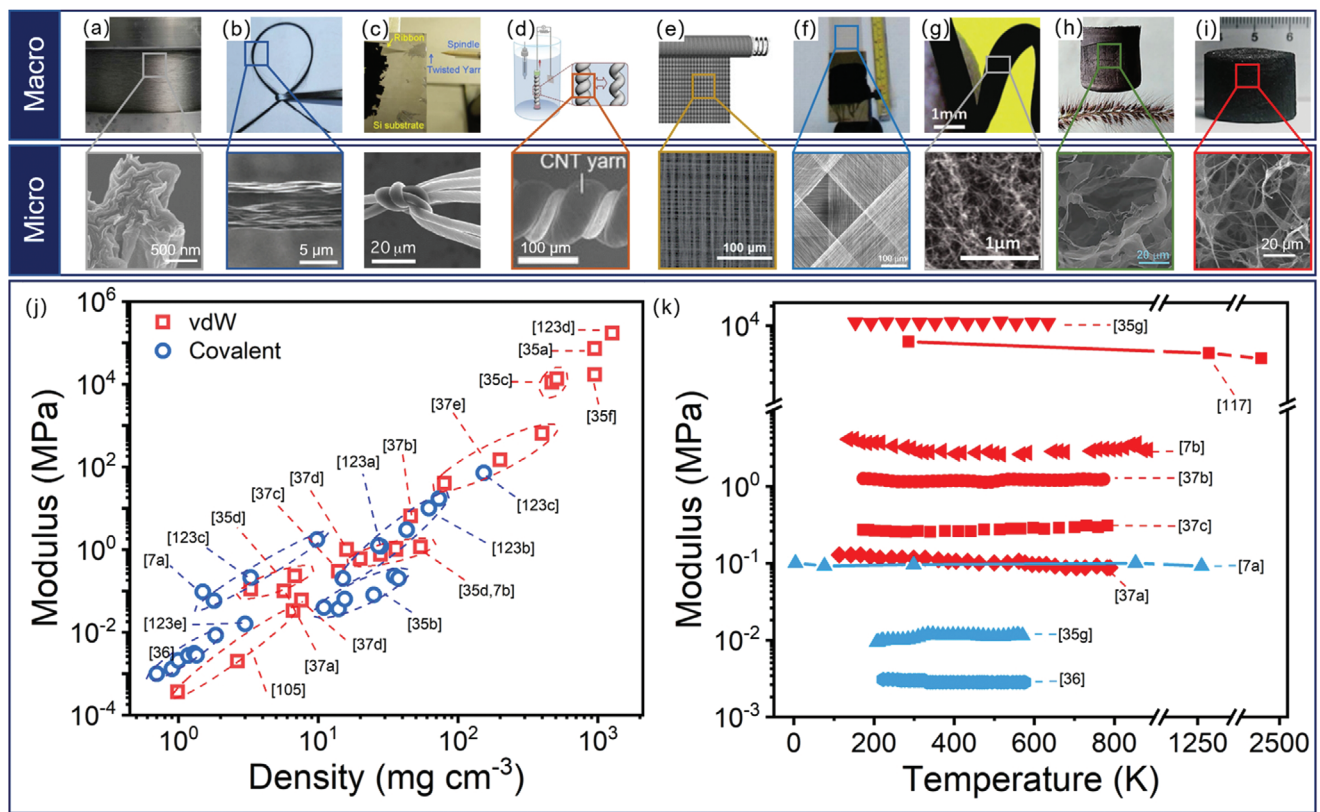


Figure 8. Neat nanocarbon materials with the stable mechanical performance across wide temperature ranges. a–d) The macro- and microschematic diagrams of 1D assemblies including yarn and fiber. a) Adapted with permission.^[45d] Copyright 2016, Wiley-VCH. b) Adapted with permission.^[118] Copyright 2020, Wiley-VCH. c) Adapted with permission.^[119] Copyright 2004, American Association for the Advancement of Science. d) Adapted with permission.^[120] Copyright 2017, The Authors, published by American Association for the Advancement of Science. e,f) The macro- and microschematic diagrams of 2D assemblies including sheet and film. e) Adapted with permission.^[121] Copyright 2015, Wiley-VCH. f) Adapted with permission.^[122] Copyright 2005, American Association for the Advancement of Science. g–i) The macro- and microschematic diagrams of 3D assemblies including forest, foam, and aerogel. g) Adapted with permission.^[7b] Copyright 2010, American Association for the Advancement of Science. h) Adapted with permission.^[37d] Copyright 2013, Wiley-VCH. i) Adapted with permission.^[36] Copyright 2015, Springer Nature. j) The relationship between modulus and density of nanocarbon materials.^[7,35a–d,f,36,37,105,123] k) The modulus of nanocarbon materials at different temperatures.^[7,35g,36,37,117]

porosity, alignment, and interaction type with the mass density being tailored from 1 to 10^3 mg cm $^{-3}$.

As shown in Figure 8j, the stiffness of neat nanocarbon materials characterized by Young's modulus increases almost linearly with their mass densities. When the mass density of neat nanocarbon materials increases, the interaction between individual nanocarbon components increases, which mainly includes two types: vdW interaction (red squares) and covalent bonding (blue dots). As described in Section 3, regardless of the synthesis method used, the vdW interaction plays a dominant role in the assembly process for neat nanocarbon materials due to their large interfacial surface area. For this reason, neat nanocarbon materials can have taken on such a rich variety of 1D, 2D, and 3D macroarchitectures with mass densities that span three orders of magnitude. The increase of mass density is a result of the increased interfacial contact between neighboring nanocarbon components. Correspondingly, their Young's modulus spans from 3.6×10^{-4} MPa, reported for a graphene foam with the density of 0.99 mg cm $^{-3}$, which is four orders of magnitude lower than polyurethane foams, to 1.7×10^5 MPa, reported for a CNT fiber with the density of 1270 mg cm $^{-3}$, which is comparable with cast iron.

In addition to providing a wide range of tunable stiffness, the vdW interaction provides neat nanocarbon materials with relatively high energy dissipation ability. For example, a series of "CNT rubbers" with densities ranging from 3.3 to 56 mg cm $^{-3}$ were fabricated. While the storage modulus was comparable with that of silicone rubber (0.3–1 MPa), the energy dissipation ability (damping ratio of 0.3) was found to be threefold that of silicone rubber (damping ratio of 0.1), which was ascribed to energy dissipation mechanism of overcoming vdW interactions of CNTs through zipping–unzipping motion.^[7b,35d]

Different from the vdW interaction, which can be naturally generated through the contact of nanocarbon components, the formation of covalent bonding (e.g., C=O, C=O, and C(=O) O) requires extra chemical modification processes. Providing stronger bond strengths, the covalent bonding has often been applied to neat nanocarbon materials for the enhancement of their elasticity and resilience during deformation. For instance, Chen and co-workers designed a lightweight 3D graphene sponge (mass density of 0.7 mg cm $^{-3}$) from covalently bonded graphene sheets.^[7a,36] As a result, its structural stability was demonstrated by exceptional recovery from deformation exemplified by 1000 cycles at 90% strain. Furthermore, Bi et al. reported a covalently bonded tubular graphene network grown by the template method, which exhibited a size distortion less than 1% after 500 cycles upon compressive strain of 90%.^[123c]

Whether vdW interaction or covalent bonding, neat nanocarbon materials have demonstrated various stable mechanical performances, including compression,^[35b,g,37c–e,123e] tensile,^[37a] torsion,^[123d] adhesion,^[78] and Poisson's ratio^[7,35c,36] across wide temperature ranges. In a plot of temperature-dependent modulus of various neat nanocarbon materials (Figure 8k), while the temperature span is greater than one thousand degrees, the variations in the moduli were within just one order of magnitude. By contrast, it is well-known that the moduli of polymeric materials commonly span nine orders of magnitude across 223–573 K. In addition, while maintaining the stiffness across

wide temperature ranges is possible, deformability and energy dissipation ability is not achievable for metals and ceramics.

4.2. Low-Temperature Energy-Storage Devices

As described in Section 2.3, nanocarbon materials possess both high specific surface area and high electrical conductivity at low temperatures, thus they are ideal materials for applications utilizing these two features, such as low-temperature energy-storage devices.

CNTs are ideal materials for constructing conductive networks due to their high electrical conductivity, aspect ratio, and specific surface area. While being combined with active materials (e.g., LiFePO₄, active carbon, metallic sulfide, and graphite),^[8g,l,132n,134] CNTs not only provide effective paths for electron transport and ion diffusion,^[8i,127] but also effectively prevent active materials from the fracture and pulverization due to their expansion/shrink during charge/discharge,^[133h,135] which is critically important for electrodes running at low temperatures. For example, You et al. prepared Prussian blue/CNTs as cathode materials and delivered a capacity of 142 mA h g $^{-1}$ and specific energy of 408 W h kg $^{-1}$ at 0.1 C at 248 K (Figure 9a), while the conductivity of electrode was increased by 47.6% with addition of CNTs.^[127] In addition, Fan et al. fabricated PI@CNT as cathodes, which showed high Coulombic efficiency, long cycle life, and a reversible capacity of 65 mAh g $^{-1}$ at 233 K (Figure 9b).^[8j] Wang et al. used SWCNT bundles (SWCNTBs) as self-adaptive substrates to create a highly resilient and conductive network which could produce radial elastic deformation to accommodate the volume change of SnO₂ during Li $^{+}$ /Na $^{+}$ insertion/extraction (Figure 9c).^[128] A capacity of 960 mAh g $^{-1}$ and a capacity retention rate of 100% after 600 cycles were reported, while cathodes without SWCNTBs only had a capacity of 550 mAh g $^{-1}$ and a capacity retention rate of 68.7% after 150 cycles.

Graphene is another excellent material for constructing electrically conductive networks. In contrast to CNTs, graphene is a 2D, planar structure and tends to possess more surface functional groups and defects, which provides abundant active sites for ion adsorption (i.e., improved ion accessibility) to improve ion storage kinetics at low temperatures. By preparing rGO with a moderate amount of surface defects and a large interlayer spacing, Wang et al. fabricated electrodes with improved ion intercalation and demonstrated a high K $^{+}$ storage capacity of 171 mAh g $^{-1}$ at 233 K (Figure 9d).^[8k] Furthermore, Wang et al. fabricated a Se/graphene composite with amorphous Se uniformly coated on the surface of a 3D conductive network composed of rGO nanosheets, which provided efficient and continuous short channels for electrons and Na $^{+}$ transmission (Figure 9e).^[129] Through this design, excellent cycle stability at 248 K with capacity retention >75% after 1000 cycles was demonstrated. In a different work, Jin et al. prepared a new ethylene glycol–water hydrogel polyelectrolyte formed by cross-linking polyacrylamide and methacrylic acid GO with a large number of micropores (Figure 9f), which improved diffusion of the electrolyte and delivered 141.7 F g $^{-1}$ at 0.5 A g $^{-1}$ at 243 K.^[130]

In addition to pure CNT or graphene constructs, hybrid materials can exhibit better performance at low temperatures

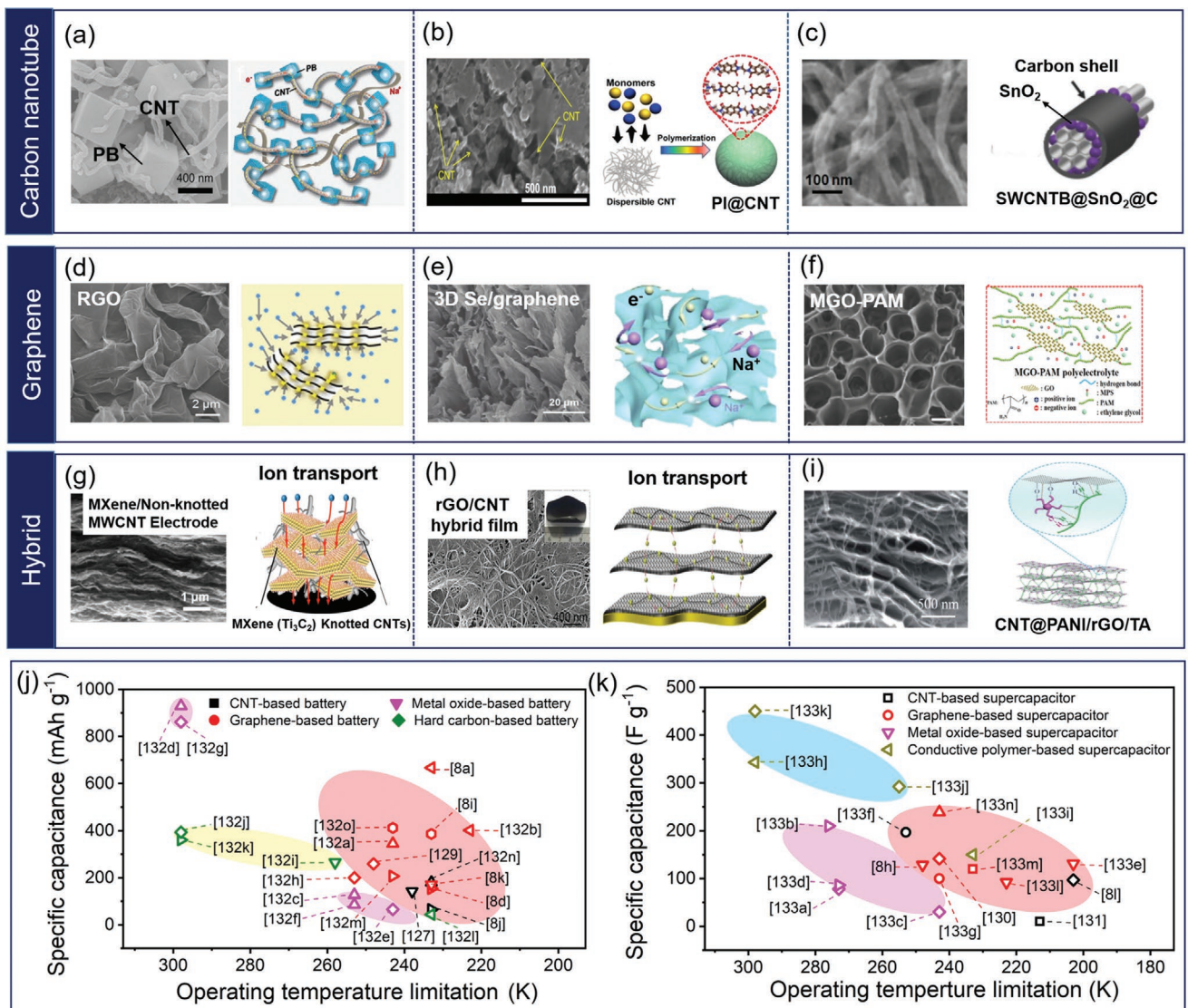


Figure 9. The effect of nanocarbon materials for low temperature energy storage. a–c) CNTs; d–f) graphene. g–i) Hybrid. a) Adapted with permission.^[127] Copyright 2016, Wiley-VCH. b) Adapted with permission.^[8j] Copyright 2018, Wiley-VCH. c) Adapted with permission.^[128] Copyright 2018, Wiley-VCH. d) Adapted with permission.^[8k] Copyright 2020, Elsevier. e) Adapted with permission.^[129] Copyright 2018, Wiley-VCH. f) Adapted with permission.^[130] Copyright 2019, Tsinghua University Press and Springer-Verlag GmbH Germany, part of Springer Nature. g) Adapted under the terms of the CC-BY Creative Commons Attribution 4.0 International license (<https://creativecommons.org/licenses/by/4.0/>).^[131] Copyright 2020, The Authors, published by Springer Nature. h) Adapted with permission.^[8e] Copyright 2017, Elsevier. i) Adapted with permission.^[8c] Copyright 2021, Royal Society of Chemistry. j) Comparison of specific capacitance and operating temperature of batteries based on nanocarbon materials with other materials.^[8a,d,i–k,127,129,132] k) Comparison of specific capacitance and operating temperature of supercapacitors based on nanocarbon materials with other materials.^[8h,l,130,131,133]

by overcoming the bundling problems of CNTs and stacking problems of graphene generally occurred due to vdW interactions. For example, Gao et al. created an open-celled electrode by inserting a specially prepared knotted CNTs into MXene sheets to maximize ion accessibility (Figure 9g).^[131] The energy density reached 59 Wh kg⁻¹ at 243 K with the lowest operating temperature to 213 K due to the high accessibility of ions and efficient ion transmission. In addition, Zang et al. fabricated rGO/CNT hybrid films with reduced internal resistance by interlacing CNTs between the rGO platelets and found that the specific capacitance only decreased by 3.2% when operated at 233 K for 140 h (Figure 9h).^[8e] Furthermore, Wu et al. also pre-

pared a hybrid structured electrode by inserting 1D CNT@polyaniline (PANI) nanowires into intermediate layers of 2D rGO to improve ion accessibility (Figure 9i).^[8c] The specific capacitance of the supercapacitor was reported as high as 454.9 F cm⁻³ at 233 K based on this porous multilayer structure.

To highlight the importance of the use of nanocarbon materials in fabricating energy devices for use at low temperatures, we constructed a graphic of the specific capacitances and operating temperatures of energy-storage devices (Figure 9j for batteries and Figure 9k for supercapacitors) which compares devices made using nanocarbon materials with those made from conventional materials, e.g., metal oxides,^[132c–g,133a–d]

conductive polymers,^[133h–k] hard carbon.^[132i–l] Energy-storage devices based on conductive polymers and metal oxides usually have high specific capacitances at room temperature, however, at low temperatures, their specific capacitances are far from ideal due to the reduction of Faradaic redox reactions. Therefore, the operating temperature of energy-storage devices based on conductive polymers and metal oxides is limited to about 253 and 243 K, respectively. By contrast, batteries based on nanocarbon materials can be operated at 223 K due to the high electrical conductivity of nanocarbon materials, and supercapacitors based on nanocarbon materials can even be operated at 203 K because their energy-storage process only involves the electrostatic adsorption and desorption of electrolyte ions.

In summary, nanocarbon-based devices exhibit superior specific capacitances at lower temperatures than those using metal oxides. Energy-storage devices based on nanocarbon materials possess great advantage in facing low-temperature environment and have great prospects for applications in the field of polar exploration, etc.

4.3. Underwater Sensing Devices

As mentioned above, nanocarbon materials have natural advantages facing severe underwater environments, such as seawater corrosion and microbial attachment due to their chemical stability. As inert materials, they can be directly used underwater without packaging to avoid packing-related performance degradation. Moreover, nanocarbon materials have good structural design ability, which can be utilized to dictate their macroscopic mechanical and electrical properties through different assemblies. When applied to underwater sensing devices, both the pressure detection range and resolution can be adjusted.

Benefiting from excellent electrical conductivity, high aspect ratio, and specific surface area of CNTs, electrochemical sensors based on macroscopic CNT materials usually have abundant of electrochemical available areas and structural deformability, leading to the combination of extraordinary sensitivity and detection range.^[90,120] Furthermore, electrochemical sensors can harvest energy due to the changes in available electrochemical areas. While the sensor itself does not require an external power supply, it can supply power for signal acquisition and transmission, thus prolonging the service life of the underwater sensing devices. For example, Kim et al. fabricated a stretchable CNT yarn sensor with superior tensile strain tolerance by cone spinning (**Figure 10a**), which not only detected the tension produced by oceanic wave motion through change of electrochemical available area of CNT yarns under twist-induced pressure (**Figure 10b**), but also demonstrated the harvesting of ocean wave energy with the peak energy of 250 W kg⁻¹ at the highest level (**Figure 10c**).^[120] In another example, Zhang et al. fabricated an electrochemical pressure sensor using nanogap-structured CNT sheets through a combination of CVD and mechanical process to sense wave pressure.^[90] This nanogap structure afforded large electrochemical surface area (**Figure 10d**) and slow deformation process of interfaces under pressure (**Figure 10e**), providing both wide pressure detection range of 10–300 KPa and the high sensitivity of 0.008 A m⁻² kPa⁻¹ at the low frequency range of wave motion (<2 Hz).

Figure 10f shows the scene of CNT-sheet-sensor monitoring inshore ships in Wuhan East Lake, which realized the real-time monitoring of ships passing by within a range of 50 m.

Compared with macroscopic materials based on CNTs, macroscopic graphene-based materials possess higher pressure tolerance because the 2D planar structure of graphene provides more interfaces that can form vdW and frictional bonding in the process of fabricating macroscopic aggregates. Thus, graphene-based sensors can exhibit a wider pressure detection range. Kaidarova et al. fabricated a piezoresistive sensor with laser-induced porous graphene foam formed by interconnected multilayer graphene sheets (**Figure 10g,h**).^[138] It showed a high pressure tolerance up to 20 MPa, indicating the working capability at depth of 2000 m, in principle. **Figure 10i** shows the scene of the graphene pressure sensor working in Al Fahal Reef of Red Sea, which successfully realized the real-time monitoring of velocity of water.

Sensors based on hybrid materials primarily utilize piezoresistive mechanism, and nanocarbon materials are usually used as active materials composited with substrates. Researchers have studied the characteristics of CNTs,^[139,140] graphene,^[141] and hybrid materials^[142] as active materials to match different structured substrates (e.g., porous foam substrates,^[139,140b,142b,143] patterned substrates^[141b,142a]) to optimize sensitivity. In particular, Li et al. fabricated a piezoresistive pressure sensor by composing porous polyurethane substrates possessing negative Poisson's ratio and CNTs for underwater sensing (**Figure 10j**).^[139] When it was placed in water, adsorbed water in sensor acted as the spacer that kept the adjacent pore walls apart. When pressure was applied, the sensor produced codirectional strain perpendicular to the direction of pressure (**Figure 10k**), and the adsorbed water was then squeezed out. This resulted in a large increase in the contact area and a corresponding decrease in resistance. Compared with its use in air, its sensitivity doubled (**Figure 10l**).

In summary, underwater sensing devices based on nanocarbon materials have great advantage in facing the complex underwater environment and have great application potential in the field of ocean exploration, etc.

4.4. High-/Low-Temperature Electronics

As addressed in Section 2.3, nanocarbon materials possess excellent electrical properties (high ampacity, high mobility, etc.) and thermal properties (high thermal conductivity, low TDP, etc.), which are useful in coping with the instabilities induced by extreme temperatures, the ampacity limits of metals, and the thermal expansion mismatch between metals and silicon.^[25c,91b,151]

CNTs are ideal materials for high-/low-temperature electronics due to their ultrahigh aspect ratios, nanoscale sizes, tunable chirality, and ultralong mean free path of carriers (>1 μm). Aligned CNT films are mainly used for the production of CNT electronics, in which CNTs as the channel materials are highly desirable for constructing field-effect-transistor (FET)-based electronics, which can be used to scale the channel length based on an effective gate control (**Figure 11a**).^[152] The performance of CNT-based FETs (CNT FETs) strongly relies on the semiconducting purity and tube

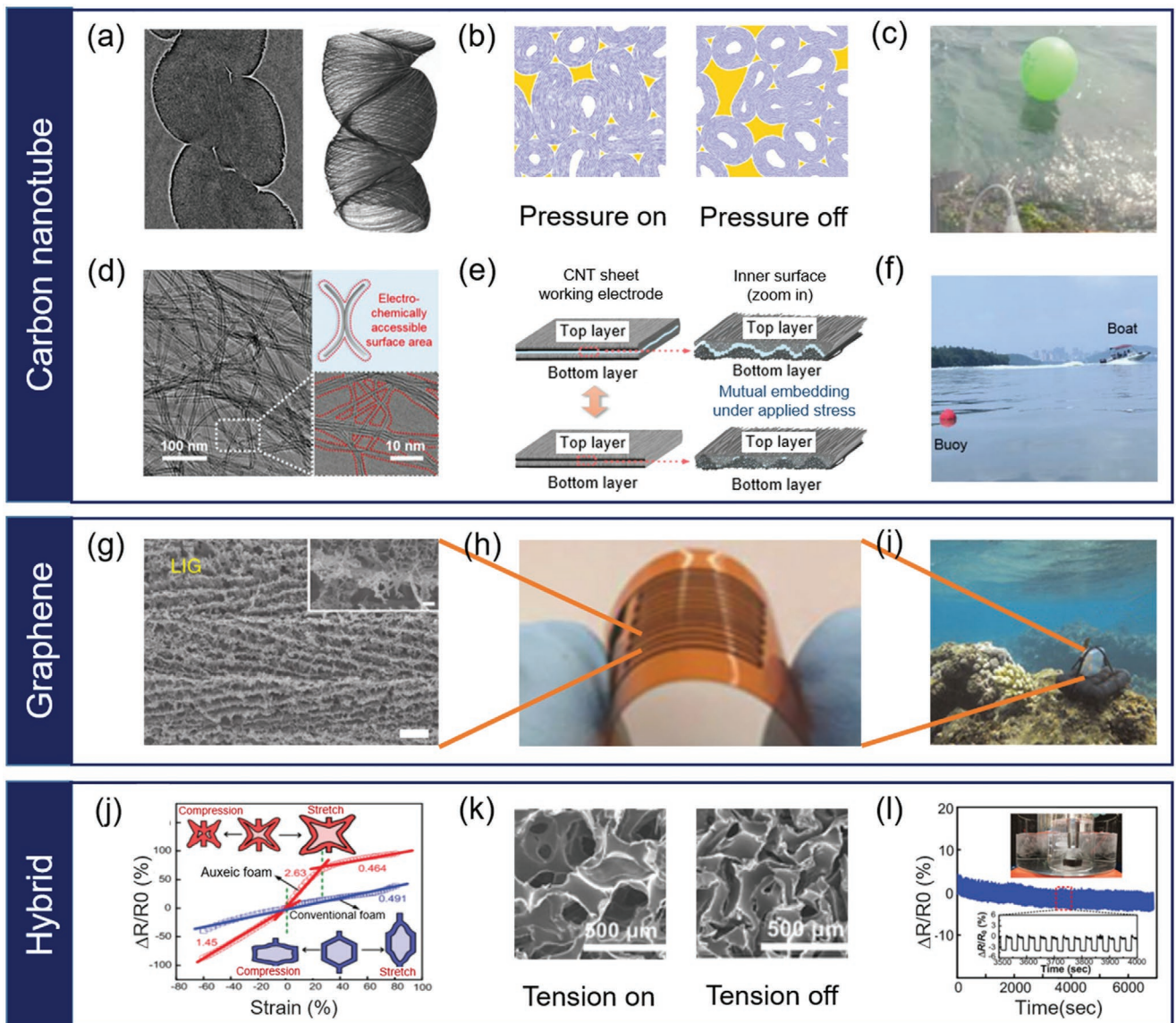


Figure 10. Underwater sensing devices using nanocarbon materials. a) Structure of CNT yarns illustrated by phase-contrast X-ray tomography image (left) and sketch image (right). b) Molecular dynamics simulation to model the effect of twist-induced pressure on the electrochemical available areas that are shown in yellow. c) Scene of CNT yarn sensor working in Gyeonpo Sea off South Korea. a–c) Adapted with permission.^[120] Copyright 2017, The Authors, published by American Association for the Advancement of Science. d) Transmission electron microscopy (TEM) image of CNT sheet with red lines expressing the electrochemical available area. Insets: magnified TEM image of the electrochemical available area of CNTs. e) Work mechanism of CNT sheet sensor. f) Scene of CNT sheet sensor working in Wuhan East Lake. d–f) Adapted with permission.^[90] Copyright 2020, Wiley-VCH. g) Scanning electron microscopy (SEM) image of laser-induced graphene foam. Inset: magnified SEM image of laser-induced graphene foam. Adapted with permission.^[136] Copyright 2014, Springer Nature. h) Photograph of the sensor based on laser-induced graphene foam. Adapted under the terms of the CC-BY Creative Commons Attribution 4.0 International license (<https://creativecommons.org/licenses/by/4.0/>).^[137] Copyright 2019, The Authors, published by Springer Nature. i) Scene of laser-induced graphene sensor working in the Red Sea. Adapted under the terms of the CC-BY Creative Commons Attribution 4.0 International license (<https://creativecommons.org/licenses/by/4.0/>).^[138] Copyright 2020, The Authors, published by Wiley-VCH. j) Work mechanism of negative-Poisson-ratio sensor. k) SEM images of the structure of negative Poisson ratio foam before and after the application of tension. l) Underwater durability tested during tube sonication in an ice bath. Insets: scene of negative Poisson ratio sensor working in water (top) and magnified in performance over 12 cycles (bottom). j–l) Adapted with permission.^[139] Copyright 2016, Wiley-VCH.

density of aligned CNT films. To date, the CNT films with high semiconducting purity up to 99.999% and high density of 100–200 CNTs μm^{-1} have been demonstrated, which meet the requirements of high-performance CNT FETs (Figure 11b,c).^[144] Notably, different from the metal–oxide–semiconductor FETs (MOSFETs) prepared by traditional doping techniques, CNT FETs can be pre-

pared without doping to avoid the diffusion of the dopants at high temperatures and the freeze-out of the dopants at low temperatures.^[139] Combined with the thermal stability of CNTs and the low intrinsic carrier excitation, the operating temperature range of CNT FETs (4–573 K) is wider than that of conventional Si-based devices (218–393 K) (Figure 11d).^[91b,102]

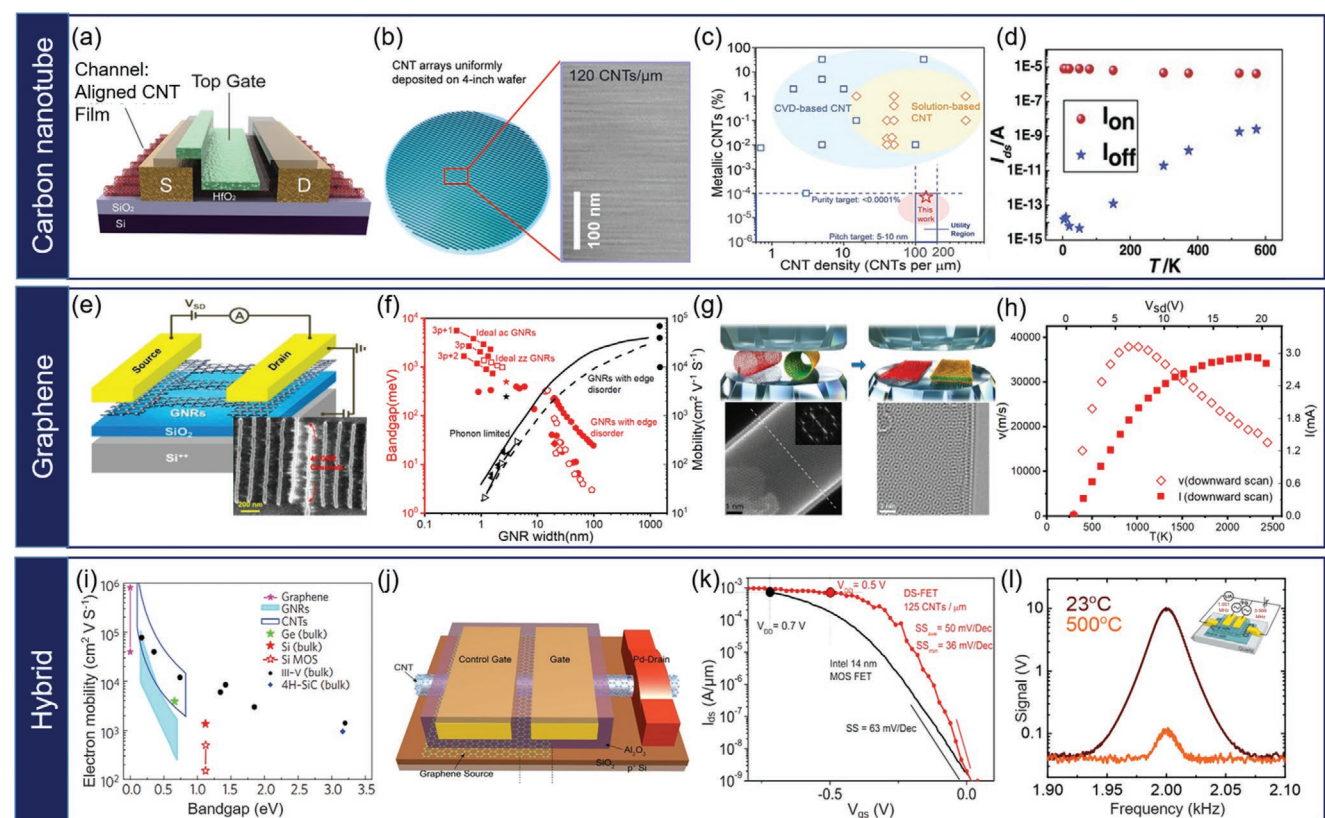


Figure 11. High- and low-temperature electronics. a) Schematic diagram of the CNT-based top-gate FET. S, source; D, drain. b) SEM image of the as-deposited CNT array obtained by using an optimal CNT solution concentration ($40 \mu\text{g mL}^{-1}$). c) Semiconducting purity versus CNT density of the arrays. a–c) Adapted with permission.^[144] Copyright 2020, The Authors, published by American Association for the Advancement of Science. d) Temperature-dependent ON- and OFF-state current. Adapted with permission.^[91b] Copyright 2011, Wiley-VCH. e) Schematic diagram of the GNR-based back-gate FET. Adapted with permission.^[145] Copyright 2016, American Chemical Society. f) Bandgap and mobility versus nanoribbon width from experiments and calculations. Adapted with permission.^[146] Copyright 2010, Springer Nature. g) Schematic of squashing a SWCNT and DWCNT (left) into GNRs (right) via a high-pressure and thermal treatment. Adapted with permission.^[147] Copyright 2021, The Authors, published by Springer Nature. h) Device I – V curve, temperature, and carrier drift velocity. Adapted with permission.^[148] Copyright 2014, The Authors, published by Springer Nature. i) Electron mobility versus bandgap in low electric fields for different materials. Adapted with permission.^[146] Copyright 2010, Springer Nature. j) Schematic diagram of the Dirac-source (DS)-FET with graphene and CNT. k) Comparison between DS-FET and a commercial Intel 14 nm Si MOSFET. j,k) Adapted with permission.^[149] Copyright 2018, The Authors, published by American Association for the Advancement of Science. l) The performance of the graphene-based heterodyne mixer at high temperature. Adapted with permission.^[150] Copyright 2019, American Institute of Physics.

Different from the chirality selectivity of CNTs, graphene possesses unique properties originating from massless fermions arising from the linear dispersion of energy bands near the Dirac points. For example, under gate voltage, charge carriers in graphene can be tuned continuously between electrons and holes and their mobilities exceed $2.5 \times 10^5 \text{ cm}^2 \text{ V}^{-1} \text{ s}^{-1}$ under ambient conditions, which makes graphene an ideal channel material to improve Si-based FETs (Figure 11e).^[153] At present, graphene-based electronics are commonly constructed from graphene nanoribbons (GNRs), and their switching ratio can be adjusted by modulating the bandgap of the GNRs.^[147,154] As shown in Figure 11f, with the ribbon width decreasing from 100 to 1 nm, the bandgap increased from ≈ 3 to $\approx 10^3$ meV (ideal)^[147,155] with the switching ratio increased to 10^4 , while the carrier mobility decreased from $\approx 10^4$ to $\approx 10 \text{ cm}^2 \text{ V}^{-1} \text{ s}^{-1}$ due to edge-scattering effects.^[147,155g,156] Chen et al. simultaneously improved the switching ratio ($>10^4$) and the carrier mobility ($2443 \text{ cm}^2 \text{ V}^{-1} \text{ s}^{-1}$) by preparing sub-10 nm wide and long GNRs with atomically smooth edges (Figure 11g).^[147] In

addition, with the increased temperature, the carrier mobility of the graphene device gradually increased, and the power consumption of the device gradually decreased across 300–1000 K. When the temperature rose above 1000 K, the declining saturation drift velocity in graphene assisted to delay the current runaway point, where the current increases with a constant driving voltage to an even higher temperature (Figure 11h).^[148]

As shown in Figure 11i, graphene with zero bandgap possesses a high carrier mobility, while CNTs have bandgap from ≈ 250 to ≈ 750 meV and their carrier mobility is higher than that of Si.^[146] Thus, the power consumption of electronics can be reduced by combining CNTs and graphene due to their high carrier mobility (Figure 11j,k).^[149,157] Qiu et al. used graphene as the source/drain electrode for sub-10 nm CNT FETs to improve gate control on the channel and suppress direct tunneling between the source and drain.^[157] Compared with the state-of-the-art Si 14 nm node FETs, this device could switch at a lower bias voltage of 0.4 V (vs 0.7 V for Si FETs), demonstrating a reduced power consumption (Figure 11k).^[149] As

described in Section 2.3.2, nanocarbon materials combined with h-BN show a good high-temperature tolerance, and the nonlinearity resulting from the recursive energy spectrum of aligned graphene/h-BN superlattices makes them appropriate for use as heterodyne frequency mixers at high temperatures (Figure 11l).^[150]

In addition, electronics are commonly prepared at relatively high temperatures (e.g., Si-based electronics prepared at 1173 K) and require some form of bond by adhesives or welding.^[93c] Ceramic adhesives and metal weldings will fail at high temperatures due to the mismatch in thermal expansion and polymer-based adhesives decompose. CNT dry adhesives are a promising choice for adhesive used in the field of electronics due to the temperature insensitivity of the vdW adhesion mechanism and the low coefficient of thermal expansion (CTE). In fact, Xu et al. reported that the adhesion strength increased with temperature increasing.^[49] In addition, it was shown that this CNT dry adhesive could also be used for efficient electrical and thermal management in the high-/low-temperature electronics due to its excellent thermal conductivity performance at extreme temperatures.^[25c,151]

In summary, high-/low-temperature electronics based on nanocarbon materials have shown great advantages in facing extreme temperatures and are hopeful to be used in the field of space exploration, industry, etc.

4.5. Aerospace and Marine Application Research

As addressed in Section 2.2, nanocarbon materials have the feature of lightweight combined with superior electrical and thermal properties, which are usually used as fillers to compound with metals, polymers, and other materials for aerospace,^[158–163,166] marine,^[164,165,167] and other fields that require high strength-to-weight ratio, corrosion resistance, and radiation resistance. The preparation methods of the above composites can be mainly divided into two types: preform-based preparation and dispersion-based preparation.

Nanocarbon-based composite materials prepared by the preform-based method are usually used to improve the properties in a specific direction.^[158,166c,d] As an example in aeronautics field, CNT arrays have been cured with the epoxy tape and used as “nanostitches” between the plies of aerospace-grade unidirectional carbon fiber laminates to enhance their interlaminar bonding and provided a significant enhancement of fracture toughness evidenced by 30% increase of tension-bearing (bolt pull out) critical strength, 14% increase of open-hole compression ultimate strength, and more than 25% increase of L-section bending energy and deflection (Figure 12a,b).^[158] CNT yarns have been adopted to solve the lunar-dust problem to assure the safety of astronauts.^[159,166a,g] Since the lunar dust is comprised of fine particles with electric charges imparted by solar winds and ultraviolet radiation, it adheres readily, and easily penetrates the smallest crevices of spacesuits. The CNT yarns with high electrical conductivity were designed as wires to be embedded into the outer layer of the spacesuit. By energizing with a multiphase AC voltage signal, a traveling wave of electric field formed around the spacesuit surface to prevent dust from entering the interior of the spacesuit and remove

80–96% of the dust adhering to the fabric.^[159] Because of the ultralight mass of the CNT yarns (~16 vs 81 646 g of the suit), there is basically no effect on astronauts (Figure 12c,d).

In addition, nanocarbon preforms have been compounded with polymers to protect the spacecraft from space radiation, high/low temperature, and electrostatic discharge.^[160,161,166e,f] For example, nanocarbon materials were fabricated into sheets (Figure 12e,f)^[160] and foams (Figure 12g,h)^[161] as preforms, and then compounded with PI for the electrostatic discharge protection layer in spacecraft thermal blankets. Compared with PI films, the electrical conductivities of CNT sheets and graphene foams were increased by 18 orders of magnitude and 10 orders of magnitude, respectively. The radiation resistance test showed that they were capable to withstand 9880 kGy of gamma radiation (⁶⁰Co source), which was equivalent to 15 years in space (geostationary-orbit electron radiation dose).^[160,161]

Nanocarbon-based composites prepared by dispersion method are usually used to improve the thermal stability and anticorrosion performances in aerospace and marine fields. For example, CNTs with their low CTE (~0) have been developed as the reinforcement for aluminum matrix composites (AMCs), which is known as a widely used material for aircraft fuselages that require superior thermal stability and lightweight. The well-dispersed CNTs can exert an effective pinning inside the Al matrix, hindering the growth of Al grains during heating and thereby enhancing the thermal stability.^[162,166h–k] With the addition content of 4.5 wt%, the CTE of CNT-based AMCs was reduced 17–19% at 373 K compared to pure Al (Figure 12i,j).^[162] In addition, nanocarbon-based aerospace grade epoxy adhesive with both structural and conductive bonding ability is being considered as the replacement of the rivets for aerospace structural applications.^[163,166l–o] For example, the peel strength of the SWCNT-adhesive composite was improved by 30% with a SWCNT loading of only 1 wt%, when its electrical conductivity exceeded 0.1 S m⁻¹ (Figure 12k,l).^[163] If the nanocarbon-based adhesives can be eventually used for the electrical bonding on aircrafts, the aircraft weight can be reduced significantly. Estimated based on an Airbus A380 with 10⁶ rivets at 2 g each, this results in a total weight reduction of 2000 kg.^[166b]

In the field of marine engineering, nanocarbon-based polymeric coatings has been remaining as a hot topic for the protection of the hull of the ships by reducing the occurrence of corrosion through restraining the migration of ions in seawater to the matrix.^[164,167a–d] Combined with superior solubility of polyhedral oligomeric silsesquioxane (POSS), a type of super-hydrophobic POSS-GO (PG) nanosheet fillers was designed and mixed with epoxy matrix (EP). After 50 days of immersion in 3.5 wt% NaCl solution (simulated marine environment), the water absorption of the composite with 0.5%-POSS-GO was 5.11%, which was much lower than that of EP (11.42%), 0.5%-GO/EP (8.35%), and 1%-PG/EP (7.55%) composite coatings (Figure 12m,n).^[164] The dispersion of GO nanosheets is critically important, which should fill the initial defects (such as microhole) and enhance the density of coating, thus reduce the penetration channel for corrosive medium. In addition, nanocarbon-based polymeric coatings can be used on the hulls to improve the stealth performance of ships. Due to the high specific areas of nanocarbon materials, abundant interfaces were created inside the coatings to enhance the scattering of

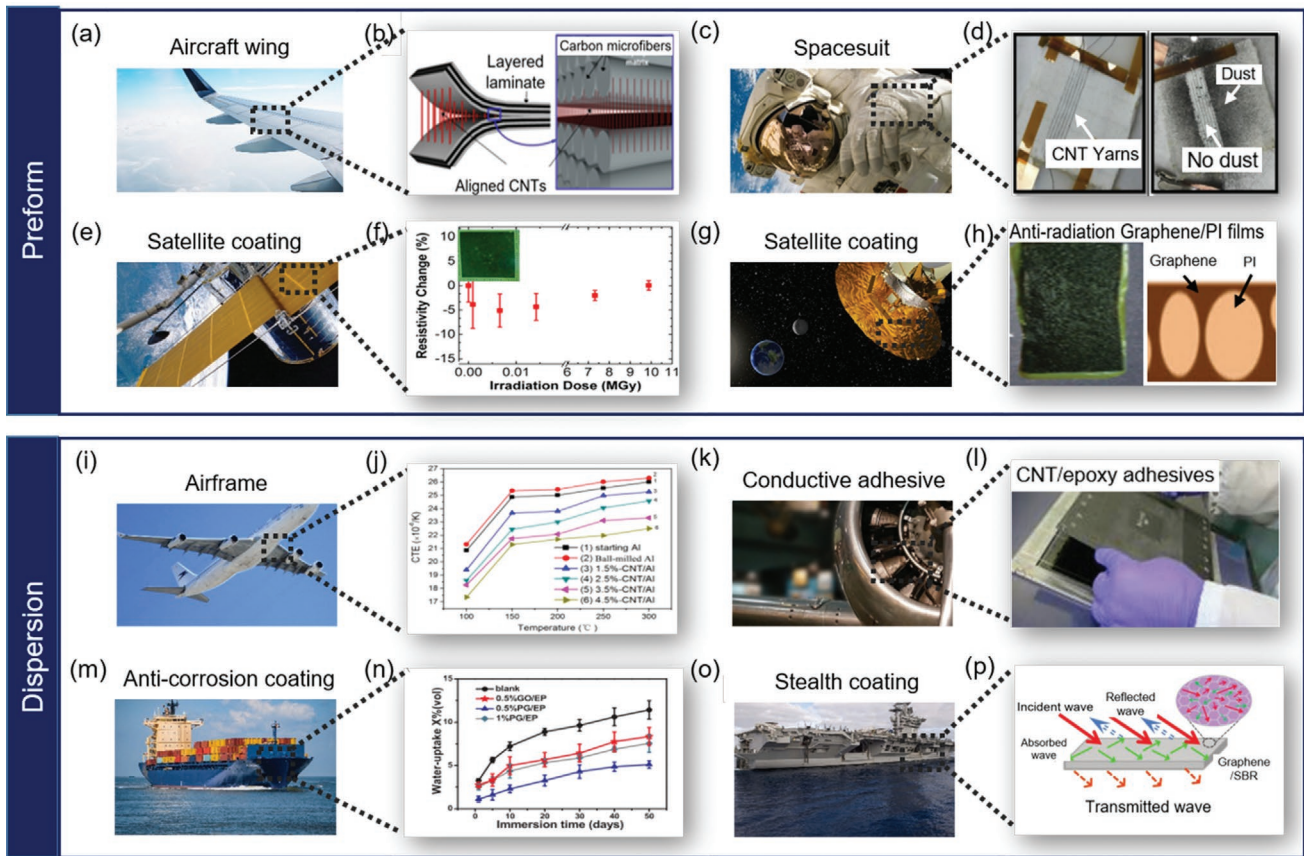


Figure 12. Application research of nanocarbon composite materials in aerospace and marine fields. a) Aircraft wing. b) CNT array used to improve mechanical properties of carbon fiber laminates. c) Spacesuit. d) CNT yarns/polymer coatings for dust removal of spacesuit. e) Satellite coating. f) CNT array/PI composite coatings with high radiation resistance. g) Satellite coating. h) Graphene foam/PI composite coatings for radiation protection. Adapted with permission.^[158] Copyright 2016, Elsevier. i) Airframe. j) CNT/Al composite with low CTE. Adapted with permission.^[162] Copyright 2016, Elsevier. k) Conductive adhesive. l) CNT/epoxy composite for aerospace adhesives. l) Adapted with permission.^[163] Copyright 2015, Elsevier. m) Anticorrosion coating. n) Graphene/epoxy composite coatings for corrosion protection. n) Adapted with permission.^[164] Copyright 2019, Elsevier. o) Stealth coating. p) Graphene/rubber composite coatings for ship stealth. p) Adapted with permission.^[165] Copyright 2017, The Royal Society of Chemistry. The images in (a,c,e,g,i,k,m,o) are from Pixabay.

electromagnetic waves and sound waves during propagation. Thus, the electromagnetic shielding and sound absorption properties of the coatings, i.e., the stealth of ships were improved (Figure 12o,p).^[165,167e-g]

In summary, nanocarbon-based composite materials have a wide range of application prospects in aerospace and marine fields due to their excellent properties, such as high strength-weight ratio, excellent radiation and corrosion resistance, low CTE, high mechanical properties, etc.

5. Conclusions and Perspectives

5.1. Conclusions

Compared with conventional materials, the C=C covalent bond of nanocarbon materials provides a unique combination of superior mechanical performance, electrical conductivity, thermal conductivity, and structural stability, which makes them ideal components for constructing macroaggregates for

extreme environments. Neat nanocarbon materials are mainly produced by CVD and self-assembly technologies, which have shown various unique extreme environmental performances, such as mechanical damping characteristics across wide temperature ranges, excellent specific conductivity at high temperatures, and thermal distortion resistance. These properties are advantageous for applications in aerospace, polar exploration, and other environments with extremely high and low temperatures. Nanocarbon-based composites are mainly fabricated by material fusion combined with structural and chemical modifications. Through the synergy between combining nanocarbon components and matrix materials, numerous examples of high-temperature tolerance, high-pressure resistance, corrosion resistance, and radiation resistance have been achieved, that show the tangible outlook of nanocarbon enabling applications in complex extreme environments. When more advanced structures are required by specific extreme environmental applications, combined processes are adopted. Based on the above structural-design principles and manufacturing strategies, nanocarbon materials have shown exceptional behavior in

the field of wide-temperature structural-material construction, low-temperature energy storage, underwater sensing, and electronics operated at high and low temperatures.

5.2. Perspectives

Although nanocarbon materials have shown various unique extreme environmental properties, there remains numerous technological challenges including the precise control of individual nanocarbon components, the precise control of macroscopic aggregates, and the improved large-scale production technology to advance their applications in extreme environments.

5.2.1. Precise Control of Individual Nanocarbon Components

At present, the challenges for the precise control of individual nanocarbon components mainly focus on the control of the chirality of CNTs and the bandgap of GNRs, which is critically important for advancing the development of nanocarbon materials in high-end applications, such as electronic devices applied in extreme environments.

To improve the precision of the chirality control of CNTs, the evolution of catalyst particles, the cracking of carbon sources, and the assembly of carbon atoms during the growth process should be further clarified at the atomic scale, while the relationship between the morphology of catalyst particles and the geometry of CNTs should be established. In addition, it is necessary to develop new types of catalysts and synthetic techniques to enable the improved chirality control and growth efficiency of CNTs simultaneously. At present, GNRs are mainly prepared by surface-based synthesis methods with precursors and substrates. But the edge structures of GNRs, i.e., width and length, are difficult to control. This precise structural control is necessary for synthesizing GNRs with controllable bandgap and for stable device fabrication. Therefore, it is still necessary to discover improved (or rationally designed) precursors and substrates as well as improved growth reactors to achieve effective control of the edge structure, nanoribbon width and length. In doing so, the complex relationship between the bandgap and mobility can be overcome. More importantly, in order to realize its application in extreme environments, it is necessary to control defects and achieve scaled-up production on the basis of the CNT chirality and graphene bandgap regulation.

In addition, the lack of *in situ* characterization techniques at the microscale to characterize the performance of nanocarbon materials in extreme environments has represented an obstacle in real-time examination of the working mechanisms. This hinders the development of working mechanisms to understand nanocarbon materials in extreme environments. Therefore, through the combination of theoretical research, nondestructive *in situ* characterization, and microscale evaluation techniques in extreme environments, the mechanism of nanocarbon materials operating in extreme environments can be elucidated to act as a guide for the design of improved materials for extreme environments.

5.2.2. Precise Control of Macroscopic Aggregates

While individual nanocarbon components theoretically can withstand pressures of 5.5 GPa at 300 K and temperatures of 3070 K in vacuum, the macroscopic aggregates of nanocarbon materials face degradation of thermal stability due to the introduction of defects within the assembly.^[24] Recently, the preparations of centimeter-long defect-free carbon nanotube bundles have been achieved, which demonstrate a tensile strength of 80 GPa with excellent impact resistance.^[168] This represents one example to avoid the obstacle of performance degradation caused by “size effect.” However, due to the limitation of synthesis, the tensile strength of the macroscopic aggregates (e.g., CNT fiber) is only 1/20–1/50 of the individual components.^[35e,f] Therefore, the preparation of macroscopic aggregates, which retain the nanoscale properties, is not a simple matter of combining individual nanocarbon components.

For the growth of neat nanocarbon materials, the size and density of the catalysts cannot be uniformly controlled in the preparation process of the existing preparation technology. Therefore, it is difficult to achieve the uniformity of the size and geometric structure of individual nanocarbon components when obtaining macroscopic aggregates. Meanwhile, agglomerations caused by molecular interactions between adjacent individual components (including tube–tube, layer–layer, and tube/layer–growth substrate interactions) also determine the overall morphology of nanocarbon materials. Additionally, the preparations of macroscopic aggregates, such as fibers, films, and foams always involve multiple postprocessing processes (solution separation, functionalization, purification, etc.), which unavoidably introduce the impurities and defects into the aggregates. This detrimentally affects the performance of such materials in extreme environments.

For the preparation of nanocarbon-based composite materials, chemical modification including the introduction of active functional groups (e.g., C=O, C–O, C–H bonds, etc.) is usually necessary to apply on the nanocarbon components to suppress the agglomeration and improve the wettability between the nanocarbon materials and the matrix. However, the degradation of the thermal and chemical stability of the materials would occur, that is, a decrease in the tolerance of extreme environments. Therefore, it is necessary to develop advanced dispersion processes to enable the thermal stability in extreme environments while the interfacial bonding between the nanocarbon materials and the matrix can be optimized. One possibility would be to design an *in situ* preparation process of nanocarbon materials to generate nanocarbon phase directly from a polymer or metal–organic framework matrix.

5.2.3. Mass Production Technology

Ultimately, the scaled-up production of nanocarbon materials with the desired structure is the key to realize the applications in extreme environments. At present, in the case of CNTs, a variety of industrial-scale synthesis methods have been developed, such as fluidized-bed CVD and rotary kiln CVD, which possess an annual production capacity of over 10 000 tons. However, the CNTs prepared by the above methods usually

have high catalyst residues and defects, which would limit their applications in high temperatures and radiation environments. In addition, for the large-scale preparation of graphene, reduced GO is still one of the most widely used methods. The method involves series of chemical procedures with a large amount of corrosive chemicals being introduced, which results in the degradation of the performance of its macroscopic aggregates in the environments such as high-temperature, high-pressure, and corrosive environments. Therefore, the development of high purity, high quality, and precision-controlled synthesis of nanomaterials, such as CNTs and graphene, is still required for their applications toward extreme environmental applications.

As one example, VACNTs are grown on flat substrates through a bottom-up, self-assembly process based on CVD. VACNTs have a number of advantages, such as controllable intrinsic properties of CNTs and easy separation from catalysts and growth substrates to obtain high-purity CNTs. In addition, it has been confirmed that high-purity, pseudo-1D fibers and horizontal arrays can be prepared from VACNTs. However, this approach has several drawbacks. First, the assembly of VACNTs limits the crystallinity of the individual CNTs due to assembly related stress at the CNT–catalyst interface.^[169] Furthermore, this method possesses a low volumetric efficiency, compared to the fluidized-bed method, due to the limited substrate surface area. Therefore, developing synthetic processes which overcome the current fundamental limiting mechanisms on purity, quality, and structural control is essential in scaling-up production.

We believe to achieve these goals requires the combination of multiple technologies, spanning theoretical research, artificial-intelligence-assisted design of both the reactor system and process, and clear understanding of the needed nanomaterial structure. Only through these approaches can we expect to move into the future and solve the remaining seemingly insurmountable scientific challenges to promote the industrial development and large-scale production of nanocarbon materials and their applications in extreme environments.

Acknowledgements

S.W. and H.L. contributed equally to this work. The authors acknowledge the financial support from the National Natural Science Foundation of China (Grant No. 51972127), the Science, Technology and Innovation Commission of Shenzhen Municipality (Grant Nos. JCYJ20190809102607400, JCYJ20210324135207020, and JCYJ20180507182530279).

Conflict of Interest

The authors declare no conflict of interest.

Keywords

carbon nanotubes, devices, extreme environments, graphene, temperature invariance

Received: January 31, 2022

Revised: April 27, 2022

Published online: September 30, 2022

- [1] a) L. J. Rothschild, R. L. Mancinelli, *Nature* **2001**, *409*, 1092; b) N. Dharmarasu, S. Arulkumaran, R. R. Surnathi, P. Jayavel, J. Kumar, P. Magudapathy, K. G. M. Nair, *Nucl. Instrum. Methods Phys. Res., Sect. B* **1998**, *140*, 119; c) V. N. Alviani, N. Hirano, N. Watanabe, M. Oba, M. Uno, N. Tsuchiya, *Appl. Energy* **2021**, *293*, 116909; d) M. Schagerl, R. W. Renaut, in *Soda Lakes of East Africa* (Ed: M. Schagerl), Springer International Publishing, Cham **2016**, p. 3.
- [2] M. Chen, Y. Zhang, G. Xing, S.-L. Chou, Y. Tang, *Energy Environ. Sci.* **2021**, *14*, 3323.
- [3] P. L. Dreike, D. M. Fleetwood, D. B. King, D. C. Sprauer, T. E. Zipperian, *IEEE Trans Compon. Packag., Manuf. Technol.: Part A* **1994**, *17*, 594.
- [4] a) F. Zhang, M. Sun, S. Xu, L. Zhao, B. Zhang, *Chem. Eng. J.* **2008**, *141*, 362; b) M. Cui, S. Ren, J. Chen, S. Liu, G. Zhang, H. Zhao, L. Wang, Q. Xue, *Appl. Surf. Sci.* **2017**, *397*, 77; c) M. T. Gudze, R. E. Melchers, *Corros. Sci.* **2008**, *50*, 3296.
- [5] a) R. D. Schrimpf, D. M. Fleetwood, M. L. Alles, R. A. Reed, G. Lucovsky, S. T. Pantelides, *Microelectron. Eng.* **2011**, *88*, 1259; b) J. R. Srour, J. M. McGarrity, *Proc. IEEE* **1988**, *76*, 1443.
- [6] a) S. Nardcchia, D. Carriazo, M. L. Ferrer, M. C. Gutierrez, F. del Monte, *Chem. Soc. Rev.* **2013**, *42*, 794; b) H. P. Cong, J. F. Chen, S. H. Yu, *Chem. Soc. Rev.* **2014**, *43*, 7295; c) Z. Li, Z. Liu, H. Y. Sun, C. Gao, *Chem. Rev.* **2015**, *115*, 7046; d) M. F. Yu, O. Lourie, M. J. Dyer, K. Moloni, T. F. Kelly, R. S. Ruoff, *Science* **2000**, *287*, 637; e) R. Zhang, Q. Wen, W. Qian, D. S. Su, Q. Zhang, F. Wei, *Adv. Mater.* **2011**, *23*, 3387; f) E. J. Askins, M. R. Zoric, M. Li, Z. Luo, K. Amine, K. D. Glusac, *Nat. Commun.* **2021**, *12*, 3288; g) G. Zhang, V. B. Koman, T. Shikdar, R. J. Oliver, N. Perez-Lodeiro, M. S. Strano, *Small* **2021**, *17*, 2006752; h) J. K. Y. Lee, N. Chen, S. Peng, L. Li, L. Tian, N. Thakor, S. Ramakrishna, *Prog. Polym. Sci.* **2018**, *86*, 40; i) E. W. Wong, P. E. Sheehan, C. M. Lieber, *Science* **1997**, *277*, 1971.
- [7] a) K. Zhao, T. Zhang, H. Chang, Y. Yang, P. Xiao, H. Zhang, C. Li, C. S. Tiwary, P. M. Ajayan, Y. Chen, *Sci. Adv.* **2019**, *5*, eaav2589; b) M. Xu, D. N. Futaba, T. Yamada, M. Yumura, K. Hata, *Science* **2010**, *330*, 1364.
- [8] a) D. R. Deng, F. Xue, C. D. Bai, J. Lei, R. Yuan, M. S. Zheng, Q. F. Dong, *ACS Nano* **2018**, *12*, 11120; b) E. Alekseeva, T. Stelmashuk, V. Ershov, O. Levin, *Electrochim. Acta* **2021**, *383*, 138309; c) D. Wu, C. Yu, W. Zhong, *J. Mater. Chem. A* **2021**, *9*, 18356; d) M. J. Lee, K. Lee, J. Lim, M. Li, S. Noda, S. J. Kwon, B. DeMattia, B. Lee, S. W. Lee, *Adv. Funct. Mater.* **2021**, *31*, 2009397; e) X. Zang, R. Zhang, Z. Zhen, W. Lai, C. Yang, F. Kang, H. Zhu, *Nano Energy* **2017**, *40*, 224; f) J. Liu, Z. Khanam, S. Ahmed, T. Wang, H. Wang, S. Song, *ACS Appl. Mater. Interfaces* **2021**, *13*, 16454; g) Y. Hu, H. Huang, D. Yu, X. Wang, L. Li, H. Hu, X. Zhu, S. Peng, L. Wang, *Nano-Micro Lett.* **2021**, *13*, 159; h) J. H. Jeong, M. J. O, K. C. Roh, *J. Alloys Compd.* **2021**, *856*, 158233; i) J.-Q. Huang, X.-F. Liu, Q. Zhang, C.-M. Chen, M.-Q. Zhao, S.-M. Zhang, W. Zhu, W.-Z. Qian, F. Wei, *Nano Energy* **2013**, *2*, 314; j) X. Fan, F. Wang, X. Ji, R. Wang, T. Gao, S. Hou, J. Chen, T. Deng, X. Li, L. Chen, C. Luo, L. Wang, C. Wang, *Angew. Chem., Int. Ed. Engl.* **2018**, *57*, 7146; k) Y. Wang, X. Gao, L. Li, M. Wang, J. Shui, M. Xu, *Nano Energy* **2020**, *67*, 104248; l) J. Xu, X. Wang, X. Zhou, N. Yuan, S. Ge, J. Ding, *Electrochim. Acta* **2019**, *301*, 478.
- [9] a) A. Kausar, *J. Thermoplast. Compos. Mater.* **2020**, <https://doi.org/10.1177/0892705720930810>; b) N. M. Nurazzi, F. A. Sabaruddin, M. M. Harussani, S. H. Kamarudin, M. Rayung, M. R. M. Asyraf, H. A. Aisyah, M. N. F. Norrrahim, R. A. Ilyas, N. Abdullah, E. S. Zainudin, S. M. Sapuan, A. Khalina, *Nanomaterials* **2021**, *11*, 2186.
- [10] a) N. H. Othman, M. C. Ismail, M. Mustapha, N. Sallih, K. E. Kee, R. A. Jaal, *Prog. Org. Coat.* **2019**, *135*, 82; b) R. Ding, W. Li, X. Wang, T. Gui, B. Li, P. Han, H. Tian, A. Liu, X. Wang, X. Liu, X. Gao, W. Wang, L. Song, *J. Alloys Compd.* **2018**, *764*, 1039.

- [11] P. Gumbsch, J. Riedle, A. Hartmaier, H. F. Fischmeister, *Science* **1998**, *282*, 1293.
- [12] a) G. Ventura, M. Perfetti, *Thermal Properties of Solids at Room and Cryogenic Temperatures*, Springer, Dordrecht **2014**; b) M. R. Ward, *Electrical Engineering Science*, McGraw Hill, Maidenhead, UK **1971**; c) D. W. Hahn, M. N. Özisik, *Heat Conduction*, Wiley, Hoboken, NJ, USA **2012**; d) X. Y. Huang, C. Y. Zhi, *Polymer Nanocomposites: Electrical and Thermal Properties*, Springer International Publishing, Switzerland **2016**; e) T. M. Tritt, *Thermal Conductivity: Theory, Properties, and Applications*, Springer, Boston, MA **2004**.
- [13] X. Li, Y. Long, L. Ma, J. Li, J. Yin, W. Guo, *2D Mater.* **2021**, *8*, 034002.
- [14] G. S. WAS, *Fundamentals of Radiation Materials Science: Metals and Alloys*, Springer, New York, USA **2016**.
- [15] a) J. He, X. Li, D. Su, H. Ji, X. Wang, *J. Eur. Ceram. Soc.* **2016**, *36*, 1487; b) F. Wang, L. Dou, J. Dai, Y. Li, L. Huang, Y. Si, J. Yu, B. Ding, *Angew. Chem., Int. Ed.* **2020**, *59*, 8285; c) C. Ferraro, E. Garcia-Tuñon, V. G. Rocha, S. Barg, M. D. Fariñas, T. E. G. Alvarez-Arenas, G. Sernicola, F. Giuliani, E. Saiz, *Adv. Funct. Mater.* **2016**, *26*, 1636; d) X. Xu, Q. Zhang, M. Hao, Y. Hu, Z. Lin, L. Peng, T. Wang, X. Ren, C. Wang, Z. Zhao, C. Wan, H. Fei, L. Wang, J. Zhu, H. Sun, W. Chen, T. Du, B. Deng, G. J. Cheng, I. Shakir, C. Darnes, T. S. Fisher, X. Zhang, H. Li, Y. Huang, X. Duan, *Science* **2019**, *363*, 723; e) X. Dong, G. Sui, J. Liu, A. Guo, S. Ren, M. Wang, H. Du, *Compos. Sci. Technol.* **2014**, *100*, 92.
- [16] Q. Ma, S. Liao, Y. Ma, Y. Chu, Y. Wang, *Adv. Mater.* **2021**, *33*, 2102096.
- [17] a) A. Sharma, R. Kositski, O. Kovalenko, D. Mordehai, E. Rabkin, *Acta Mater.* **2020**, *198*, 72; b) B. Gludovatz, A. Hohenwarter, D. Catoor, E. H. Chang, E. P. George, R. O. Ritchie, *Science* **2014**, *345*, 1153; c) S. Lv, Y. Zu, G. Chen, B. Zhao, X. Fu, W. Zhou, *Mater. Sci. Eng., A* **2020**, *795*, 140035.
- [18] K. Yang, J. Guan, K. Numata, C. Wu, S. Wu, Z. Shao, R. O. Ritchie, *Nat. Commun.* **2019**, *10*, 3786.
- [19] J. Peng, B. Chen, Z. Wang, J. Guo, B. Wu, S. Hao, Q. Zhang, L. Gu, Q. Zhou, Z. Liu, S. Hong, S. You, A. Fu, Z. Shi, H. Xie, D. Cao, C. Lin, G. Fu, L. Zheng, Y. Jiang, N. Zheng, *Nature* **2020**, *586*, 390.
- [20] G. Ackland, *Science* **2010**, *327*, 1587.
- [21] C. Lu, L. Niu, N. Chen, K. Jin, T. Yang, P. Xiu, Y. Zhang, F. Gao, H. Bei, S. Shi, M. R. He, I. M. Robertson, W. J. Weber, L. Wang, *Nat. Commun.* **2016**, *7*, 13564.
- [22] R. Al-Jishi, G. Dresselhaus, *Phys. Rev. B* **1982**, *26*, 4514.
- [23] C. Lee, X. Wei, W. Kysar Jeffrey, J. Hone, *Science* **2008**, *321*, 385.
- [24] M. Zhang, D. He, X. Zhang, Y. Xu, W. Wang, J. Liang, B. Wei, D. Wu, *Chin. J. High Pressure Phys.* **1998**, *12*, 17.
- [25] a) W. J. Evans, L. Hu, P. Kebinski, *Appl. Phys. Lett.* **2010**, *96*, 203112; b) A. A. Balandin, S. Ghosh, W. Bao, I. Calizo, D. Teweldebrhan, F. Miao, C. N. Lau, *Nano Lett.* **2008**, *8*, 902; c) C. Subramaniam, Y. Yasuda, S. Takeya, S. Ata, A. Nishizawa, D. N. Futaba, T. Yamada, K. Hata, *Nanoscale* **2014**, *6*, 2669.
- [26] a) K. I. Bolotin, K. J. Sikes, Z. Jiang, M. Klima, G. Fudenberg, J. Hone, P. Kim, H. L. Stormer, *Solid State Commun.* **2008**, *146*, 351; b) X. Du, I. Skachko, A. Barker, E. Y. Andrei, *Nat. Nanotechnol.* **2008**, *3*, 491; c) Y. Cui, Z. Zhong, D. Wang, W. U. Wang, C. M. Lieber, *Nano Lett.* **2003**, *3*, 149.
- [27] T. W. Ebbesen, H. J. Lezec, H. Hiura, J. W. Bennett, H. F. Ghaemi, T. Thio, *Nature* **1996**, *382*, 54.
- [28] a) G. Chen, D. N. Futaba, H. Kimura, S. Sakurai, M. Yumura, K. Hata, *ACS Nano* **2013**, *7*, 10218; b) P. Kim, L. Shi, A. Majumdar, P. L. McEuen, *Phys. Rev. Lett.* **2001**, *87*, 215502; c) C. Yu, L. Shi, Z. Yao, D. Li, A. Majumdar, *Nano Lett.* **2005**, *5*, 1842.
- [29] E. Pop, D. Mann, Q. Wang, K. Goodson, H. Dai, *Nano Lett.* **2006**, *6*, 96.
- [30] M. F. Ashby, *Acta Metall.* **1989**, *37*, 1273.
- [31] a) Y. Si, X. Wang, L. Dou, J. Yu, B. Ding, *Sci. Adv.* **2018**, *4*, 8925; b) L. Dou, X. Cheng, X. Zhang, Y. Si, J. Yu, B. Ding, *J. Mater. Chem. A* **2020**, *8*, 7775; c) X. Zhang, F. Wang, L. Dou, X. Cheng, Y. Si, J. Yu, B. Ding, *ACS Nano* **2020**, *14*, 15616.
- [32] a) M. F. El-Amin, *Viscoelastic and Viscoplastic Materials*, Intech, Rijeka, Croatia **2016**; b) M. F. Ashby, *Materials Selection in Mechanical Design*, Elsevier, Burlington, MA, USA **2011**.
- [33] T. A. Schaedler, A. J. Jacobsen, A. Torrents, A. E. Sorensen, J. Lian, J. R. Greer, L. Valdevit, W. B. Carter, *Science* **2011**, *334*, 962.
- [34] a) D. Akbarimehr, K. Fakharian, *Soil Dyn. Earthquake Eng.* **2021**, *140*, 106435; b) X. Wang, S. Zhan, Z. Lu, J. Li, X. Yang, Y. Qiao, Y. Men, J. Sun, *Adv. Mater.* **2020**, *32*, 2005759.
- [35] a) S. Pathak, Z. G. Cambaz, S. R. Kalidindi, J. G. Swadener, Y. Gogotsi, *Carbon* **2009**, *47*, 1969; b) C. Li, Y.-W. Ding, B.-C. Hu, Z.-Y. Wu, H.-L. Gao, H.-W. Liang, J.-F. Chen, S.-H. Yu, *Adv. Mater.* **2020**, *32*, 1904331; c) Q. Liu, M. Li, Y. Gu, S. Wang, Y. Zhang, Q. Li, L. Gao, Z. Zhang, *Carbon* **2015**, *86*, 46; d) M. Xu, D. N. Futaba, M. Yumura, K. Hata, *Nano Lett.* **2011**, *11*, 3279; e) X. Yu, X. Zhang, J. Zou, Z. Lan, C. Jiang, J. Zhao, D. Zhang, M. Miao, Q. Li, *Adv. Mater. Interfaces* **2016**, *3*, 1600352; f) J. Zhao, X. Zhang, Z. Pan, Q. Li, *Adv. Mater. Interfaces* **2015**, *2*, 1500093; g) Z. L. Yu, B. Qin, Z. Y. Ma, J. Huang, S. C. Li, H. Y. Zhao, H. Li, Y. B. Zhu, H. A. Wu, S. H. Yu, *Adv. Mater.* **2019**, *31*, 1900651.
- [36] Y. Wu, N. Yi, L. Huang, T. Zhang, S. Fang, H. Chang, N. Li, J. Oh, J. A. Lee, M. Kozlov, A. C. Chipara, H. Terrones, P. Xiao, G. Long, Y. Huang, F. Zhang, L. Zhang, X. Lepro, C. Haines, M. D. Lima, N. P. Lopez, L. P. Rajukumar, A. L. Elias, S. Feng, S. J. Kim, N. T. Narayanan, P. M. Ajayan, M. Terrones, A. Aliev, P. Chu, et al., *Nat. Commun.* **2015**, *6*, 6141.
- [37] a) F. Guo, Y. Jiang, Z. Xu, Y. Xiao, B. Fang, Y. Liu, W. Gao, P. Zhao, H. Wang, C. Gao, *Nat. Commun.* **2018**, *9*, 881; b) L. Jing, H. Li, J. Lin, R. Y. Tay, S. H. Tsang, E. H. T. Teo, A. I. Y. Tok, *ACS Appl. Mater. Interfaces* **2018**, *10*, 9688; c) K. H. Kim, M. N. Tsui, M. F. Islam, *Chem. Mater.* **2017**, *29*, 2748; d) H. Sun, Z. Xu, C. Gao, *Adv. Mater.* **2013**, *25*, 2554; e) M. N. Tsui, K. H. Kim, M. F. Islam, *ACS Appl. Mater. Interfaces* **2017**, *9*, 37954.
- [38] a) F. Azimpour-Shishevan, H. Akbulut, M. Mohtadi-Bonab, *Polym. Test.* **2020**, *90*, 106745; b) Q. Cheng, J. Bao, J. Park, Z. Liang, C. Zhang, B. Wang, *Adv. Funct. Mater.* **2009**, *19*, 3219; c) B. Cho, J. Lee, S. Hwang, J. Han, H. Chae, Y. Park, *Composites, Part A* **2020**, *135*, 105938; d) Y. Han, X. Zhang, X. Yu, J. Zhao, S. Li, F. Liu, P. Gao, Y. Zhang, T. Zhao, Q. Li, *Sci. Rep.* **2015**, *5*, 11533; e) S. Saha, S. Bal, *Emerging Mater. Res.* **2019**, *8*, 408; f) X. Zhang, W. Li, P. Song, B. You, G. Sun, *Chem. Eng. J.* **2020**, *381*, 122784; g) R. Ismail, A. Ibrahim, M. Rusop, A. Adnan, *AIP Conf. Proc.* **2018**, *1963*, 020005.
- [39] a) D. Bansal, S. Pillay, U. Vaidya, *Carbon* **2013**, *55*, 233; b) Y. Wang, C. Sun, X. Sun, J. Hinkley, G. M. Odegard, T. S. Gates, *Compos. Sci. Technol.* **2003**, *63*, 1581.
- [40] E. E. Martinez-Flores, J. Negrete, G. Torres-Villaseñor, *J. Therm. Anal. Calorim.* **2009**, *97*, 891.
- [41] a) E. Wittenberg, A. Meyer, S. Eggers, V. Abetz, *Soft Matter* **2018**, *14*, 2701; b) J. Huang, Y. Xu, S. Qi, J. Zhou, W. Shi, T. Zhao, M. Liu, *Nat. Commun.* **2021**, *12*, 3610; c) T. Wang, M. Long, H. Zhao, B. Liu, H. Shi, W. An, S. Li, S. Xu, Y. Wang, *J. Mater. Chem. A* **2020**, *8*, 18698; d) W. Xu, D. Ravichandran, S. Jambulkar, Y. Zhu, K. Song, *Adv. Funct. Mater.* **2021**, *31*, 2009311.
- [42] Q. Zhang, X. Xu, D. Lin, W. Chen, G. Xiong, Y. Yu, T. S. Fisher, H. Li, *Adv. Mater.* **2016**, *28*, 2229.
- [43] H. Gotoh, C. Liu, A. B. Imran, M. Hara, T. Seki, K. Mayumi, K. Ito, Y. Takeoka, *Sci. Adv.* **2018**, *4*, eaat7629.
- [44] a) J. R. Lloyd, J. Clemens, R. Snede, *Microelectron. Reliab.* **1999**, *39*, 1595; b) J. R. Black, *Proc. IEEE* **1969**, *57*, 1587; c) W. H. Preece, *Proc. R. Soc. London* **1888**, *43*, 280.
- [45] a) J. G. Park, S. Li, R. Liang, X. Fan, C. Zhang, B. Wang, *Nanotechnology* **2008**, *19*, 185710; b) L. Song, G. Toth, J. Wei, Z. Liu, W. Gao, L. Ci, R. Vajtai, M. Endo, P. M. Ajayan, *Nanotechnology* **2012**, *23*,

- 015703; c) R. Murali, Y. Yang, K. Brenner, T. Beck, J. D. Meindl, *Appl. Phys. Lett.* **2009**, *94*, 243114; d) Z. Xu, Y. Liu, X. Zhao, L. Peng, H. Sun, Y. Xu, X. Ren, C. Jin, P. Xu, M. Wang, C. Gao, *Adv. Mater.* **2016**, *28*, 6449; e) Z. Yao, C. L. Kane, C. Dekker, *Phys. Rev. Lett.* **2000**, *84*, 2941; f) X. Wang, N. Behabtu, C. C. Young, D. E. Tsentalovich, M. Pasquali, J. Kono, *Adv. Funct. Mater.* **2014**, *24*, 3241; g) Y. Zhao, J. Wei, R. Vajtai, P. M. Ajayan, E. V. Barrera, *Sci. Rep.* **2011**, *1*, 83.
- [46] a) C. Subramaniam, T. Yamada, K. Kobashi, A. Sekiguchi, D. N. Futaba, M. Yumura, K. Hata, *Nat. Commun.* **2013**, *4*, 2202; b) K. Zhao, T. Zhang, A. Ren, Y. Yang, P. Xiao, Z. Ge, Y. Ma, Y. Chen, *Carbon* **2019**, *141*, 198; c) X. Chen, J. Tao, J. Yi, Y. Liu, R. Bao, C. Li, *J. Alloys Compd.* **2018**, *735*, 163; d) J. Zou, D. Liu, J. Zhao, L. Hou, T. Liu, X. Zhang, Y. Zhao, Y. T. Zhu, Q. Li, *ACS Appl. Mater. Interfaces* **2018**, *10*, 8197; e) X. Ye, M. Li, D. Li, B. Li, Y. Zhang, *J. Appl. Phys.* **2018**, *124*, 175105; f) S. J. Kim, D. H. Shin, Y. S. Choi, H. Rho, M. Park, B. J. Moon, Y. Kim, S. K. Lee, D. S. Lee, T. W. Kim, S. H. Lee, K. S. Kim, B. H. Hong, S. Bae, *ACS Nano* **2018**, *12*, 2803.
- [47] a) K. Hayashi, M. Eguchi, Y. Miyazaki, *J. Electron. Mater.* **2016**, *46*, 2710; b) Y. Ocak, S. Aksöz, N. Maraşlı, K. Keşlioğlu, *J. Non-Cryst. Solids* **2010**, *356*, 1795; c) A. L. Smirnov, S. G. Taluts, A. D. Ivliev, V. I. Gorbatov, V. F. Polev, I. G. Korshunov, *High Temp.* **2017**, *55*, 380; d) V. B. Loboda, S. N. Khursenko, *J. Exp. Theor. Phys.* **2006**, *103*, 790; e) T. Pieríkos, S. Hałas, M. Czarnacki, *Vacuum* **2010**, *85*, 498.
- [48] a) H. Zhang, J. Li, B. Zhang, K. Yao, W. Liu, H. Wang, *Phys. Rev. B* **2007**, *75*, 205407; b) Y. Wei, K. Jiang, X. Feng, P. Liu, L. Liu, S. Fan, *Phys. Rev. B* **2007**, *76*, 045423; c) N. Behabtu, C. C. Young, D. E. Tsentalovich, O. Kleinerman, X. Wang, A. W. K. Ma, E. A. Bengio, R. F. ter Waarbeek, J. de Jong, R. E. Hoogerwerf, S. B. Fairchild, J. B. Ferguson, B. Maruyama, J. Kono, Y. Talmon, Y. Cohen, M. J. Otto, M. Pasquali, *Science* **2013**, *339*, 182; d) A. E. Aliev, C. Guthy, M. Zhang, S. Fang, A. A. Zakhidov, J. E. Fischer, R. H. Baughman, *Carbon* **2007**, *45*, 2880; e) Q. Shao, G. Liu, D. Teweldebrhan, A. A. Balandin, *Appl. Phys. Lett.* **2008**, *92*, 202108.
- [49] M. Xu, F. Du, S. Ganguli, A. Roy, L. Dai, *Nat. Commun.* **2016**, *7*, 13450.
- [50] G. Chen, D. N. Futaba, S. Sakurai, M. Yumura, K. Hata, *Carbon* **2014**, *67*, 318.
- [51] a) S. D. Shandakov, A. V. Kosobutsky, A. I. Vershinina, O. G. Sevostyanov, I. M. Chirkova, D. M. Russakov, M. V. Lomakin, M. S. Rybakov, T. V. Glushkova, E. A. Ovcharenko, M. A. Zhilyaeva, A. G. Nasibulin, *Mater. Sci. Eng. B* **2021**, *269*, 115178; b) Y. H. Song, J. T. Di, C. Zhang, J. N. Zhao, Y. Y. Zhang, D. M. Hu, M. Li, Z. G. Zhang, H. Z. Wei, Q. W. Li, *Nanoscale* **2019**, *11*, 13909.
- [52] a) A. B. Kaiser, *Rep. Prog. Phys.* **2001**, *64*, <https://doi.org/10.1088/0034-4885/64/1/201>; b) A. B. Kaiser, G. Dusberg, S. Roth, *Phys. Rev. B* **1998**, *57*, 1418.
- [53] H. M. Xiang, Y. Xing, F. Z. Dai, H. J. Wang, L. Su, L. Miao, G. J. Zhang, Y. G. Wang, X. W. Qi, L. Yao, H. L. Wang, B. Zhao, J. Q. Li, Y. C. Zhou, *J. Adv. Ceram.* **2021**, *10*, 385.
- [54] a) A. A. Balandin, *Nat. Mater.* **2011**, *10*, 569; b) A. Miranda, N. Barekar, B. J. McKay, *J. Alloys Compd.* **2019**, *774*, 820; c) C. Yu, K. Chen, H. Cheng, W. Chen, *Comput. Mater. Sci.* **2016**, *117*, 127; d) Alamusi, N. Hu, B. Jia, M. Arai, C. Yan, J. Li, Y. Liu, S. Atobe, H. Fukunaga, *Comput. Mater. Sci.* **2012**, *54*, 249; e) Q. Liang, X. Yao, W. Wang, Y. Liu, C. Wong, *ACS Nano* **2011**, *5*, 2392.
- [55] a) F. Mohammadi, N. Arab, S. S. Li, *Mater. Trans.* **2018**, *59*, 1251; b) I. H. Tseng, J. C. Chang, S. L. Huang, M. H. Tsai, *Polym. Int.* **2013**, *62*, 827; c) F. Zarei, S. Sheibani, *Diamond Relat. Mater.* **2021**, *113*, 108273.
- [56] a) P. Miranzo, M. Osendi, *Scr. Mater.* **2008**, *58*, 973; b) Q. Lü, S. F. Wang, L. J. Li, J. L. Wang, S. Y. Dai, W. Yu, G. S. Fu, *Sci. China Phys. Mech. Astron.* **2014**, *57*, 1644; c) S. Li, C. Wang, F. Yang, L. An, K. So, J. Li, *Mater. Today* **2021**, *46*, 35; d) L. Su, H. Wang, M. Niu, X. Fan, M. Ma, Z. Shi, S. Guo, *ACS Nano* **2018**, *12*, 3103.
- [57] S. Li, X. Yang, J. Hou, W. Du, *J. Magnesium Alloys* **2020**, *8*, 78.
- [58] a) X. H. Zhang, X. X. Ni, C. X. Li, B. You, G. Sun, *J. Mater. Chem. A* **2020**, *8*, 9701; b) W. Fan, X. Zhang, Y. Zhang, Y. F. Zhang, T. X. Liu, *Compos. Sci. Technol.* **2019**, *173*, 47; c) X. Y. Zhao, F. Yang, Z. C. Wang, P. M. Ma, W. F. Dong, H. Q. Hou, W. Fan, T. X. Liu, *Composites, Part B* **2020**, *182*, 107624.
- [59] a) J. Hone, M. C. Llaguno, N. M. Nemes, A. T. Johnson, J. E. Fischer, D. A. Walters, M. J. Casavant, J. Schmidt, R. E. Smalley, *Appl. Phys. Lett.* **2000**, *77*, 666; b) L. Peng, Z. Xu, Z. Liu, Y. Guo, P. Li, C. Gao, *Adv. Mater.* **2017**, *29*, 1700589.
- [60] S. Rouhi, R. Ansari, M. Ahmadi, *Mod. Phys. Lett. B* **2017**, *31*, 1750053.
- [61] a) G. X. Cao, X. Chen, J. W. Kysar, *J. Mech. Phys. Solids* **2006**, *54*, 1206; b) C. Li, T.-W. Chou, *Phys. Rev. B* **2005**, *71*, 235414.
- [62] G. Q. Xin, T. K. Yao, H. T. Sun, S. M. Scott, D. L. Shao, G. K. Wang, J. Lian, *Science* **2015**, *349*, 1083.
- [63] G. Q. Xin, H. T. Sun, T. Hu, H. R. Fard, X. Sun, N. Koratkar, T. Borca-Tasciuc, J. Lian, *Adv. Mater.* **2014**, *26*, 4521.
- [64] G. H. Chen, R. Sundaram, A. Sekiguchi, K. Hata, D. N. Futaba, *ACS Appl. Nano Mater.* **2021**, *4*, 869.
- [65] a) Z. Yan, G. Liu, J. M. Khan, A. A. Balandin, *Nat. Commun.* **2012**, *3*, 827; b) Y. Zhang, H. Han, N. Wang, P. Zhang, Y. Fu, M. Murugesan, M. Edwards, K. Jeppson, S. Volz, J. Liu, *Adv. Funct. Mater.* **2015**, *25*, 4430.
- [66] a) A. R. Abu Talib, L. H. Abbud, A. Ali, F. Mustapha, *Mater. Des.* **2012**, *35*, 12; b) P. Murugan, K. Naresh, K. Shankar, R. Velmurugan, G. Balaganesan, *Mater. Today Proc.* **2018**, *5*, 16946; c) G. Balaganesan, R. Velmurugan, M. Srinivasan, N. K. Gupta, K. Kanniy, *Int. J. Impact Eng.* **2014**, *74*, 57.
- [67] a) A. K. Bandaru, S. Ahmad, N. Bhatnagar, *Composites, Part A* **2017**, *97*, 151; b) L. Sorrentino, C. Bellini, A. Corrado, W. Polini, R. Aricò, *Procedia Eng.* **2014**, *88*, 255.
- [68] a) K. S. Pandya, J. R. Pothnis, G. Ravikumar, N. K. Naik, *Mater. Des.* **2013**, *44*, 128; b) S. Y. Lee, G. D. Kim, S. J. Kim, C. H. Chang, *Shock Vib.* **2018**, *2018*, 7626075; c) R. Muñoz, F. Martínez-Hergueta, F. Gálvez, C. González, J. Llorca, *Compos. Struct.* **2015**, *127*, 141; d) J. Cheon, M. Kim, *Composites, Part B* **2021**, *217*, 108872; e) M. De Farias, S. Amico, L. Coelho, S. Pezzin, *Polym.-Plast. Technol. Mater.* **2019**, *59*, 517.
- [69] a) E. Sevkat, B. Liaw, F. Delale, B. B. Raju, *Composites, Part A* **2009**, *40*, 1090; b) V. S. Gálvez, F. Gálvez, D. Cendón, L. Sánchez, *Procedia Eng.* **2016**, *167*, 116; c) M. Pushparaja, G. Balaganesan, R. Velmurugan, N. K. Gupta, *Procedia Eng.* **2017**, *173*, 175.
- [70] a) J. Gibson, J. McKee, G. Freihofer, S. Raghavan, J. Gou, *Int. J. Smart Nano Mater.* **2013**, *4*, 212; b) K. S. Pandya, N. K. Naik, *Int. J. Impact Eng.* **2015**, *76*, 49; c) L. Zhang, R. Wang, J. Wang, L. Wu, X. Zhang, *Nanoscale* **2019**, *11*, 2343; d) N. M. Hassan, Z. Bahroun, A. Mohamed, A. Baker, K. Jijakli, A. Saqr, *Compos. Struct.* **2021**, *258*, 113432; e) F. Heidari, M. Aghalari, A. C. Tehran, K. Shelesh-Nezhad, *J. Thermoplast. Compos. Mater.* **2020**, *34*, 1037; f) E. Randjbaran, D. L. Majid, R. Zahari, M. T. H. Sultan, N. Mazlan, *Facta Univ. Ser. Mech. Eng.* **2020**, *18*, 229; g) K. L. Xiao, X. D. Lei, Y. Y. Chen, Q. An, D. M. Hu, C. Wang, X. Q. Wu, C. G. Huang, *Carbon* **2021**, *175*, 478; h) Z. Zhan, Y. Ma, J. Ren, X. Gao, L. Li, M. Xu, *Carbon* **2020**, *170*, 146.
- [71] S. Si, W. Li, X. Zhao, M. Han, Y. Yue, W. Wu, S. Guo, X. Zhang, Z. Dai, X. Wang, X. Xiao, C. Jiang, *Adv. Mater.* **2017**, *29*, 1604623.
- [72] K. P. So, D. Chen, A. Kushima, M. D. Li, S. Kim, Y. Yang, Z. G. Wang, J. G. Park, Y. H. Lee, R. I. Gonzalez, M. Kiwi, E. M. Bringa, L. Shao, J. Li, *Nano Energy* **2016**, *22*, 319.
- [73] J. Tang, G. Wei, X. C. Cai, S. L. Hu, T. D. Shen, T. Cheng, R. Yin, J. Zhang, X. F. Ruan, B. Yang, Y. Q. Wang, G. X. Cai, C. Z. Jiang, F. Ren, *Matter* **2020**, *3*, 1631.

- [74] J. Tang, T. Cheng, Y. Q. Wang, L. L. Hu, M. Q. Hong, W. J. Qin, G. X. Cai, C. Z. Jiang, F. Ren, *J. Eur. Ceram. Soc.* **2021**, *41*, 5280.
- [75] Y. Kim, J. Baek, S. Kim, S. Kim, S. Ryu, S. Jeon, S. M. Han, *Sci. Rep.* **2016**, *6*, 24785.
- [76] a) W. Sun, L. Wang, Z. Yang, J. Wang, G. Liu, *Mater. Lett.* **2021**, *284*, 128963; b) W. Sun, L. Wang, T. Wu, C. Dong, G. Liu, *Mater. Lett.* **2019**, *240*, 262; c) W. Sun, L. Wang, T. Wu, M. Wang, Z. Yang, Y. Pan, G. Liu, *Chem. Mater.* **2015**, *27*, 2367; d) S. Qiu, W. Li, W. Zheng, H. Zhao, L. Wang, *ACS Appl. Mater. Interfaces* **2017**, *9*, 34294; e) D. S. Chauhan, M. A. Quraishi, K. R. Ansari, T. A. Saleh, *Prog. Org. Coat.* **2020**, *147*, 105741; f) X. Wang, C. Li, M. Zhang, D. Lin, S. C. Yuan, F. Xu, Y. X. Zhou, C. J. Wang, Y. J. Zhu, H. Y. Wang, *Chern. Eng. J.* **2022**, *430*, 133156.
- [77] a) M. Zhu, Z. Du, Z. Yin, W. Zhou, Z. Liu, S. H. Tsang, E. H. Teo, *ACS Appl. Mater. Interfaces* **2016**, *8*, 502; b) N.-W. Pu, G.-N. Shi, Y.-M. Liu, X. Sun, J.-K. Chang, C.-L. Sun, M.-D. Ger, C.-Y. Chen, P.-C. Wang, Y.-Y. Peng, C.-H. Wu, S. Lawes, *J. Power Sources* **2015**, *282*, 248; c) Z. Zhao, T. Hou, N. Wu, S. Jiao, K. Zhou, J. Yin, J. W. Suk, X. Cui, M. Zhang, S. Li, Y. Qu, W. Xie, X. B. Li, C. Zhao, Y. Fu, R. D. Hong, S. Guo, D. Lin, W. Cai, W. Mai, Z. Luo, Y. Tian, Y. Lai, Y. Liu, L. Colombo, Y. Hao, *Nano Lett.* **2021**, *21*, 1161.
- [78] X. Jin, H. Tan, Z. Wu, J. Liang, W. Miao, C. S. Lian, J. Wang, K. Liu, H. Wei, C. Feng, P. Liu, Y. Wei, Q. Li, J. Wang, L. Liu, X. Li, S. Fan, W. Duan, K. Jiang, *Nano Lett.* **2019**, *19*, 6756.
- [79] D. Hu, W. Gong, J. Di, D. Li, R. Li, W. Lu, B. Gu, B. Sun, Q. Li, *Carbon* **2017**, *118*, 659.
- [80] P. Lv, X. W. Tan, K. H. Yu, R. L. Zheng, J. J. Zheng, W. Wei, *Carbon* **2016**, *99*, 222.
- [81] Z. Xu, Y. Zhang, P. Li, C. Gao, *ACS Nano* **2012**, *6*, 7103.
- [82] X. Yang, P. Liu, D. Zhou, F. Gao, X. Wang, S. Lv, Z. Yuan, X. Jin, W. Zhao, H. Wei, L. Zhang, J. Gao, Q. Li, S. Fan, K. Jiang, *Nano Res.* **2019**, *12*, 1855.
- [83] B. Román-Manso, J. J. Moyano, D. Pérez-Coll, M. Belmonte, P. Miranzo, M. I. Osendí, *J. Eur. Ceram. Soc.* **2018**, *38*, 2265.
- [84] Y. K. Choi, Y. Gotoh, K. I. Sugimoto, S. M. Song, T. Yanagisawa, M. Endo, *Polymer* **2005**, *46*, 11489.
- [85] T. Hayashi, Y. A. Kim, T. Natsuki, M. Endo, *ChemPhysChem* **2007**, *8*, 999.
- [86] L. S. Walker, V. R. Marotto, M. A. Rafiee, N. Koratkar, E. L. Corral, *ACS Nano* **2011**, *5*, 3182.
- [87] S. Zhang, L. Kang, X. Wang, L. Tong, L. Yang, Z. Wang, K. Qi, S. Deng, Q. Li, X. Bai, F. Ding, J. Zhang, *Nature* **2017**, *543*, 234.
- [88] Y. S. Yeom, K. Y. Cho, H. Y. Seo, J. S. Lee, D. H. Im, C. Y. Nam, H. G. Yoon, *Compos. Sci. Technol.* **2020**, *186*, 107915.
- [89] H. M. Jeong, J. W. Lee, W. H. Shin, Y. J. Choi, H. J. Shin, J. K. Kang, J. W. Choi, *Nano Lett.* **2011**, *11*, 2472.
- [90] M. Zhang, S. Fang, J. Nie, P. Fei, A. E. Aliev, R. H. Baughman, M. Xu, *Adv. Funct. Mater.* **2020**, *30*, 2004564.
- [91] a) W. Zhou, Z. Han, J. Wang, Y. Zhang, Z. Jin, X. Sun, Y. Zhang, C. Yan, Y. Li, *Nano Lett.* **2006**, *6*, 2987; b) T. Pei, Z. Zhang, Z. Wang, L. Ding, S. Wang, L.-M. Peng, *Adv. Funct. Mater.* **2011**, *21*, 1843.
- [92] a) Y. Wu, Y. Lin, A. Bol, K. Jenkins, F. Xia, D. Farmer, Y. Zhu, P. Avouris, *Nature* **2011**, *472*, 74; b) F. Zhu, X. Lin, P. Liu, K. Jiang, Y. Wei, Y. Wu, J. Wang, S. Fan, *Nano Res.* **2015**, *7*, 553; c) W. Cai, A. Moore, Y. Zhu, X. Li, S. Chen, L. Shi, R. Ruoff, *Nano Lett.* **2010**, *10*, 1645; d) X. Li, W. Cai, J. An, S. Kim, J. Nah, D. Yang, R. Piner, A. Velamakanni, I. Jung, E. Tutuc, S. K. Banerjee, L. Colombo, R. S. Ruoff, *Science* **2009**, *324*, 1312.
- [93] a) L. Qu, L. Dai, *Adv. Mater.* **2007**, *19*, 3844; b) C. Lutz, Z. Ma, R. Thelen, J. Syurik, O. Il'in, O. Ageev, P. Jouanne, H. Hölscher, *Tribol. Lett.* **2019**, *67*, 10; c) Y. Eun, J.-I. Lee, J. Choi, Y. Song, J. Kim, *Adv. Mater.* **2011**, *23*, 4285.
- [94] M. Xu, D. N. Futaba, M. Yumura, K. Hata, *ACS Nano* **2012**, *6*, 5837.
- [95] a) Q. Song, F. Ye, X. Yin, W. Li, H. Li, Y. Liu, K. Li, K. Xie, X. Li, Q. Fu, L. Cheng, L. Zhang, B. Wei, *Adv. Mater.* **2017**, *29*, 1701583;
- b) X. F. Zhao, C. Z. Hang, X. H. Wen, M. Y. Liu, H. Zhang, F. Yang, R. G. Ma, J. C. Wang, D. W. Zhang, H. L. Lu, *ACS Appl. Mater. Interfaces* **2020**, *12*, 14136.
- [96] Y. Bai, H. Yue, J. Wang, B. Shen, S. Sun, S. Wang, H. Wang, X. Li, Z. Xu, R. Zhang, F. Wei, *Science* **2020**, *369*, 1104.
- [97] a) M. Kumar, Y. Ando, J. Nanosci. Nanotechnol. **2010**, *10*, 3739; b) J. P. Tessonner, D. S. Su, *ChemSusChem* **2011**, *4*, 824.
- [98] V. Jourdain, C. Bichara, *Carbon* **2013**, *58*, 2.
- [99] R. Muñoz, C. Gómez-Aleixandre, *Chem. Vap. Deposition* **2013**, *19*, 297.
- [100] J. Pang, A. Bachmatiuk, I. Ibrahim, L. Fu, D. Placha, G. S. Martynkova, B. Trzebicka, T. Gemming, J. Eckert, M. H. Rümmeli, *J. Mater. Sci.* **2015**, *51*, 640.
- [101] a) Y. Hu, L. Kang, Q. Zhao, H. Zhong, S. Zhang, L. Yang, Z. Wang, J. Lin, Q. Li, Z. Zhang, L. Peng, Z. Liu, J. Zhang, *Nat. Commun.* **2015**, *6*, 6099; b) L. Kang, Y. Hu, H. Zhong, J. Si, S. Zhang, Q. Zhao, J. Lin, Q. Li, Z. Zhang, L. Peng, J. Zhang, *Nano Res.* **2015**, *8*, 3694.
- [102] Y. Xie, D. Zhong, C. Fan, X. Deng, L.-M. Peng, Z. Zhang, *Adv. Electron. Mater.* **2021**, *7*, 1701583.
- [103] a) K. Kim, Y. Oh, M. Islam, *Nat. Nanotechnol.* **2012**, *7*, 562; b) J. Afroze, L. Tong, M. Abden, Z. Yuan, Y. Chen, *Carbon* **2021**, *175*, 312.
- [104] Y. Li, L. Sun, F. Xu, S. Wang, Q. Peng, Z. Yang, X. He, Y. Li, *Nanoscale* **2019**, *11*, 1692.
- [105] L. Qiu, J. Z. Liu, S. L. Y. Chang, Y. Z. Wu, D. Li, *Nat. Commun.* **2012**, *3*, 1241.
- [106] Z. Xu, H. Sun, X. Zhao, C. Gao, *Adv. Mater.* **2013**, *25*, 188.
- [107] P.-X. Hou, J. Du, C. Liu, W. Ren, E. I. Kauppinen, H.-M. Cheng, *MRS Bull.* **2017**, *42*, 825.
- [108] Q. M. Zou, L. M. Deng, D. W. Li, Y. S. Zhou, H. R. Golgir, K. Keramatnejad, L. S. Fan, L. Jiang, J. F. Silvain, Y. F. Lu, *ACS Appl. Mater. Interfaces* **2017**, *9*, 37340.
- [109] a) W. Wu, J. Gui, W. Sai, Z. Xie, *J. Alloys Compd.* **2017**, *691*, 778; b) P. Cao, K. P. So, Y. Yang, J. G. Park, M. Li, L. Yan, J. Hu, M. Kirk, M. Li, Y. H. Lee, M. P. Short, J. Li, *Acta Mater.* **2021**, *203*, 116483.
- [110] a) M. Wang, S. Cai, C. Pan, C. Wang, X. Lian, Y. Zhuo, K. Xu, T. Cao, X. Pan, B. Wang, S.-J. Liang, J. J. Yang, P. Wang, F. Miao, *Nat. Electron.* **2018**, *1*, 130; b) Y. Yang, X. Yang, L. Liang, Y. Gao, H. Cheng, X. Li, M. Zou, A. Cao, R. Ma, Q. Yuan, X. Duan, *Science* **2019**, *364*, 1057; c) H. Wang, S. Hu, K. Takahashi, X. Zhang, H. Takamatsu, J. Chen, *Nat. Commun.* **2017**, *8*, 15843; d) Y. Wang, L. Xiang, W. Yang, Z. Li, Z. Fang, D. Zhou, P. Liu, X. Wei, *Adv. Funct. Mater.* **2019**, *30*, 1907814.
- [111] a) L. Lin, J. Li, Q. Yuan, Q. Li, J. Zhang, L. Sun, D. Rui, Z. Chen, K. Jia, M. Wang, Y. Zhang, M. Rummeli, N. Kang, H. Xu, F. Ding, H. Peng, Z. Liu, *Sci. Adv.* **2019**, *5*, 8337; b) J. Alvarenga, P. R. Jarosz, C. M. Schauer, B. T. Moses, B. J. Landi, C. D. Cress, R. P. Raffaelle, *Appl. Phys. Lett.* **2010**, *97*, 182106.
- [112] M. Lima, N. Li, M. Jung de Andrade, S. Fang, J. Oh, G. Spinks, M. Kozlov, C. Haines, D. Suh, J. Foroughi, S. Kim, Y. Chen, T. Ware, M. Shin, L. Machado, A. Fonseca, J. Madden, W. Voit, D. Galvao, R. Baughman, *Science* **2012**, *338*, 928.
- [113] P. Liu, L. Liu, Y. Wei, K. Liu, Z. Chen, K. Jiang, Q. Li, S. Fan, *Adv. Mater.* **2009**, *21*, 3563.
- [114] F. Luo, Y. Fan, G. Peng, S. Xu, Y. Yang, K. Yuan, J. Liu, W. Ma, W. Xu, Z. H. Zhu, X.-A. Zhang, A. Mishchenko, Y. Ye, H. Huang, Z. Han, W. Ren, K. S. Novoselov, M. Zhu, S. Qin, *ACS Photonics* **2019**, *6*, 2117.
- [115] Z. Liang, Y. Yao, B. Jiang, X. Wang, H. Xie, M. Jiao, C. Liang, H. Qiao, D. Kline, M. R. Zachariah, L. Hu, *Adv. Funct. Mater.* **2021**, *31*, 2102994.
- [116] J. Foroughi, G. M. Spinks, D. Antiohos, A. Mirabedini, S. Gambhir, G. G. Wallace, S. R. Ghorbani, G. Peleckis, M. E. Kozlov, M. D. Lima, R. H. Baughman, *Adv. Funct. Mater.* **2014**, *24*, 5859.

- [117] C. Zhang, Y. Song, H. Zhang, B. Lv, J. Qiao, N. Yu, Y. Zhang, J. Di, Q. Li, *Nanoscale* **2019**, *11*, 4585.
- [118] P. Li, Y. Liu, S. Shi, Z. Xu, W. Ma, Z. Wang, S. Liu, C. Gao, *Adv. Funct. Mater.* **2020**, *30*, 2006584.
- [119] M. Zhang, K. R. Atkinson, R. H. Baughman, *Science* **2004**, *306*, 1358.
- [120] S. H. Kim, C. S. Haines, N. Li, K. J. Kim, T. J. Mun, C. Choi, J. Di, Y. J. Oh, J. P. Oviedo, J. Bykova, S. Fang, N. Jiang, Z. Liu, R. Wang, P. Kumar, R. Qiao, S. Priya, K. Cho, M. Kim, M. S. Lucas, L. F. Drummy, B. Maruyama, D. Y. Lee, X. Lepró, E. Gao, D. Albarq, R. Ovalle-Robles, S. J. Kim, R. H. Baughman, *Science* **2017**, *357*, 773.
- [121] Y. Xu, Y. Zhang, Z. Guo, J. Ren, Y. Wang, H. Peng, *Angew. Chem., Int. Ed.* **2015**, *54*, 15390.
- [122] M. Zhang, S. L. Fang, A. A. Zakhidov, S. B. Lee, A. E. Aliev, C. D. Williams, K. R. Atkinson, R. H. Baughman, *Science* **2005**, *309*, 1215.
- [123] a) D. P. Hashim, N. T. Narayanan, J. M. Romo-Herrera, D. A. Cullen, M. G. Hahm, P. Lezzi, J. R. Suttle, D. Kelkhoff, E. Muñoz-Sandoval, S. Ganguli, A. K. Roy, D. J. Smith, R. Vajtai, B. G. Sumpter, V. Meunier, H. Terrones, M. Terrones, P. M. Ajayan, *Sci. Rep.* **2012**, *2*, 363; b) M. A. Worsley, S. O. Kucheyev, J. H. Satcher, A. V. Hamza, T. F. Baumann, *Appl. Phys. Lett.* **2009**, *94*, 073115; c) H. Bi, I. W. Chen, T. Lin, F. Huang, *Adv. Mater.* **2015**, *27*, 5943; d) J. Di, S. Fang, F. A. Moura, D. S. Galvão, J. Bykova, A. Aliev, M. J. de Andrade, X. Lepró, N. Li, C. Haines, R. Ovalle-Robles, D. Qian, R. H. Baughman, *Adv. Mater.* **2016**, *28*, 6598; e) H. Hu, Z. Zhao, W. Wan, Y. Gogotsi, J. Qiu, *Adv. Mater.* **2013**, *25*, 2219.
- [124] Y. Wei, D. Weng, Y. Yang, X. Zhang, K. Jiang, L. Liu, S. Fan, *Appl. Phys. Lett.* **2006**, *89*, 063101.
- [125] M. Li, Y. Song, C. Zhang, Z. Yong, J. Qiao, D. Hu, Z. Zhang, H. Wei, J. Di, Q. Li, *Carbon* **2019**, *146*, 627.
- [126] H. Sun, R. Che, X. You, Y. Jiang, Z. Yang, J. Deng, L. Qiu, H. Peng, *Adv. Mater.* **2014**, *26*, 8120.
- [127] Y. You, H. R. Yao, S. Xin, Y. X. Yin, T. T. Zuo, C. P. Yang, Y. G. Guo, Y. Cui, L. J. Wan, J. B. Goodenough, *Adv. Mater.* **2016**, *28*, 7243.
- [128] Y. Wang, J. Ren, X. Gao, W. Zhang, H. Duan, M. Wang, J. Shui, M. Xu, *Small* **2018**, *14*, 1802913.
- [129] Y.-Y. Wang, B.-H. Hou, J.-Z. Guo, Q.-L. Ning, W.-L. Pang, J. Wang, C.-L. Lü, X.-L. Wu, *Adv. Energy Mater.* **2018**, *8*, 1703252.
- [130] X. Jin, G. Sun, G. Zhang, H. Yang, Y. Xiao, J. Gao, Z. Zhang, L. Qu, *Nano Res.* **2019**, *12*, 1199.
- [131] X. Gao, X. Du, T. S. Mathis, M. Zhang, X. Wang, J. Shui, Y. Gogotsi, M. Xu, *Nat. Commun.* **2020**, *11*, 6160.
- [132] a) Z. Luo, D. Chen, X. Wang, J. Huang, Y. Pan, W. Lei, J. Pan, *Small* **2021**, *17*, 2008163; b) Z. Yu, B. Wang, X. Liao, K. Zhao, Z. Yang, F. Xia, C. Sun, Z. Wang, C. Fan, J. Zhang, Y. Wang, *Adv. Energy Mater.* **2020**, *10*, 2000907; c) S. J. Shi, J. P. Tu, Y. Y. Tang, Y. Q. Zhang, X. Y. Liu, X. L. Wang, C. D. Gu, *J. Power Sources* **2013**, *225*, 338; d) G. Backert, B. Oschmann, M. N. Tahir, F. Mueller, I. Lieberwirth, B. Balke, W. Tremel, S. Passerini, R. Zentel, *J. Colloid Interface Sci.* **2016**, *478*, 155; e) X. Wei, Y. Ren, *Electrochim. Acta* **2015**, *180*, 323; f) S.-J. Yoon, S.-T. Myung, Y.-K. Sun, *J. Electrochem. Soc.* **2014**, *161*, A1514; g) X. Xu, R. Cao, S. Jeong, J. Cho, *Nano Lett.* **2012**, *12*, 4988; h) Y. Yan, L. Ben, Y. Zhan, X. Huang, *Electrochim. Acta* **2016**, *187*, 186; i) A. Ponrouch, M. R. Palacín, *Electrochim. Commun.* **2015**, *54*, 51; j) Y. Li, Y. Yuan, Y. Bai, Y. Liu, Z. Wang, L. Li, F. Wu, K. Amine, C. Wu, J. Lu, *Adv. Energy Mater.* **2018**, *8*, 1702781; k) L. Xiao, H. Lu, Y. Fang, M. L. Sushko, Y. Cao, X. Ai, H. Yang, J. Liu, *Adv. Energy Mater.* **2018**, *8*, 1703238; l) Y. Liu, B. Yang, X. Dong, Y. Wang, Y. Xia, *Angew. Chem., Int. Ed. Engl.* **2017**, *56*, 16606; m) R. Raccichini, A. Varzi, V. S. K. Chakravadhanula, C. Kübel, A. Balducci, S. Passerini, *J. Power Sources* **2015**, *281*, 318; n) J. Xu, X. Wang, N. Yuan, B. Hu, J. Ding, S. Ge, *J. Power Sources* **2019**, *430*, 74; o) S. Xu, L. Zhang, H. Zhang, M. Wei, X. Guo, S. Zhang, *Mater. Today Energy* **2020**, *18*, 100495; p) X. Wang, W. Zhao, W. Zhang, K. W. Wong, J. Wu, T. Chen, S. Huang, *ACS Sustainable Chem. Eng.* **2021**, *9*, 11705.
- [133] a) W. Li, K. Xu, L. An, F. Jiang, X. Zhou, J. Yang, Z. Chen, R. Zou, J. Hu, *J. Mater. Chem. A* **2014**, *2*, 1443; b) J. Yan, E. Khoo, A. Sumboja, P. S. Lee, *ACS Nano* **2010**, *4*, 4247; c) A. J. Roberts, A. F. Danil de Namor, R. C. Slade, *Phys. Chem. Chem. Phys.* **2013**, *15*, 3518; d) W. Meng, W. Chen, L. Zhao, Y. Huang, M. Zhu, Y. Huang, Y. Fu, F. Geng, J. Yu, X. Chen, C. Zhi, *Nano Energy* **2014**, *8*, 133; e) J. Tian, C. Cui, Q. Xie, W. Qian, C. Xue, Y. Miao, Y. Jin, G. Zhang, B. Guo, *J. Mater. Chem. A* **2018**, *6*, 3593; f) Y. Liu, H. Li, X. Wang, T. Lv, K. Dong, Z. Chen, Y. Yang, S. Cao, T. Chen, *J. Mater. Chem. A* **2021**, *9*, 12051; g) Z. Lin, P.-L. Taberna, P. Simon, *Electrochim. Acta* **2016**, *206*, 446; h) N. Kurra, M. K. Hota, H. N. Alshareef, *Nano Energy* **2015**, *13*, 500; i) Z. Z. Liu, J. M. Zhang, J. Liu, Y. J. Long, L. M. Fang, Q. W. Wang, T. Liu, *J. Mater. Chem. A* **2020**, *8*, 6219; j) Y.-T. Weng, H.-A. Pan, N.-L. Wu, G. Z. Chen, *J. Power Sources* **2015**, *274*, 1118; k) J. Lei, Z. Jiang, X. Lu, G. Nie, C. Wang, *Electrochim. Acta* **2015**, *176*, 149; l) Y. Zhou, M. Ghaffari, M. Lin, H. Xu, H. Xie, C. M. Koo, Q. M. Zhang, *RSC Adv.* **2015**, *5*, 71699; m) W.-Y. Tsai, R. Lin, S. Murali, L. Li Zhang, J. K. McDonough, R. S. Ruoff, P.-L. Taberna, Y. Gogotsi, P. Simon, *Nano Energy* **2013**, *2*, 403; n) J. Kong, G. Xiong, Z. Bo, X. Lu, K. Yi, W. Kuang, S. Yang, H. Yang, S. Tian, J. Yan, K. Cen, *ChemElectroChem* **2019**, *6*, 2788.
- [134] G. L. Wang, Z. P. Ma, G. J. Shao, L. X. Kong, W. M. Gao, *J. Power Sources* **2015**, *291*, 209.
- [135] a) C. Xia, W. Chen, X. Wang, M. N. Hedhili, N. Wei, H. N. Alshareef, *Adv. Energy Mater.* **2015**, *5*, 1401805; b) Y. Sun, N. Liu, Y. Cui, *Nat. Energy* **2016**, *1*, 16071; c) M. Keppeler, N. Shen, S. Nageswaran, M. Srinivasan, *J. Mater. Chem. A* **2016**, *4*, 18223.
- [136] J. Lin, Z. Peng, Y. Liu, F. Ruiz-Zepeda, R. Ye, E. L. G. Samuel, M. J. Yacaman, B. I. Yakobson, J. M. Tour, *Nat. Commun.* **2014**, *5*, 5714.
- [137] A. Kaidarova, M. A. Khan, M. Marengo, L. Swanepoel, A. Przybysz, C. Muller, A. Fahlman, U. Buttner, N. R. Geraldi, R. P. Wilson, C. M. Duarte, J. Kosel, *npj Flexible Electron.* **2019**, *3*, 15.
- [138] A. Kaidarova, N. Alsharif, B. N. M. Oliveira, M. Marengo, N. R. Geraldi, C. M. Duarte, J. Kosel, *Global Challenges* **2020**, *4*, 2000001.
- [139] Y. Li, S. Luo, M. C. Yang, R. Liang, C. Zeng, *Adv. Funct. Mater.* **2016**, *26*, 2900.
- [140] a) D. Kim, J. Yoon, *ACS Appl. Mater. Interfaces* **2020**, *12*, 20965; b) X. Su, H. Li, X. Lai, Z. Chen, X. Zeng, *Adv. Funct. Mater.* **2019**, *29*, 1900554; c) Y. Liang, P. Xiao, F. Ni, L. Zhang, T. Zhang, S. Wang, W. Zhou, W. Lu, S.-W. Kuo, T. Chen, *Nano Energy* **2021**, *81*, 105617; d) P. Ahuja, S. K. Ujjaini, K. Uruta, A. Furuse, I. Moriguchi, K. Kaneko, *Chem. Eng. J.* **2020**, *388*, 124174; e) X. Sun, S. He, Z. Qin, J. Li, F. Yao, *Compos. Commun.* **2021**, *26*, 100784.
- [141] a) H. Liu, Q. Li, Y. Bu, N. Zhang, C. Wang, C. Pan, L. Mi, Z. Guo, C. Liu, C. Shen, *Nano Energy* **2019**, *66*, 104143; b) Z. Chu, W. Jiao, Y. Huang, Y. Zheng, R. Wang, X. He, *J. Mater. Chem. A* **2021**, *9*, 9634.
- [142] a) M. Jian, K. Xia, Q. Wang, Z. Yin, H. Wang, C. Wang, H. Xie, M. Zhang, Y. Zhang, *Adv. Funct. Mater.* **2017**, *27*, 1606066; b) B. B. Bhatt, L. Kumar, A. Kushwaha, D. Gupta, *Sens. Actuators, A* **2021**, *331*, 112875.
- [143] Y. Ni, J. Huang, S. Li, X. Dong, T. Zhu, W. Cai, Z. Chen, Y. Lai, *ACS Appl. Mater. Interfaces* **2021**, *13*, 53271.
- [144] L. Liu, J. Han, L. Xu, J. Zhou, C. Zhao, S. Ding, H. Shi, M. Xiao, L. Ding, Z. Ma, C. Jin, Z. Zhang, L. Peng, *Science* **2020**, *368*, 850.
- [145] S. J. Jeong, S. Jo, J. Lee, K. Yang, H. Lee, C. S. Lee, H. Park, S. Park, *Nano Lett.* **2016**, *16*, 5378.
- [146] F. Schwierz, *Nat. Nanotechnol.* **2010**, *5*, 487.
- [147] C. Chen, Y. Lin, W. Zhou, M. Gong, Z. He, F. Shi, X. Li, J. Z. Wu, K. T. Lam, J. N. Wang, F. Yang, Q. Zeng, J. Guo, W. Gao, J.-M. Zuo,

- J. Liu, G. Hong, A. L. Antaris, M.-C. Lin, W. L. Mao, H. Dai, *Nat. Electron.* **2021**, *4*, 653.
- [148] Y. Yin, Z. Cheng, L. Wang, K. Jin, W. Wang, *Sci. Rep.* **2014**, *4*, 5758.
- [149] C. Qiu, F. Liu, L. Xu, B. Deng, M. Xiao, J. Si, L. Lin, Z. Zhang, J. Wang, H. Guo, H. Peng, L.-M. Peng, *Science* **2018**, *361*, 387.
- [150] M. Šiškins, C. Mullan, S.-K. K. Son, J. Yin, K. Watanabe, T. Taniguchi, D. Ghazaryan, K. S. Novoselov, A. Mishchenko, *Appl. Phys. Lett.* **2019**, *114*, 123104.
- [151] C. Subramaniam, A. Sekiguchi, T. Yamada, D. N. Futaba, K. Hata, *Nanoscale* **2016**, *8*, 3888.
- [152] L. Qian, Y. Xie, M. Zou, J. Zhang, *J. Am. Ceram. Soc.* **2021**, *143*, 18805.
- [153] K. Kim, J. Y. Choi, T. Kim, S. H. Cho, H. J. Chung, *Nature* **2011**, *479*, 338.
- [154] a) Y. Gao, J. Chen, G. Chen, C. Fan, X. Liu, *Small Methods* **2021**, *5*, 2100771; b) D. V. Kosynkin, A. L. Higginbotham, A. Sinitskii, J. R. Lomeda, A. Dimiev, B. K. Price, J. M. Tour, *Nature* **2009**, *458*, 872; c) M. Kolmer, A.-K. Steiner, I. Izquierdo, W. Ko, M. Engelund, M. Szymonski, A.-P. Li, K. Amsharov, *Science* **2020**, *369*, 571.
- [155] a) M. Y. Han, B. Oezilmaz, Y. Zhang, P. Kim, *Phys. Rev. Lett.* **2007**, *98*, 206805; b) P. Kim, M. Y. Han, A. F. Young, I. Meric, K. L. Shepard, in *2009 IEEE Int. Electron Devices Meeting (IEDM)*, IEEE, Piscataway, NJ, USA, December, **2009**, <https://doi.org/10.1109/IEDM.2009.5424379>; c) X. Li, X. Wang, L. Zhang, S. Lee, H. Dai, *Science* **2008**, *319*, 1229; d) L. Yang, C. H. Park, Y. W. Son, M. L. Cohen, S. G. Louie, *Phys. Rev. Lett.* **2007**, *99*, 186801; e) Z. Chen, Y. M. Lin, M. J. Rooks, P. Avouris, *Phys. E* **2007**, *40*, 228; f) M. Evaldsson, I. V. Zozoulenko, H. Xu, T. Heinzel, *Phys. Rev. B* **2008**, *78*, 161407; g) H. S. Wang, L. Chen, K. Elbilo, L. He, H. Wang, C. Chen, C. Jiang, C. Li, T. Wu, C. X. Cong, T. J. Pennycook, G. Argentero, D. Zhang, K. Watanabe, T. Taniguchi, W. Wei, Q. Yuan, J. C. Meyer, X. Xie, *Nat. Mater.* **2021**, *20*, 202.
- [156] a) J. H. Chen, C. Jang, S. Xiao, M. Ishigami, M. S. Fuhrer, *Nat. Nanotechnol.* **2008**, *3*, 206; b) F. Chen, J. Xia, D. K. Ferry, N. Tao, *Nano Lett.* **2009**, *9*, 2571; c) A. Betti, G. Fiori, G. Iannaccone, Y. Mao, presented at *2009 IEEE Int. Electron Devices Meeting (IEDM)*, IEEE, Piscataway, NJ, USA, December, **2009**, <https://doi.org/10.1109/IEDM.2009.5424276> d) X. Wang, Y. Ouyang, X. Li, H. Wang, J. Guo, H. Dai, *Phys. Rev. Lett.* **2008**, *100*, 206803.
- [157] C. Qiu, Z. Zhang, M. Xiao, Y. Yang, D. Zhong, L.-M. Peng, *Science* **2017**, *355*, 271.
- [158] R. Guzman de Villoria, P. Hallander, L. Ydrefors, P. Nordin, B. L. Wardle, *Compos. Sci. Technol.* **2016**, *133*, 33.
- [159] K. K. Manyapu, L. Peltz, P. De Leon, *Acta Astronaut.* **2019**, *157*, 134.
- [160] N. Atar, E. Grossman, I. Gouzman, A. Bolker, Y. Hanein, *ACS Appl. Mater. Interfaces* **2014**, *6*, 20400.
- [161] M. Loeblein, A. Bolker, S. H. Tsang, N. Atar, C. Uzan-Sagiv, R. Verker, I. Gouzman, E. Grossman, E. H. T. Teo, *Small* **2015**, *11*, 6369.
- [162] X. Yang, T. Zou, C. Shi, E. Liu, C. He, N. Zhao, *Mater. Sci. Eng., A* **2016**, *660*, 11.
- [163] M. B. Jakubinek, B. Ashrafi, Y. Zhang, Y. Martinez-Rubi, C. T. Kingston, A. Johnston, B. Simard, *Composites, Part B* **2015**, *69*, 87.
- [164] Y. Ye, D. Zhang, T. Liu, Z. Liu, W. Liu, J. Pu, H. Chen, H. Zhao, X. Li, *J. Hazard. Mater.* **2019**, *364*, 244.
- [165] Y. Li, F. Xu, Z. Lin, X. Sun, Q. Peng, Y. Yuan, S. Wang, Z. Yang, X. He, Y. Li, *Nanoscale* **2017**, *9*, 14476.
- [166] a) K. K. Manyapu, P. De Leon, L. Peltz, J. R. Gaier, D. Waters, *Acta Astronaut.* **2017**, *137*, 472; b) A. C. Nogueira, K. Drechsler, E. Hombergsmeyer, in *53rd AIAA/ASME/ASCE/AHS/ASC Structures, Structural Dynamics and Materials Conf.*, American Institute of Aeronautics and Astronautics, Reston, VA, USA **2012**, <https://doi.org/10.2514/6.2012-1893>; c) X. Ni, R. Kopp, E. Kalfon-Cohen, C. Furtado, J. Lee, A. Arteiro, G. Borstnar, M. N. Mavrogordato, L. Helfen, I. Sinclair, S. M. Spearing, P. P. Camanho, B. L. Wardle, *Composites, Part B* **2021**, *217*, 108623; d) X. Ni, C. Furtado, N. K. Fritz, R. Kopp, P. P. Camanho, B. L. Wardle, *Compos. Sci. Technol.* **2020**, *190*, 108014; e) R. Shivakumar, A. Bolker, S. H. Tsang, N. Atar, R. Verker, I. Gouzman, M. Hala, N. Moshe, A. Jones, E. Grossman, T. K. Minton, E. H. Tong Teo, *Polymer* **2020**, *191*, 122270; f) N. Atar, E. Grossman, I. Gouzman, A. Bolker, V. J. Murray, B. C. Marshall, M. Qian, T. K. Minton, Y. Hanein, *ACS Appl. Mater. Interfaces* **2015**, *7*, 12047; g) P. Weiss, M. P. Mohamed, T. Gobert, Y. Chouard, N. Singh, T. Chalal, S. Schmed, M. Schweins, T. Stegmaier, G. T. Gresser, G. Groemer, N. Sejkora, S. Das, R. Rampini, M. Hoříška, *Adv. Mater. Technol.* **2020**, *5*, 2000028; h) K. Doğan, M. İ. Özgün, H. Sübüütay, E. Salur, Y. Eker, M. Kuntoğlu, A. Aslan, M. K. Gupta, M. Acarer, *Arch. Civ. Mech. Eng.* **2022**, *22*, 55; i) B. Sadeghi, G. Fan, Z. Tan, Z. Li, A. Kondo, M. Naito, *KONA Powder Part. J.* **2022**, *39*, 219; j) S. Bi, Z. Y. Liu, B. L. Xiao, P. Xue, D. Wang, Q. Z. Wang, D. R. Ni, Z. Y. Ma, *Carbon* **2021**, *184*, 364; k) A. P. Usef, V. Bhajantri, V. Kannoth, S. C. Jambagi, *J. Alloys Compd.* **2021**, *888*, 160844; l) U. Marathe, M. Padhan, J. Bijwe, *Compos. Sci. Technol.* **2021**, *210*, 108813; m) N. J. Kanu, S. Bapat, H. Deodhar, E. Gupta, G. K. Singh, U. K. Vates, G. C. Verma, V. Pandey, *Smart Sci.* **2022**, *10*, 40; n) X. F. Sánchez-Romate, J. Martin, M. Sánchez, A. Ureña, *Nanomaterials* **2020**, *10*, 2290; o) P. Jojibabu, Y. X. Zhang, A. N. Rider, J. Wang, *Composites, Part B* **2020**, *186*, 107813.
- [167] a) S. Pourhashem, M. R. Vaezi, A. Rashidi, M. R. Bagherzadeh, *Corros. Sci.* **2017**, *115*, 78; b) K.-C. Chang, M.-H. Hsu, H.-I. Lu, M.-C. Lai, P.-J. Liu, C.-H. Hsu, W.-F. Ji, T.-L. Chuang, Y. Wei, J.-M. Yeh, W.-R. Liu, *Carbon* **2014**, *66*, 144; c) M. Cui, S. Ren, H. Zhao, Q. Xue, L. Wang, *Chem. Eng. J.* **2018**, *335*, 255; d) Y. Ye, D. Yang, D. Zhang, H. Chen, H. Zhao, X. Li, L. Wang, *Chem. Eng. J.* **2020**, *383*, 123160; e) Y. Fu, I. I. Kabir, G. H. Yeoh, Z. Peng, *Polym. Test.* **2021**, *96*, 107115; f) B. E. Gu, C. Y. Huang, T. H. Shen, Y. L. Lee, *Prog. Org. Coat.* **2018**, *121*, 226; g) Y. F. Fu, J. Fischer, K. Q. Pan, G. H. Yeoh, Z. X. Peng, *Appl. Acoust.* **2021**, *171*, 107668.
- [168] Y. X. Bai, R. F. Zhang, X. Ye, Z. X. Zhu, H. H. Xie, B. Y. Shen, D. L. Cai, B. F. Liu, C. X. Zhang, Z. Jia, S. L. Zhang, X. D. Li, F. Wei, *Nat. Nanotechnol.* **2018**, *13*, 589.
- [169] T. Tsuji, G. H. Chen, T. Morimoto, Y. Shimizu, J. Kim, H. Sakakita, K. Hata, S. Sakurai, K. Kobashi, D. N. Futaba, *Nanomaterials* **2021**, *11*, 3461.



Sijia Wu received her bachelor's degree in materials science and engineering from Wuhan University of Technology (2020). She is currently a Master's degree candidate in the group of Prof. Ming Xu at the Huazhong University of Science and Technology.



Huajian Li received his bachelor's degree in material forming and control engineering from Northeastern University (2020). He is currently a Master's degree candidate in the group of Prof. Ming Xu at the Huazhong University of Science and Technology.



Ming Xu obtained her bachelor's (2003) and Ph.D. degrees (2007) from the Shanghai JiaoTong University and continued her research work in Hong Kong, Japan, and USA. She won the 7th Iijima Prize, which is recognized as one of the most distinguished honors in the field of carbon nanotube research. She joined the Huazhong University of Science and Technology (HUST) as a Full Professor since 2012 and has founded the lab for "Research and Development of Nanocarbon materials for Extreme-Environmental Applications" (www.nanocarbon-hust.cn). She has published more than 50 papers in the most prestigious journals including *Science*, *Nature Catalysis*, *Advanced Materials*, etc.